Characterizing Interference in Wireless Mesh Networks

HUI, Ka Hung

A Thesis Submitted in Partial Fulfilment
of the Requirements for the Degree of
Master of Philosophy
in
Information Engineering

August 2007

Abstract of thesis entitled:

Characterizing Interference in Wireless Mesh Networks

Submitted by HUI, Ka Hung

for the degree of Master of Philosophy

at The Chinese University of Hong Kong in August 2007

The relationship between interference and capacity has been a main focus in the study of *wireless mesh networks*. To find out the capacity of a wireless mesh network, we have to accurately model the interference among the wireless links. Then we can design *traffic engineering algorithms* to allocate flows on each link to achieve the capacity.

Existing traffic engineering algorithms were designed based on the celebrated interference model - *protocol model*, and the existence of a perfect scheduler. However, these assumptions only help simplify the problem, and may not be achieved in reality. Therefore, these works may have little value in current wireless mesh networks.

In this thesis, we first introduce a new interference model - *partial interference*, predicting the result of a transmission in a wireless network to be probabilistic based on the corresponding signal-to-noise ratio (SNR) and the modulation scheme used. We illustrate there is a gain in terms of capacity by considering partial interference.

Second, towards designing traffic engineering algorithms in wireless random access networks, we study the stability regions of 802.11 and slotted ALOHA networks under partial interference. The results show that the protocol model is not accurate

enough to model interference in a wireless network. By considering partial interference, we show that the stability region is larger, and the gain in network capacity can be provisioned.

It is difficult to have a complete characterization on the stability regions of 802.11 and slotted ALOHA networks, as illustrated in this thesis. Therefore, as a third contribution, we propose FRASA, *Feedback Retransmission Approximation for Slotted ALOHA*, as a surrogate to approximate the stability region of slotted ALOHA. From this, we derive the *convex hull bound* and the *supporting hyperplane bound* to outer-bound and inner-bound the stability region of FRASA respectively. These bounds are guaranteed to be convex and piecewise linear. By using these bounds, the traffic engineering problem can be formulated as linear programming, which can be solved by standard techniques. We hope our work can serve as a basis in designing traffic engineering algorithms in wireless random access networks.

摘要

在無線網狀網路的研究中，無線訊號間干擾和網路容量之間的關係是一個研究的主要範圍。我們需要準確的模型估計網路中鏈接間的干擾，才能找出網路容量。然後我們可以據此制定交通工程算法來分配網路中的流量來達致預計的容量。

現時的交通工程算法中，大多是根據著名的干擾摸型—協議模型，和完善的調度來制定的。但這些假設只能幫助簡化問題，在現實中是難以實現的。所以在現行的無線網狀網路中實行這些算法的作用並不大。

在這份論文，我們首先建立一個新的訊號干擾模型—部分干擾，其中無線網路中的傳輸結果是取決於由對應的信號噪音比(SNR)及所使用的調變制式所定的機率。我們指出，如果我們考慮無線鏈接之間的部分干優，網路容量將會得到提升。

其次，為了在無線隨機存取網路中設計交通工程算法，我們研究802.11及分段ALOHA網路在部分干擾下的穩定區域。結果顯示，協議模型並不能準確描述網路中的干擾情況。在考慮部分干擾下，我們可以得到較大的穩定區域，於是我們預期考慮部分干擾能帶來網路容量的提升。

我們指出，要完全找出802.11及分段ALOHA的穩定區域是非常困難的。於是，我們提出FRASA—分段ALOHA的續傳反饋模型，來模擬分段ALOHA並尋求分段ALOHA穩定區域的近似解。由此，我們衍生出分別由凸包和支撐超平面所產生的FRASA穩定區域的外邊界及內邊界。這兩個邊界所圍成的區域都是片段線性及凸面的。透過這兩個邊界，我們可以利用已有標準方法解決的線性規劃來制定交通工程算法。我們希望這份論文能作為設計無線隨機存取網路交通工程算法的藍本。

Acknowledgement

First of all, I would like to express my sincere gratitude to my supervisors, Prof. Wing-Cheong Lau and Prof. On-Ching Yue, for their support and giving me freedom to explore interesting research areas in these two years. Throughout these years, their advices, guidance, inspiration and patience have provided me tremendous support. I wish to thank Prof. Jack Lee for his advices and suggestions in research group meetings.

I am grateful to Prof. Raymond Yeung, Prof. Peter Yum and my supervisors for writing reference letters and helping me in various applications.

I also thank all my friends, in particular, Wilson Ip, Michael Cheung, Jack Chan, Ryan Ho, Silas Fong and Derek Cheung, for their help, support and entertainment. Thanks also to my new friends in my graduate study: Ka-Ming Lau, Jack Chui, Gina Yuen, Kin-Fai Li, Chun-Pong Luk, Deng Yun, Martin Choy, Terry Lo and Wing-Kai Lin, for their encouragement and sharing of experiences in research and other areas.

Finally, I want to give my wholehearted thankfulness for the support, care and understanding from my family.

This work is dedicated to my family and friends for their love and support.

Contents

List of Figures

List of Tables

Chapter 1

Introduction / Motivation

In a *wireless mesh network*, all stations communicate with each other through wireless links. A fundamental difference between a wireless network and its wired counterpart is that wireless links may *interfere* with each other, resulting in performance degradation. Therefore in the study of wireless mesh networks, one important performance measure is the capacity of the network when the effects of inter-link interference are considered.

In establishing the capacity of a wireless network, we have to predict whether the wireless links interfere with each other. Several interference models, *e.g.*, *protocol model* and *physical model* [4], were proposed to predict whether transmissions in a wireless network are successful. Many researchers have focused on the design of *interference-aware routing / traffic engineering algorithms* based on the protocol model to optimize the capacity of wireless mesh networks [1, 5, 6].

In these interference models, one key assumption is that interference is a *binary* phenomenon, *i.e.*, either the links mutually interfere with each other, or they do not interfere. However, it was reported that this assumption is not valid, both in single-channel [7] and multi-channel [8] scenarios, which means that it is possible for interfering links to be active simultaneously and realize some throughput. We term this as *partial interference*. This implies that the interference models used are overly sim-

plified, and motivates us to develop more accurate models to capture this partial behavior.

In Chapter 3, we introduce the idea of *partial interference* and point out why the protocol and physical models are not accurate. We demonstrate that if we exploit partial interference in scheduling traffic in a regular wireless network, the gain in *capacity across unit cut* can be as high as 67%. We also illustrate that there is a tradeoff between the *capacity* and the *density* of the links in a wireless network.

In previous works like [1, 5, 6] about designing traffic engineering algorithms in a wireless mesh network, the authors assumed the existence of an ideal scheduler which can, in a centralized manner, coordinate and control link-level access of different nodes across the network. However, practical wireless networks pre-dominantly use distributed *random access* protocols. The ability to characterize the capacity region of wireless random access networks has therefore become a pre-requisite for traffic engineering / optimization of such networks.

In Chapter 4, we study partial interference in 802.11 networks, the most prevalent random access networks nowadays. We propose an analytical framework to characterize partial interference in a single-channel wireless network. We extend the Markov model in [9] to take into account the unsaturated traffic conditions, the signal-to-noise ratio (SNR) attained at the receivers and the modulation scheme employed. These modifications result in a *partial interference region*, implying that the interference models used in previous works are not accurate enough. We also find out the *stability (admissible) region* of 802.11 networks with two links. Moreover, we provide an intuitive analogy between our results and time division multiple access (TDMA) with code division multiple access (CDMA) to explain our analytical results and illustrate the importance of carrier sensing threshold in our model.

Due to the complexity of the 802.11 MAC protocol, the results in Chapter 4 can only be computed numerically. The analytical characterization of the capacity region of general 802.11-based networks therefore seems to be forbiddingly intractable. We therefore choose to study slotted-ALOHA-based networks instead, in order to gain insights on the capacity region and thus, the design of interference-aware traffic engineering algorithms for general wireless random access networks.

In Chapter 5, we study the stability region of slotted ALOHA networks. We extend the model in [10] to derive the exact stability region of slotted ALOHA with two links while considering partial interference. We show that as the link separation increases, the stability region obtained expands *gradually* under partial interference. Due to the similarities in the results with those in Chapter 4, the results here can be applied to 802.11 networks. The stability region can be either convex or nonconvex, depending on the link separation and the transmission probability vector. We also give in *closed form* a partial characterization on the boundary of the stability region under partial interference with general number of links.

The study of the stability region of slotted ALOHA has attracted many researchers [2, 3, 10–15]. Despite the simplicity of slotted ALOHA, this problem is extremely difficult when M, the number of links in the system, exceeds two, even on the collision channel assumption. Under this assumption, successful transmissions occur if and only if there is one active transmitter, because of the interference among the stations. The inherent difficulty in the analysis is due to the effect of queueing in each transmitter. More specifically, the probability of successful transmission depends on the number of active transmitters, which in turn depends on whether the queues in the transmitters are empty or not. However, it is still an open problem to obtain the stationary joint queue statistics in closed form. This is the

reason why we can only give a partial characterization on the boundary of the stability region of slotted ALOHA in Chapter 5 when there are more than two links.

Instead of finding the exact stability region, previous researchers have attempted to bound the stability region [2, 3, 10–12]. However, they did not require the bounds to be *convex* or *piecewise linear*, which are important in traffic engineering. Requiring such properties reduces the traffic engineering problem into convex or linear programming, which are relatively more tractable. Therefore, we are motivated to derive convex and piecewise linear bounds on the stability region.

In Chapter 6, we propose FRASA, *Feedback Retransmission Approximation for Slotted ALOHA*, as a surrogate to approximate finite-link slotted ALOHA. By considering FRASA, we obtain in *closed form* the exact stability region of FRASA under collision channel for *any* number of links. We show that the result from FRASA is identical to the analytical result of finite-link slotted ALOHA when there are two links. We demonstrate by simulation that the stability region obtained from FRASA is a good approximation to the stability region of finite-link slotted ALOHA. We also illustrate that FRASA has a wider range of applicability than the existing bounds. We provide a *convex hull bound*, which is convex, piecewise linear, and outer-bounds the stability region of FRASA. This bound can be computed by using the transmission probability vector only. Moreover, we introduce $\mathbf{p}$-*convexity*, which is essential to ensure the convex hull bound to be close to the boundary of the stability region of FRASA. The nonconvexity of the stability region of FRASA when $M > 2$ follows from these results. A separate inner bound, called *supporting hyperplane bound*, which is also convex and piecewise linear, is also introduced. Furthermore, we also extend these results to cover other interference models like binary and partial interference.

In summary, the major contributions of this thesis are:

1. The notion of partial interference in wireless mesh networks is introduced. The benefits of considering partial interference in terms of capacity are illustrated.
2. The stability regions of wireless networks with random access protocols like 802.11 and slotted ALOHA under partial interference are studied. When partial interference is considered instead of binary interference, the stability region is larger. This implies that by exploiting partial interference, more combinations of flows on the links can be admitted and the capacity of the network can be potentially increased.
3. A new model, FRASA, is introduced to approximate the stability region of finite-link slotted ALOHA. Two convex and piecewise linear bounds on the stability region of FRASA are derived, which can be used to formulate the traffic engineering problem in wireless networks as convex or linear programming.

In conclusion, although we do not completely solve the traffic engineering problem in wireless mesh networks with random access protocols under partial interference, we hope this work can serve as a basis in obtaining insights in the design of traffic engineering algorithms in such networks.

□ **End of chapter.**

Chapter 2

Literature Review

2.1 Introduction

We give a survey on calculating the capacity of a wireless mesh network in this Chapter. The capacity of a wireless mesh network is highly related to the interference among the links in the network. Therefore it is crucial to model the interference accurately. We illustrate how the capacity-finding problem can be augmented to consider the effects of inter-link interference in a wireless mesh network. We also present the works on finding the stability region of wireless networks with slotted ALOHA, the simplest random access protocol.

2.2 The Capacity-Finding Problem

We use a *directed* graph $\mathtt{G} = (V_{\mathtt{G}}, E_{\mathtt{G}})$, called the *connectivity graph*, to model a wireless mesh network. Each vertex $v \in V_{\mathtt{G}}$ represents a node in the network, and each edge $(u, v) \in E_{\mathtt{G}} = \{(u, v) \colon u \in V_{\mathtt{G}}, v \in V_{\mathtt{G}}, u \neq v\}$ denotes the *directed* wireless link from u to v.

Previous researches have focused on finding the capacity of a wireless network, given a fixed placement of nodes in the network [1, 5, 6]. Assume the capacity of each link is ρ_0, and there are F

source-destination pairs $\{\mathsf{s}_f - \mathsf{d}_f\}_{f\in\mathcal{F}}$, where $\mathcal{F} = \{f\}_{f=1}^{F}$.

When there is only one source-destination pair $\mathsf{s} - \mathsf{d}$, the capacity-finding problem can be formulated as a *maximum flow* problem. Let $\lambda_{u,v}$ denote the amount of traffic that can be carried by link (u, v). The maximum flow problem can be represented by the following linear programming problem:

$$\max \sum_{(\mathsf{s},v)\in E_{\mathsf{G}}} \lambda_{\mathsf{s},v}$$

subject to

$$\sum_{(u,v)\in E_{\mathsf{G}}} \lambda_{u,v} = \sum_{(v,u)\in E_{\mathsf{G}}} \lambda_{v,u}, \qquad \forall v \in V_{\mathsf{G}} \setminus \{\mathsf{s}, \mathsf{d}\}, \tag{2.1}$$

$$\sum_{(v,\mathsf{s})\in E_{\mathsf{G}}} \lambda_{v,\mathsf{s}} = 0, \tag{2.2}$$

$$\sum_{(\mathsf{d},v)\in E_{\mathsf{G}}} \lambda_{\mathsf{d},v} = 0, \tag{2.3}$$

$$\lambda_{u,v} \le \rho_0, \qquad \forall (u, v) \in E_{\mathsf{G}}, \tag{2.4}$$

$$\lambda_{u,v} \ge 0, \qquad \forall (u, v) \in E_{\mathsf{G}}. \tag{2.5}$$

The polytope defined by (2.1)-(2.5) is called the *flow polytope*. (2.1) represents flow conservation for every node that is neither source nor destination. (2.2) and (2.3) state that there is no incoming flow for the source and no outgoing flow for the destination respectively. (2.4) and (2.5) specify that the flow on each link cannot exceed the capacity and is non-negative.

For the more general case of F source-destination pairs where $F > 1$, the capacity-finding problem can be modeled as a *multi-commodity flow* problem. In this setting, we are given a traffic matrix $\{\Lambda_f\}_{f\in\mathcal{F}}$, where Λ_f is the amount of traffic that we want to deliver from the source s_f to the destination d_f. Let $\lambda_{u,v,f}$ denote the amount of traffic for commodity f or the f-th source-destination pair that can be carried by link (u, v). The multi-commodity flow problem can be represented by the following

linear programming problem:

$$\max \psi$$

subject to

$$\sum_{(\mathtt{s}_f,v)\in E_{\mathtt{G}}} \lambda_{\mathtt{s}_f,v,f} = \psi\Lambda_f, \qquad \forall f \in \mathcal{F}, \tag{2.6}$$

$$\sum_{(u,v)\in E_{\mathtt{G}}} \lambda_{u,v,f} = \sum_{(v,u)\in E_{\mathtt{G}}} \lambda_{v,u,f}, \forall v \in V_{\mathtt{G}} \setminus \{\mathtt{s}_f, \mathtt{d}_f\}, \forall f \in \mathcal{F}, \tag{2.7}$$

$$\sum_{(v,\mathtt{s}_f)\in E_{\mathtt{G}}} \lambda_{v,\mathtt{s}_f,f} = 0, \qquad \forall f \in \mathcal{F}, \tag{2.8}$$

$$\sum_{(\mathtt{d}_f,v)\in E_{\mathtt{G}}} \lambda_{\mathtt{d}_f,v,f} = 0, \qquad \forall f \in \mathcal{F}, \tag{2.9}$$

$$\sum_{f\in\mathcal{F}} \lambda_{u,v,f} \leq \rho_0, \qquad \forall (u,v) \in E_{\mathtt{G}}, \tag{2.10}$$

$$\lambda_{u,v,f} \geq 0, \qquad \forall (u,v) \in E_{\mathtt{G}}, \forall f \in \mathcal{F}. \tag{2.11}$$

This multi-commodity flow problem finds out how much we can scale up the traffic matrix while still preserving the flow constraints. (2.6) represents that we scale up the traffic for each commodity by the same amount; (2.7), (2.8), (2.9) and (2.11) are generalizations of (2.1), (2.2), (2.3) and (2.5) for each commodity respectively; while (2.10) is the bundle constraint: it generalizes (2.4) in the sense that the sum of the flows across all commodities on a link cannot exceed the capacity of a link. If $\psi < 1$, the original traffic matrix $\{\Lambda_f\}_{f\in\mathcal{F}}$ is infeasible.

2.3 Interference Models

The linear programming formulations in previous Section are insufficient to find the capacity of a wireless mesh network because of the shared nature of the wireless medium. In particular, the

optimal solutions computed from the linear programming in previous Section do not prevent interfering links from being active simultaneously. Two interference models were proposed in [4] to determine whether the wireless links in a network interfere with one another, which may be used to tackle this problem. The first one is the *protocol model*. In this model, each node v has a *transmission range* of R_v and a potentially larger *interference range* of R'_v. A transmission from node v to node u is successful if

- $d_{v,u} \leq \mathsf{R}_v$; and
- Any node v' with $d_{v',u} \leq \mathsf{R}'_{v'}$ is not active in transmission.

In the above formulation, $d_{v,u}$ represents the distance between nodes v and u.

Another model is the *physical model*. In this model, a transmission from node v to node u is successful if

- $\gamma_{v,u} \geq \gamma_0$.

Here, $\gamma_{v,u}$ is the SNR at node u due to the transmission from node v, and γ_0 is the SNR threshold for the receivers to decode properly.

2.4 Considering Interference in the Capacity-Finding Problem with Perfect Scheduling

In this Section, we review some works on how to incorporate the effects of interference into the capacity-finding problem. The wireless networks under consideration are assumed to operate under *perfect scheduling*. After solving the capacity-finding problem for this type of networks, we get the proportion of time that each link in a wireless network should be active. Time slots are then allocated to each link in order to achieve the predicted capacity while excluding interfering links from being active simultaneously.

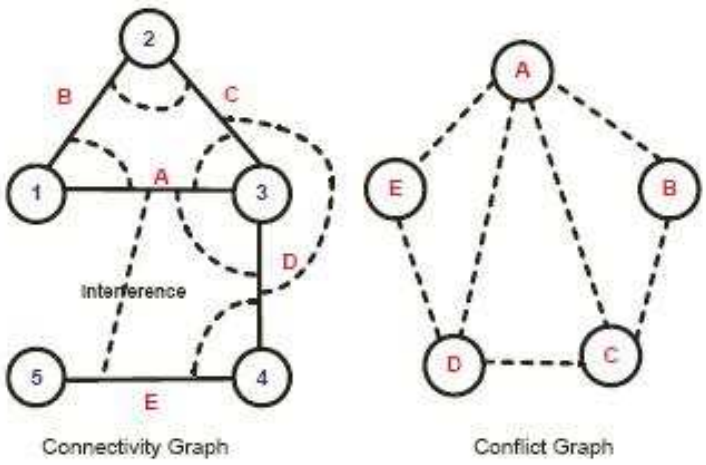

Figure 2.1: A connectivity graph and its corresponding conflict graph [1].

2.4.1 Conflict Graph

Previous researches have studied the effects of interference on the capacity of a wireless mesh network mainly using the protocol model. To represent the interference relationship between wireless links in a network using the protocol model, we use another *directed* graph called the *conflict graph* $\mathtt{F} = (V_{\mathtt{F}}, E_{\mathtt{F}})$. In the conflict graph, each vertex $l_{u,v}$ represents link (u, v) in the connectivity graph, and the edge from $l_{u,v}$ to $l_{u',v'}$ indicates that a transmission on link (u, v) interferes with that on link (u', v').

The following Subsections describe the constraints derived in previous researches on flow scheduling. In deriving the constraints, the *undirected* version of the connectivity graph and the conflict graph were used. A vertex $l_{u,v}$ in the undirected conflict graph represents vertices $l_{u,v}$ and $l_{v,u}$ in the directed conflict graph. An edge $(l_{u,v}, l_{u',v'})$ in the undirected conflict graph is equivalent to the following eight edges in the directed conflict graph: $(l_{u,v}, l_{u',v'})$, $(l_{u,v}, l_{v',u'})$, $(l_{v,u}, l_{u',v'})$, $(l_{v,u}, l_{v',u'})$, $(l_{u',v'}, l_{u,v})$, $(l_{u',v'}, l_{v,u})$, $(l_{v',u'}, l_{u,v})$ and $(l_{v',u'}, l_{v,u})$. An example of the *undirected* connectivity graph and the conflict graph are shown in Fig. 2.1 [1].

2.4.2 Independent Set Constraints

An *independent set* in a graph is a set of vertices such that there is no edge between any two of the vertices. It represents a set of links that can be active simultaneously in the conflict graph. A *maximal independent set* means an independent set that is not contained in other independent sets. Suppose $\mathfrak{I}$ is the collection of all maximal independent sets in the conflict graph. Let $\mathsf{i} \in \mathfrak{I}$ be any maximal independent set and f_i be the fraction of time that all links in i can be active simultaneously. Then the independent set constraints state that:

$$\sum_{\mathsf{i} \in \mathfrak{I}} \mathsf{f}_\mathsf{i} \leq 1 \tag{2.12}$$

$$\lambda_{u,v} \leq \rho_0 \sum_{\mathsf{i}: l_{u,v} \in \mathsf{i}} \mathsf{f}_\mathsf{i}, \forall l_{u,v} \in V_\mathrm{F} \tag{2.13}$$

(2.12) and (2.13) form the *independent set polytope*. (2.12) means that at most only one maximal independent set can be active at a particular time. (2.13) indicates that the fraction of time that a link is active should be upper-bounded by the sum of the amount of the time that it is allowed to be active.

The independent set constraints are *necessary and sufficient conditions* for the flows to be scheduled without interference. However, finding all maximal independent sets in a graph is NP-complete [1, 5]. So alternative constraints were proposed.

2.4.3 Row Constraints

The row constraints state that:

$$\lambda_{u,v} + \sum_{l_{u',v'} \in V_\mathrm{F}: (l_{u',v'}, l_{u,v}) \in E_\mathrm{F}} \lambda_{u',v'} \leq \rho_0, \forall l_{u,v} \in V_\mathrm{F} \tag{2.14}$$

(2.14) forms the *row polytope*. (2.14) means that the sum of the traffic carried by a link and its interferers should not exceed the capacity.

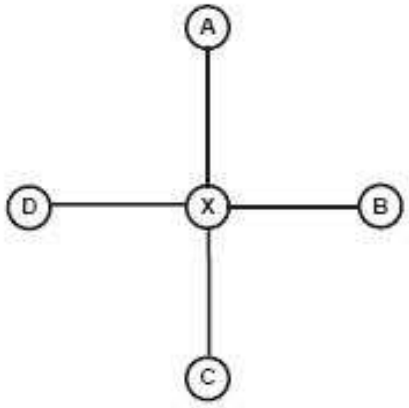

Figure 2.2: A counterexample for the unnecessity of row constraints [1].

The row constraints are only *sufficient conditions*. A counterexample for its unnecessity is shown in Fig. 2.2 [1]. From row constraints, one can derive the followings:

$$\begin{aligned} \lambda_A + \lambda_X &\leq \rho_0, \\ \lambda_B + \lambda_X &\leq \rho_0, \\ \lambda_C + \lambda_X &\leq \rho_0, \\ \lambda_D + \lambda_X &\leq \rho_0, \\ \lambda_A + \lambda_B + \lambda_C + \lambda_D + \lambda_X &\leq \rho_0. \end{aligned}$$

If $\lambda_X = 0$, then at most $\lambda_A = \lambda_B = \lambda_C = \lambda_D = \dfrac{\rho_0}{4}$ is feasible. However, $\lambda_A = \lambda_B = \lambda_C = \lambda_D = \rho_0$ is feasible because links A, B, C, D form a maximal independent set and can be active simultaneously.

2.4.4 Clique Constraints

A *clique* in a graph is a set of vertices such that there is an edge between any two of the vertices. It represents a set of links that mutually conflict with each other in the conflict graph. A *maximal clique* means a clique that is not contained in other cliques. Suppose $\mathfrak{C}$ is the collection of all maximal cliques in the

conflict graph. Let $\mathsf{c} \in \mathfrak{C}$ be any maximal clique. The clique constraints state that:

$$\sum_{l_{u,v} \in \mathsf{c}} \lambda_{u,v} \leq \rho_0, \forall \mathsf{c} \in \mathfrak{C} \tag{2.15}$$

(2.15) forms the *clique polytope*. (2.15) specifies that the sum of the traffic carried by the links belonging to the same clique should not exceed the capacity.

The clique constraints are only *necessary conditions*. A counterexample for its insufficiency is shown in Fig. 2.3 [1]. From clique constraints, we can derive the followings:

$$\begin{aligned}
\lambda_A + \lambda_B &\leq \rho_0, \\
\lambda_B + \lambda_C &\leq \rho_0, \\
\lambda_C + \lambda_D &\leq \rho_0, \\
\lambda_D + \lambda_E &\leq \rho_0, \\
\lambda_E + \lambda_A &\leq \rho_0,
\end{aligned}$$

which means $\lambda_A = \lambda_B = \lambda_C = \lambda_D = \lambda_E = \dfrac{\rho_0}{2}$ is feasible. However, at most $\lambda_A = \lambda_B = \lambda_C = \lambda_D = \lambda_E = \dfrac{2\rho_0}{5}$ is feasible because at most two links can be active at the same time.

2.4.5 Using the physical model

Here we review the extension of the capacity-finding problem to the physical model. We make use of a *weighted* conflict graph to reflect the effect on the SNR induced by the amount of interference received, by assigning the following weight to $(l_{u',v'}, l_{u,v})$, where u, v, u', v' are all distinct, in the conflict graph [5]:

$$w(l_{u',v'}, l_{u,v}) = \frac{P_{u',v}}{\frac{P_{u,v}}{\gamma_0} - N_v} \tag{2.16}$$

In (2.16), $P_{u,v}$ denotes the power received at node v as a result of a transmission from node u, and N_v represents the background

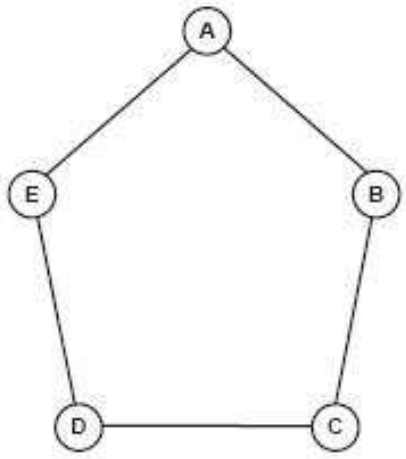

Figure 2.3: A counterexample for the insufficiency of clique constraints [1].

noise power at node v. In case u, v, u', v' are not all distinct, we let $w(l_{u',v'}, l_{u,v}) = \infty$ to represent that links (u, v) and (u', v') cannot be active simultaneously. As suggested by the formula, the amount of interference caused by an interfering link depends on the position of the transmitter, so two vertices $l_{u,v}$ and $l_{v,u}$ should be used in the conflict graph to represent the links between nodes u and v in opposite directions.

We define a counterpart of independent set, called *schedulable set*, which means a set s such that the following constraint is satisfied:

$$\sum_{l_{u',v'} \in \mathsf{s}: (l_{u',v'}, l_{u,v}) \in E_{\mathrm{F}}} w(l_{u',v'}, l_{u,v}) \leq 1, \forall l_{u,v} \in \mathsf{s} \tag{2.17}$$

(2.17) means that for any link in a schedulable set, the cumulative interference of other links in the schedulable set should be small enough so that the resultant SNR is well-above the threshold γ_0, implying that all links in the schedulable set can be active simultaneously. We also define a *maximal schedulable set*, which means that addition of any links to this set will violate (2.17).

Suppose $\mathfrak{S}$ is the collection of all maximal schedulable sets in

the conflict graph. Let s be any maximal schedulable set and f_s be the fraction of time that all links in s can be active simultaneously. The schedulable sets impose the following constraints:

$$\sum_{\mathsf{s}\in\mathfrak{S}} \mathsf{f}_\mathsf{s} \leq 1 \tag{2.18}$$

$$\lambda_{u,v} \leq \rho_0 \sum_{\mathsf{s}:\, l_{u,v}\in\mathsf{s}} \mathsf{f}_\mathsf{s}, \forall l_{u,v} \in V_\mathtt{F} \tag{2.19}$$

(2.18) means that at most only one maximal schedulable set can be active at a particular time. (2.19) indicates that the fraction of time that a link is active should be upper-bounded by the sum of the amount of the time that it is allowed to be active. The schedulable set constraints are *necessary and sufficient conditions* for the flows to be schedulable.

2.5 Considering Interference in the Capacity-Finding Problem with Random Access

To find the capacity of wireless mesh networks with random access protocols, first we need to characterize the *stability region* of this type of networks. After solving the capacity-finding problem augmented with the stability region, we get the loadings on each link. We just need to allocate the amount of flows on each link according to the results from the capacity-finding problem and we can achieve the capacity. However, there is little work on relating the capacity of a wireless random access network to the stability region of such a network. Therefore, we only provide a brief review on the study of the stability region of wireless networks with slotted ALOHA, the simplest random access protocol.

Almost all works assumed the *collision channel* model, *i.e.*, any transmission in the network is successful if and only if there

is one active transmitter. This assumption is true only when all stations in the network are sufficiently close to each other.

The study of the stability region of M-link infinite-buffer slotted ALOHA was initiated by [11] decades before, and is still an ongoing research. The authors in [11] obtained the exact stability region when $M = 2$ under collision channel. [2] and [12] used *stochastic dominance* and derived the same result as in [11] for the case of $M = 2$.

For general M, there were attempts to find the exact stability region, but there was only limited success. [14] established the boundary of the stability region, but it involves stationary joint queue statistics, which still do not have closed form to date.

Instead of finding the boundary, many researchers focused on finding bounds on the stability region for general M. [11] obtained separate sufficient and necessary conditions for stability. [2] and [12] derived tighter bounds on the stability region by using stochastic dominance in different ways. [3] introduced *instability rank* and used it to improve the bounds on the stability region. However, the bounds in [2] and [3] are not always applicable. Also, the bounds obtained may not be piecewise linear.

With the advances in multi-user detection, researchers also studied this stability problem with the *multipacket reception* (MPR) model. [15] studied this problem in the infinite-link, single-buffer and symmetric MPR case. [10] considered the problem with finite links and infinite buffer. They obtained the boundary for the asymmetric MPR case with two links, and also the inner bound on the stability region for general M.

2.6 Chapter Summary

In this Chapter, we have reviewed the capacity-finding problem in wireless mesh networks. We have also introduced various ways to incorporate the effects of inter-link interference into the capacity-finding problem. For wireless mesh networks under perfect scheduling, we have the independent set constraints, the row constraints, the clique constraints and the schedulable set constraints. With wireless mesh networks under random access, we have to characterize the stability region. However, little work has been done in studying the capacity of wireless mesh networks with random access protocols. Also, there are other shortcomings in modeling interference in a wireless network. These shortcomings will be further elaborated in next Chapter.

□ **End of chapter.**

Chapter 3

Partial Interference - Basic Idea

3.1 Introduction

In this Chapter, we point out the deficiencies in the models in Chapter 2. Motivated by experimental results in previous studies, we introduce the notion of partial interference in wireless networks, contrasting with binary interference that can be represented by a single threshold. Partial interference takes into account the SNR at the receivers and the modulation scheme employed by the network. We illustrate that by considering partial interference, the gain in capacity across unit cut can be as high as 67% under scheduling in a modified Manhattan network.

3.2 Deficiencies in Previous Models

The capacity-finding problem together with the effects of interlink interference listed in Chapter 2 are formulated based on the assumptions of protocol model and perfect scheduling. However, we comment that these assumptions only help simplify the capacity-finding problem and may not be valid in reality.

3.2.1 Multiple Interferers

The constraints based on the protocol model ignore the case of multiple interferers. Consider the topology as shown in Fig. 3.1. Assume the path loss model is $pl(d) = Cd^{-\alpha}$ where d is the propagation distance, α is the path loss exponent and C is a constant. Also assume the effect of background noise is negligible. In this topology, node v transmits to node u. The transmitters, *i.e.*, nodes v, v', v'', all transmit with power P and have the same transmission range R and interference range R'. Suppose $d_{v,u} = \mathsf{R}$ and R' is defined by $\frac{PC\mathsf{R}^{-\alpha}}{PC\mathsf{R}'^{-\alpha}} = \gamma_0$. Let $d_{v',u} = d_{v'',u}$ and $\frac{PCd_{v,u}^{-\alpha}}{PCd_{v',u}^{-\alpha}} = 1.5\gamma_0$. Therefore, $d_{v',u} = d_{v'',u} > \mathsf{R}'$, and from the protocol model the transmissions from v' and v'' do not interfere with the transmission from v to u. From the perspective of the physical model, when either v' or v'' is active but not both, the SNR at u is greater than the required threshold γ_0, therefore the transmission from v to u will be successful. But when both v' and v'' are active simultaneously, the SNR at u becomes $\frac{PCd_{v,u}^{-\alpha}}{2PCd_{v',u}^{-\alpha}} = 0.75\gamma_0$, implying that the transmission from v to u will be unsuccessful. The primary reason for this discrepancy is that in the protocol model, only two transmitters are considered each time, and the possibility of multiple interferers is ignored. Therefore, we should use the physical model, which takes the SNR together with the case of multiple interferers into account, to model the interference in wireless networks.

3.2.2 Non-binary Behavior of Interference

In the protocol model, it is assumed that when there is interference between two links, it is not possible for both receivers to decode the signals from the corresponding transmitters when

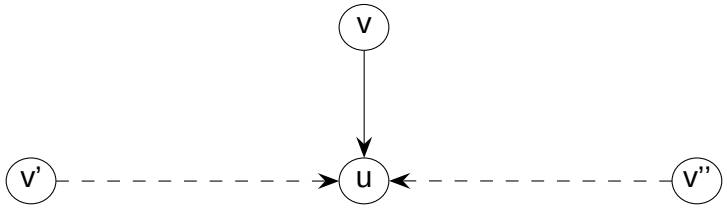

Figure 3.1: Protocol model ignores the case of multiple interferers.

both transmitters are active at the same time. This implies when interference exists between two links, each link can only achieve half of the capacity if the links share the wireless medium exclusively, or the links can hardly realize any throughput if they always attempt transmissions. In both cases, the relationship between the throughput of each link and the separation between the links can be modeled as a step function. We can obtain similar relationship from the physical model, in which the abrupt change is induced by the SNR threshold instead of the threshold distance, *i.e.*, the interference range.

However, such an abrupt change does not appear in reality. In [7], the authors measured the interference among links in a single-channel, static 802.11 multi-hop wireless network. They measured the interference between pairs of links by the *link interference ratio*, and observed that this ratio exhibited a continuum between 0 and 1. In [8], two interfering links were set up in a wireless network with multiple partially overlapped channels to measure TCP and UDP throughputs of an individual link. It was found that the throughputs increased smoothly when the separation between the links increased. The throughputs increased more rapidly as the channel separation between the links increased. These experimental results suggest that the *threshold-based* or *binary* assumption in the protocol and the physical models may not be valid.

3.2.3 Impractical Perfect Scheduling

When we include the independent set polytope or clique polytope in the capacity-finding problem, we make an assumption that the underlying wireless network operates in a time-division manner with perfect scheduling. After getting the proportion of time that each link in a wireless network should be active, time slot assignment algorithms are designed to schedule when the links should be active. This requires a centralized scheduler to coordinate and control the access to the wireless medium by the links. However, such a perfect scheduling is hard to achieve in reality. Moreover, practical wireless networks pre-dominantly use distributed random access protocols. Therefore, we study the capacity-finding problem in random access networks.

3.3 Refining the Relationship between Interference and Throughput Degradation

There have been some preliminary works on finding the relationship between the SNR attained at a receiver and the throughput achieved by the corresponding wireless link. In [16], a methodology for estimating the packet error rate in the *affected wireless network* due to the interference from the *interfering wireless network* was presented. The throughput of the affected wireless network was found to increase continuously with the SNR attained at the corresponding receiver, which increased with the separation between the networks.

As an illustration to the methodology in [16], assume the underlying modulation scheme used is binary phase shift keying (BPSK). The distance between the transmitter and the receiver and that between the interferer and the receiver are d_S and d_I meters respectively. The transmission power of the transmitter and the interferer are P_S and P_I watts respectively.

Assuming the interfering signal can be modeled as additive white Gaussian noise (AWGN) and the background noise can be ignored. We use the two-ray ground reflection model

$$pl(d) = \frac{G_T G_R h_T^2 h_R^2}{d^4} = \frac{C}{d^4} \tag{3.1}$$

to represent the path loss, where G_T and G_R are the gain of transmitter and receiver antenna respectively, h_T and h_R are the height of transmitter and receiver antenna respectively, and $C = G_T G_R h_T^2 h_R^2$. The path loss exponent is 4 in this model. We let $G_T = G_R = 1$ and $h_T = h_R = 1.5$. Then the bit error rate is $\frac{1}{2} erfc(\sqrt{\gamma})$ [17], where γ is the SNR attained at the receiver and is equal to $\frac{P_S pl(d_S)}{P_I pl(d_I)}$. Suppose all packets consist of L bits. Then the normalized throughput ρ as a result of the interference is calculated as follows, assuming both the transmitter and the interferer are always active:

$$\rho = \left[1 - \frac{1}{2} erfc(\sqrt{\gamma})\right]^L.$$

We call this *partial interference*, stating that the result of a wireless transmission to be probabilistic based on the corresponding signal-to-noise ratio (SNR) and the modulation scheme used. Fig. 3.2 shows a plot of throughput against distance between the interferer and the receiver in partial interference for $P_S = P_I = 25$ dBm, $d_S = 300$ meters, d_I ranging from 400 to 700 meters and $L = 12000$ bits.

In Fig. 3.2 we also plot the variation of throughput against distance between the interferer and the receiver if the physical model is used. The SNR threshold γ_0 is calculated by assuming that when $\gamma = \gamma_0$, the packet error rate is 10^{-3}, *i.e.*,

$$10^{-3} = 1 - \left[1 - \frac{1}{2} erfc(\sqrt{\gamma_0})\right]^L.$$

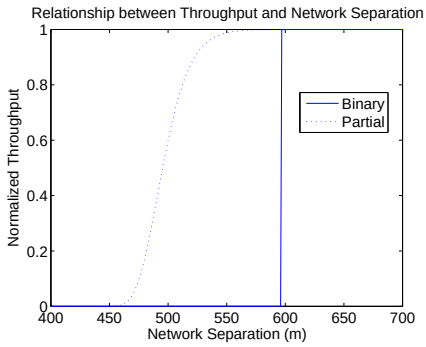

Figure 3.2: Throughput degradation and network separation.

We observe that if the value we assign to γ_0 is too large (or the threshold distance is too large), we underestimate the throughput that the links can achieve. On the other hand, if γ_0 is too small (or the threshold distance is too small), we introduce excessive interference into the network. In other words, it is difficult to use a single threshold to describe accurately the relationship between interference and throughput of each link in a network.

3.4 Capacity Gain by Exploiting Partial Interference

In this Section, we demonstrate that there is a gain in capacity by exploiting partial interference. We consider one variation of the Manhattan network [18], *i.e.*, a network consisting of a rectangular grid extending to infinity in both dimensions. The horizontal and vertical separation between neighboring stations are denoted by r and d respectively. The capacity of each link without interference is denoted by ρ_0.

We assume differential binary phase shift keying (DBPSK) is employed and a packet consists of L bits. We use the two-ray ground reflection model (3.1) as in previous Section to model the path loss. To apply the physical model, we let the SNR

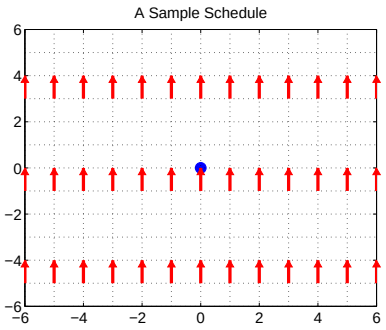

Figure 3.3: A scheduling pattern in the modified Manhattan network.

threshold γ_0 be the case that the packet error rate is ϵ, *i.e.*, $1-\left[1-\frac{1}{2}\exp(-\gamma_0)\right]^L = \epsilon$, where $\frac{1}{2}\exp(-\gamma)$ is the bit error rate of DBPSK [17]. We let $L = 8192$ and $\epsilon = 10^{-3}$, therefore the SNR requirement is $\gamma_0 = 15.23$. Assuming there is no interferer, this SNR requirement is met when the length of a link is smaller than 493 meters.

We use a Cartesian coordinate plane to represent the modified Manhattan network. One station is placed at every point with integral coordinates in the network. Suppose we schedule flows in the modified Manhattan network from the South to the North using the pattern shown in Fig. 3.3 and its shifted versions. In Fig. 3.3, an arrow is used to represent an active link, where the tail and the head of an arrow denote the transmitter and the receiver of the link respectively.

We use the *capacity across unit cut* $\eta(\mu)$ as the performance metric, where $\mu = \frac{r}{d}$ is the ratio of the horizontal separation to the vertical separation. It is a measure on how much we can send through a cut on average while packing the links together. Consider the SNR attained at the receiver marked with the blue circle, which has the position assigned as the origin in the Cartesian coordinate plane. We assume all stations transmit with power P, and each station has a background noise power

of N. The SNR is defined by $\gamma(\mu) = \dfrac{S}{N + I(\mu)}$, where S is the received power from the intended transmitter and $I(\mu)$ is the power received from all interferers. The capacity achieved by each link is $\rho(\mu) = \rho_0 \left\{ 1 - \frac{1}{2} \exp[-\gamma(\mu)] \right\}^L$ under partial interference; while in the physical model, we let $\rho(\mu) = \rho_0$ if $\gamma(\mu) \geq \gamma_0$ and $\rho(\mu) = 0$ otherwise. A *cut* $\mathcal{C}$ in the network is an infinitely long horizontal line. Let $\{T_n\}_{n \in \mathbb{N}}$ be the set of all active transmitters such that $\mathcal{C}$ intersects the link used by T_n. We divide $\mathcal{C}$ into segments $\mathcal{C}(T_n), n \in \mathbb{N}$, where

$$\mathcal{C}(T_n) = \left\{ x \in \mathcal{C} \colon \|x - T_n\| = \min_{n' \in \mathbb{N}} \|x - T_{n'}\| \right\}$$

and $\|\cdot\|$ is the Euclidean norm. Then the length $\mathcal{L}$ of the cut occupied by an active transmitter is the length of $\mathcal{C}(T_n)$, and the capacity across unit cut is therefore $\eta(\mu) = \dfrac{\mathsf{f}\rho(\mu)}{\mathcal{L}}$, where f is the fraction of time that a link is active.

In the following we assume $d = 450$ meters, $P = 24.5$ dBm and $N = -88$ dBm. For the schedule in Fig. 3.3, the signal power is $S = \dfrac{PC}{d^4}$. All transmitters in Fig. 3.3 are located at positions $(x, 4y-1)$, where x and y are integers. The interference power is

$$\begin{aligned} I(\mu) &= \left\{ \sum_{x=-\infty}^{\infty} \sum_{y=-\infty}^{\infty} \frac{PC}{\left((xr)^2 + [(4y-1)d]^2\right)^2} - \frac{PC}{d^4} \right\} \\ &= \left\{ \sum_{x=-\infty}^{\infty} \sum_{y=-\infty}^{\infty} [(x\mu)^2 + (4y-1)^2]^{-2} - 1 \right\} \frac{PC}{d^4}. \end{aligned}$$

Considering the physical model, if the schedule is allowed to be active, we need $\mu \geq \mu_0 = 5.58$, as listed in Table 3.1 and depicted in Fig. 3.4 by the blue dashed line. The value of μ_0 is obtained from $\gamma(\mu_0) = \gamma_0$. Each active transmitter occupies

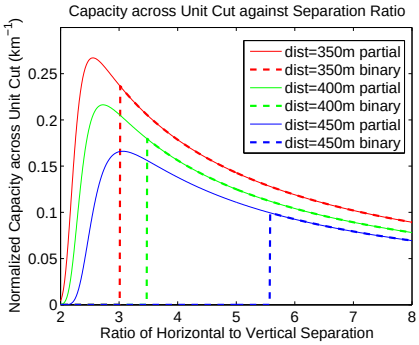

Figure 3.4: Capacity across unit cut for different length of links under the physical model (binary interference) and partial interference.

Table 3.1: Capacity gain in the modified Manhattan network with different length of links.

d	μ_0	$\eta(\mu_0)$	μ_{opt}	$\eta(\mu_{opt})$	% increase
350	3.02	0.2365 ρ_0	2.55	0.2671 ρ_0	12.93%
400	3.48	0.1796 ρ_0	2.73	0.2163 ρ_0	20.45%
450	5.58	0.0996 ρ_0	3.06	0.1661 ρ_0	66.82%

a cut of length $r = \mu d$ and each link is active for one quarter of a cycle. Therefore, for $\mu = \mu_0$, the maximum capacity across unit cut under the physical model is $\dfrac{\rho_0}{4\mu_0 d} = 0.0996\rho_0$ bits per second per kilometer.

If we allow partial interference, the active transmitters can be packed more closely. When μ decreases, more spatial reuse is allowed. The increase in the density of active transmitters outweighs the degradation in capacity, so there is an increase in the capacity across unit cut. However, if μ decreases further, interference will be the dominant factor in determining the capacity across unit cut. Therefore, the capacity across unit cut drops, and there exists μ_{opt} for the optimal performance under partial interference. This behavior is depicted by the blue solid line in Fig. 3.4. The optimal value of μ under partial interference is $\mu_{opt} = 3.06$, and the capacity across unit cut is $0.1661\rho_0$

bits per second per kilometer. There is a percentage increase of 66.82% in the capacity across unit cut by exploiting partial interference. Similar results are shown in Table 3.1 and Fig. 3.4 for $d = 350, 400$ meters. The percentage increase is larger when the links are longer, but the capacity achieved by each link reduces. We can view $\mu_0 d$ as the carrier sensing range in the modified Manhattan network with the scheduling pattern in Fig. 3.3, as it is the smallest horizontal separation allowed by the physical model. We observe that if the length of the links increases, the carrier sensing range needs to be increased in a larger proportion. Also, this carrier sensing range is much larger than double of the length of the links, which is the usual convention used in defining the relationship between carrier sensing range and transmission range.

3.5 Chapter Summary

In this Chapter, we have reviewed the deficiencies in the models in previous Chapter. We also introduced the notion of partial interference in wireless networks, and illustrated that by exploiting partial interference in scheduling in a regular wireless network, the performance gain in terms of capacity across unit cut can be as high as 67%. The example included here only considered partial interference in wireless networks with perfect scheduling. In the next two Chapters, we will study partial interference in wireless networks with random access protocols, *i.e.*, 802.11 and slotted ALOHA. Performance gain in terms of capacity by exploiting partial interference in random access networks will be demonstrated.

□ **End of chapter.**

Chapter 4

Partial Interference in 802.11

4.1 Introduction

In this Chapter, we study partial interference in 802.11 networks, the prevalent wireless random access networks. We present an analytical framework to characterize partial interference in a single-channel wireless network under unsaturated traffic conditions, which uses 802.11b with basic access scheme and DBPSK. We show that there is a partial interference region, in which the throughput of each link increases continuously with the separation between the links in the network. An analogy is drawn between partial interference and code division multiple access to demonstrate their similarities. As a first attempt to relate the capacity-finding problem in wireless random access networks to the stability region of such networks, we derive the admissible (stability) region of an 802.11 network with two links numerically.

4.2 The 802.11 Model

We present our framework to characterize partial interference in a wireless network with random access protocols. In this framework, we derive the *transmission probabilities* τ_n and the

packet corruption probabilities c_n of the links in the network. τ_n is the probability that a station transmits in a randomly chosen slot, while c_n is the probability that a packet is received with error.

4.2.1 Assumptions

For illustration, we choose the MAC and PHY protocols to be 802.11b with basic access scheme and 1Mbps DBPSK. Our model can be readily extended to consider other modulation schemes. In addition, we make the following assumptions:

- The network consists of two links (T_1, R_1) and (T_2, R_2), where T_n and R_n denote the transmitter and the receiver of the links respectively, $n = 1, 2$.
- There are a constant *buffer nonempty probability* q_n that the transmission buffer of T_n is nonempty and a constant *channel idle probability* i_n that T_n senses the channel to be idle, $n = 1, 2$.
- T_n transmits with power P_n, and the background noise power at R_n is N_n, $n = 1, 2$.
- Channel defects like shadowing and fading are neglected, and a generic path loss model $pl(d) = Cd^{-\alpha}$ is used to model the wireless channel, where d is the propagation distance, α is the path loss exponent and C is a constant.
- The interference from other transmitters plus the receiver background noise is assumed to be Gaussian distributed.
- All bits in a packet must be received correctly for correct reception of the packet.
- The size of an acknowledgement is much smaller than that of the payload, so the bit errors on acknowledgement are negligible.

4.2.2 Transmission Probability Calculation

We follow the approach as in [9], using a discrete-time Markov chain to model the 802.11 Distributed Coordination Function (DCF) and obtain the transmission probability of a station. An ordered pair (j, k) is used to denote the state of the Markov chain, where j represents the backoff stage, and k is the current backoff counter value. In stage j, k is in the range $[0, W_j - 1]$, where W_j is the contention window size in stage j. m is the maximum number of backoff stages. However, there are some discrepancies between this model and the actual behavior of 802.11 DCF. First, the model assumes that a station retransmits indefinitely until the packet is successfully transmitted. This assumption is inconsistent with 802.11 basic access scheme. Also, the model does not account for the unsaturated traffic conditions, which is the scenario appeared in practical situations.

We adopt the following modifications on the Markov chain to obtain a better model. First, we take into account the limited number of retransmissions in 802.11 as in [19], by restricting the Markov chain to leave the m-th backoff stage once the station transmits a packet in that backoff stage. Second, we follow [19] to modify the values of W_j in accordance with the 802.11 MAC and PHY specifications [20], with m' corresponding to the first backoff stage using the maximum contention window size:

$$W_j = \begin{cases} 2^j W_0, & 0 \leq j \leq m' \\ 2^{m'} W_0, & m' < j \leq m \end{cases}.$$

In addition, to model the unsaturated conditions, we follow [21] to augment the Markov chain by introducing new states $(-1, k), k \in [0, W_0 - 1]$. These new states represent the states of being in the post-backoff stage. The post-backoff stage is entered whenever the station has no packets queued in its transmission buffer after a successful transmission. The corresponding Markov chain is depicted in Fig. 4.1.

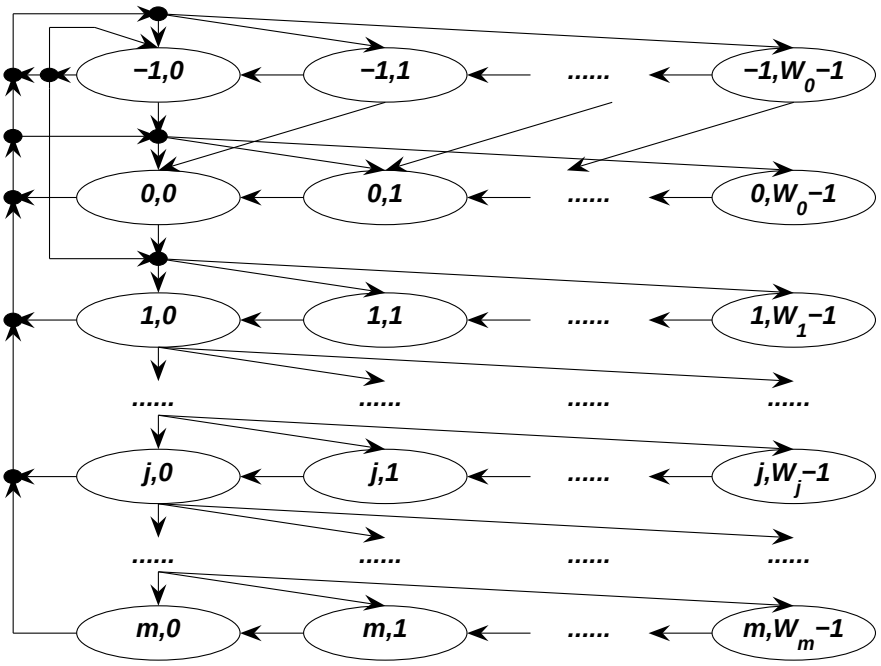

Figure 4.1: A Markov chain model for 802.11 DCF in unsaturated conditions.

We use $\Pr(j_1, k_1|j_0, k_0)$ to denote the transition probability from (j_0, k_0) to (j_1, k_1), and the transition probabilities are as follows:

$$\Pr(j, k|j, k+1) = 1, \quad j \in [0, m], k \in [0, W_j - 2], \tag{4.1}$$

$$\Pr(0, k|-1, k+1) = q_n, k \in [0, W_0 - 2], \tag{4.2}$$

$$\Pr(-1, k|-1, k+1) = 1 - q_n, k \in [0, W_0 - 2], \tag{4.3}$$

$$\Pr(0, k|j, 0) = \frac{(1 - c_n)q_n}{W_0}, \quad j \in [0, m-1], k \in [0, W_0 - 1], \tag{4.4}$$

$$\Pr(-1, k|j, 0) = \frac{(1 - c_n)(1 - q_n)}{W_0}, \quad j \in [0, m-1], k \in [0, W_0 - 1], \tag{4.5}$$

$$\Pr(0,k|m,0) = \frac{q_n}{W_0}, k \in [0, W_0 - 1], \tag{4.6}$$

$$\Pr(-1,k|m,0) = \frac{1-q_n}{W_0}, k \in [0, W_0 - 1], \tag{4.7}$$

$$\Pr(j,k|j-1,0) = \frac{c_n}{W_j}, \quad j \in [1,m], k \in [0, W_j - 1], \tag{4.8}$$

$$\Pr(0,k|-1,0) = \frac{q_n(1-i_n) + q_n^2 i_n(1-c_n)}{W_0}, \quad k \in [0, W_0 - 1], \tag{4.9}$$

$$\Pr(1,k|-1,0) = \frac{q_n i_n c_n}{W_1}, k \in [0, W_1 - 1], \tag{4.10}$$

$$\Pr(-1,k|-1,0) = \frac{q_n i_n (1-c_n)(1-q_n)}{W_0}, \quad k \in [1, W_0 - 1], \tag{4.11}$$

$$\Pr(-1,0|-1,0) = \frac{q_n i_n (1-c_n)(1-q_n)}{W_0} + (1-q_n). \tag{4.12}$$

The equations above describe the following behaviors:

- the decrement of backoff counter at the beginning of each slot by (4.1)-(4.3);
- the reset of backoff procedure to stage 0 or -1 after a successful transmission by (4.4)-(4.5);
- the reset of backoff procedure to stage 0 or -1 after the last transmission attempt by (4.6)-(4.7);
- the increment of backoff stage after an unsuccessful transmission by (4.8);
- the transition after post-backoff finishes by (4.9)-(4.12).

Let $\pi_{j,k}$ denote the stationary probability of the state (j,k) in the Markov chain. The transmission probability of a station is

given by

$$\begin{aligned}\tau_n &= \pi_{-1,0} q_n i_n + \sum_{j=0}^{m} \pi_{j,0} \\ &= \left(2q_n^2 W_0 \sum_{j=0}^{m} c_n^j\right)\Bigg\{ q_n^2 W_0 \sum_{j=0}^{m} c_n^j (W_j + 1) \\ &\quad + (1-q_n)\Big[1-(1-q_n)^{W_0}\Big] \\ &\quad \times [q_n(1-i_n)(W_0+1) + 2(1-q_n)]\Bigg\}^{-1}. \qquad (4.13)\end{aligned}$$

The derivation of this equation is given in Appendix.

4.2.3 Packet Corruption Probability Calculation

The packet corruption probability is calculated according to the modulation scheme used in the PHY layer, the distance between the transmitter and the receiver, and the existence of nearby interferer(s). For a fixed *carrier sensing threshold* β, we differentiate into two cases, whether both transmitters can sense the transmission of each other or not.

If T_1 can sense the transmission of T_2, *i.e.*, $P_2 pl\big(d_{T_1,T_2}\big) > \beta$, where $d_{X,Y}$ is the distance between X and Y, then the SNR at R_1 is

$$\gamma_1 = \frac{P_1 pl\big(d_{T_1,R_1}\big)}{N_1}.$$

The bit error rate attained by (T_1, R_1) is $e(\gamma_1) = \frac{1}{2}\exp(-\gamma_1)$, and the packet corruption probability for (T_1, R_1) is

$$c_1 = 1 - [1 - e(\gamma_1)]^{H_P + H_M + L}, \qquad (4.14)$$

where H_P, H_M and L represent the number of bits in the PHY header, the MAC header and the payload respectively.

On the other hand, if T_1 cannot sense the transmission of T_2, *i.e.*, $P_2 pl\big(d_{T_1,T_2}\big) \leq \beta$, then the SNR at R_1 depends on whether T_2 is active in transmission or not, *i.e.*,

$$\Pr\{\gamma_1 = \gamma\} = \begin{cases} 1-\tau_2, & \gamma = \dfrac{P_1 pl\big(d_{T_1,R_1}\big)}{N_1} \\ \tau_2, & \gamma = \dfrac{P_1 pl\big(d_{T_1,R_1}\big)}{N_1 + P_2 pl\big(d_{T_2,R_1}\big)} \end{cases}.$$

The packet corruption probability is calculated by the average bit error rate $E[e(\gamma_1)]$:

$$c_1 = 1 - \big(1 - E[e(\gamma_1)]\big)^{H_P+H_M+L}. \tag{4.15}$$

The channel idle probability is defined as follows. If T_1 can sense the transmission of T_2, then T_1 will consider the channel to be idle whenever T_2 is inactive, *i.e.*, $i_1 = 1-\tau_2$; otherwise T_1 always senses the channel to be idle and $i_1 = 1$.

4.2.4 Loading Calculation

Suppose we want to schedule a flow of λ_n bits per second on (T_n, R_n), and ρ_n bits per second is achieved by (T_n, R_n), $n = 1, 2$. We refer λ_n and ρ_n to the *offered load* and the *carried load* respectively. We calculate ρ_n by

$$\rho_n = \frac{\tau_n(1-c_n)L}{E[S_n]}, \tag{4.16}$$

where $E[S_n]$ is the expected length of a slot as seen by (T_n, R_n). Let a_n be the probability that at least one station is transmitting, and s_n be the probability that there is at least one successful transmission given that at least one station is transmitting. Then $E[S_n] = (1-a_n)\sigma + a_n s_n(T_s+\sigma) + a_n(1-s_n)(T_c+\sigma)$, where σ, T_s and T_c are the time spent in an idle slot, a successful transmission and an unsuccessful transmission respectively. When T_1

can sense the transmission of T_2, we consider both links to be one system:

$$a_1 = 1 - (1-\tau_1)(1-\tau_2),$$
$$s_1 = \frac{1 - [1-\tau_1(1-c_1)][1-\tau_2(1-c_2)]}{a_1}.$$

Otherwise, we treat both links to be separate systems:

$$a_1 = \tau_1,$$
$$s_1 = 1 - c_1.$$

We approximate the packet arrival of (T_n, R_n) to be a Poisson process with rate $\frac{\lambda_n}{L}$, $n = 1, 2$, and estimate the buffer nonempty probability by

$$q_n = 1 - \exp\left\{-\frac{\lambda_n}{L} E[S_n]\right\}. \tag{4.17}$$

4.2.5 Summary

In summary, if T_1 can sense the transmission of T_2, then we obtain the following set of equations for (T_1, R_1):

$$\begin{aligned}
\tau_1 = {} & \left(2q_1^2 W_0 \sum_{j=0}^{m} c_1^j\right)\Bigg\{q_1^2 W_0 \sum_{j=0}^{m} c_1^j (W_j + 1) \\
& + (1-q_1)\Big[1 - (1-q_1)^{W_0}\Big] \\
& \times [q_1\tau_2(W_0+1) + 2(1-q_1)]\Bigg\}^{-1}, \\
c_1 = {} & 1 - [1 - e(\gamma_1)]^{H_P + H_M + L}, \\
q_1 = {} & 1 - \exp\Bigg\{-\big[\big(1 - [1-\tau_1(1-c_1)][1-\tau_2(1-c_2)]\big)T_s \\
& + [\tau_1 c_1 + \tau_2 c_2 - \tau_1\tau_2(c_1 + c_2 - c_1 c_2)]T_c + \sigma\big]\frac{\lambda_1}{L}\Bigg\}.
\end{aligned}$$

Otherwise, we obtain another set of equations for (T_1, R_1):

$$\tau_1 = \left(2q_1^2 W_0 \sum_{j=0}^{m} c_1^j\right)\Bigg\{q_1^2 W_0 \sum_{j=0}^{m} c_1^j (W_j + 1) + 2(1-q_1)^2\Big[1-(1-q_1)^{W_0}\Big]\Bigg\}^{-1},$$

$$c_1 = 1 - \big(1 - E[e(\gamma_1)]\big)^{H_P + H_M + L},$$

$$q_1 = 1 - \exp\Big\{-[\tau_1(1-c_1)T_s + \tau_1 c_1 T_c + \sigma]\frac{\lambda_1}{L}\Big\}.$$

Similarly, we can obtain three equations for link (T_2, R_2). With these six equations we can solve for the variables $\tau_1, c_1, q_1, \tau_2, c_2, q_2$ by Newton's method [22], and obtain the loadings of these two links by (4.16).

4.3 Some Analytical Results

We use the two-ray ground reflection model

$$pl(d) = \frac{G_T G_R h_T^2 h_R^2}{d^4} = \frac{C}{d^4}$$

to represent the path loss as in Chapter 3 and the values in Table 4.1 to obtain numerical results from our model. These values are defined in or derived from the values in the 802.11 MAC and PHY specifications [20] or NS-2 [23].

In the following we attempt to find the maximum carried loads of each link in various scenarios. One observation from solving the system of equations in Section 4.2 is that the carried load will be smaller than the offered load when the offered load is too large. This corresponds to the instability of 802.11 observed in previous works (*e.g.*, [9]). Therefore, we use binary search to find the maximum carried load under stable conditions. Initially, the search range for the offered load is between 0 and 1Mbps. We

Table 4.1: Parameters used for the analytical results of 802.11.

H_P	192 bits	H_M	272 bits	m	7	m'	5
T_s	9020 μs	T_c	9020 μs	σ	20 μs	W_0	32
P_1, P_2	24.5 dBm	N_1, N_2	-88 dBm	G_t, G_r	1	h_t, h_r	1.5 m

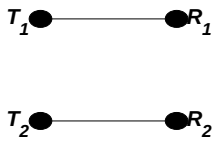

Figure 4.2: A sample topology.

choose the midpoint of the search range to be the offered load and solve the system of equations. If the resultant carried load is the same as the offered load, the offered load can be increased and the next search range will be the upper half of the original one. Otherwise, the offered load results in instability and the next search range will be the lower half of the original one. This procedure is repeated until the search range is sufficiently small.

We consider a network of two parallel links as shown in Fig. 4.2, with d and r representing the length of the links and the link separation respectively. The link separation is defined as the perpendicular distance between the links. We let $L = 8192$ bits, $d = 450$ meters, and $\beta = -70, -75, -78, -80$ dBm to solve for the maximum carried loads and obtain the curves as shown in Figs. 4.3(a)-4.3(d).

Consider the curve corresponding to the carrier sensing threshold of -78 dBm in Fig. 4.3(c), which is a common value used in NS-2 simulation and the practical value used in Orinoco wireless LAN card. The corresponding carrier sensing range is 550 meters, which is in line with the carrier sensing range used in practice. In our model, we assume that carrier sensing works when the separation is within the carrier sensing range and fails otherwise, and use two different sets of equations to model the

system in these situations. Therefore there is an abrupt change in the aggregate throughput when the separation equals the carrier sensing range. If there is no carrier sensing in the system, the aggregate throughput will reduce to zero smoothly when the link separation reduces.

The curve in Fig. 4.3(c) can be divided into three parts according to the link separation r. When $r < 550$ meters, both transmitters are in the carrier sensing range of each other. As a result, at most only one transmitter is active at a time. If $r \geq 550$ meters, the transmitters are unaware of the existence of each other, and they contend for the wireless channel as if there were no interferers nearby. When $r > 800$ meters, the separation is so large that there will not be any interference between the links. When r lies between 550 and 800 meters, the aggregate throughput of the links increases smoothly as r increases. We label this range of r as the *partial interference region*. The existence of this partial interference region suggests that the interference models proposed by [4] that a single threshold can represent the interference relationship in wireless networks may be overly simplified.

The width of this partial interference region depends on the carrier sensing threshold β used. Smaller β, *e.g.*, -80 dBm, results in a narrower partial interference region as in Fig. 4.3(d). Simultaneous transmissions are allowed only for the links separated far enough, and the throughput is suppressed significantly. For larger β, *e.g.*, -75 and -70 dBm, more *spatial reuse* is allowed, and the width of the partial interference region is larger, as shown in Figs. 4.3(a)-4.3(b). However, excessive interference is introduced for larger β, so there is a reduction in the aggregate throughput.

Besides carrier sensing threshold, the length of the links d also affects the partial interference region. We reduce d to be 400 meters, and obtain the results in Figs. 4.4(a)-4.4(d). As shown

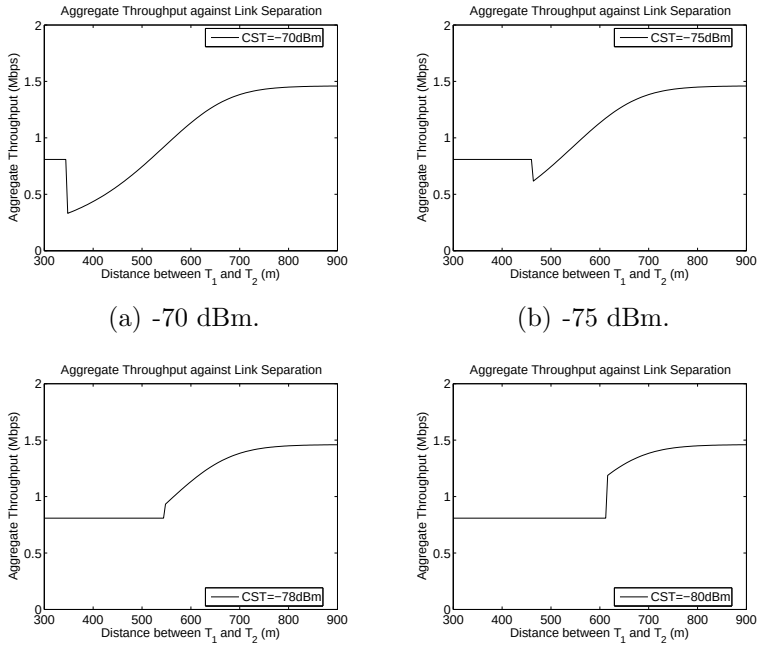

(a) -70 dBm. (b) -75 dBm.

(c) -78 dBm. (d) -80 dBm.

Figure 4.3: Aggregate throughput for the topology in Fig. 4.2 with length of links = 450 meters and various carrier sensing thresholds.

in Figs. 4.4(a)-4.4(d), the partial interference region becomes narrower for all values of carrier sensing threshold. Also, the aggregate throughput achieved by the links is larger for the same link separation when the links are shortened.

4.4 A TDMA/CDMA Analogy

In this Section, we use TDMA, CDMA and Shannon's capacity to establish an analogy to our results in previous Section. Consider the same network as in Fig. 4.2. The bandwidth of the channel is denoted by B. Both transmitters transmit with power P and the background noise power at each receiver is N.

If the links use TDMA as the multiplexing scheme to share the wireless channel, then only one link can be active at a time. So there is no interference, and the SNR at the receiver of each

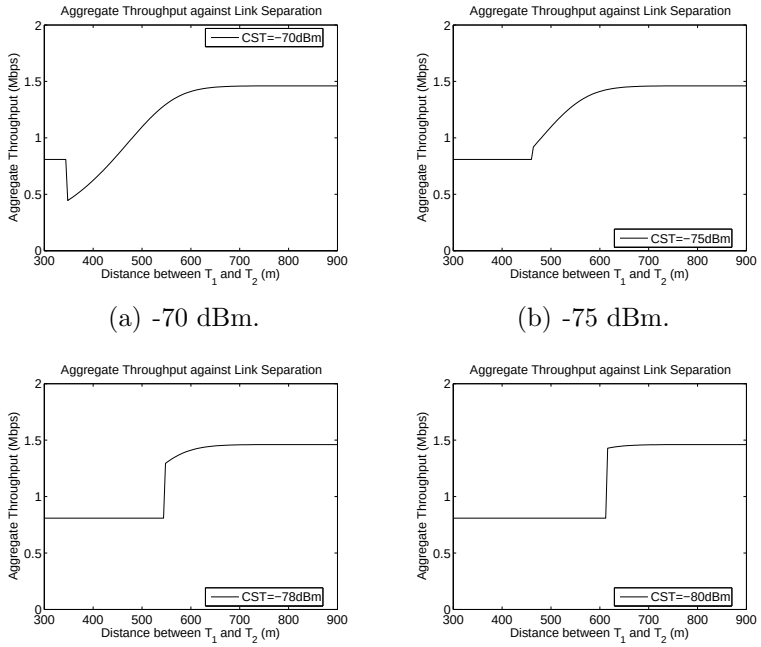

(a) -70 dBm. (b) -75 dBm.

(c) -78 dBm. (d) -80 dBm.

Figure 4.4: Aggregate throughput for the topology in Fig. 4.2 with length of links = 400 meters and various carrier sensing thresholds.

link is $\gamma = \dfrac{PCd^{-\alpha}}{N}$. Then by Shannon's capacity formula [17], the aggregate capacity is

$$\rho_{TDMA} = B \log_2(1 + \gamma).$$

If CDMA is used instead, then the SNR at the receiver of each link will be $\dfrac{PCd^{-\alpha}}{N + PC(d^2 + r^2)^{-\frac{\alpha}{2}}} = \dfrac{1}{\gamma^{-1} + z}$, where $z = \left(\dfrac{d^2}{d^2 + r^2}\right)^{\frac{\alpha}{2}}$. The aggregate capacity is

$$\rho_{CDMA} = 2B \log_2\left(1 + \frac{1}{\gamma^{-1} + z}\right).$$

Fig. 4.5 shows the variation of aggregate capacity against link separation in TDMA and CDMA, normalized by the capacity in TDMA, with $d = 450$ meters. The aggregate capacity

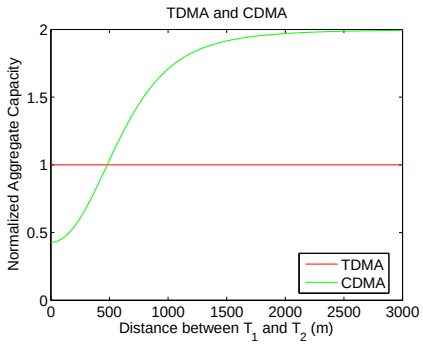

Figure 4.5: A TDMA/CDMA analogy for the results in Section 4.3.

is independent of the link separation in TDMA, and increases smoothly with the link separation in CDMA. There exists a crossover point r_0 such that, when $r < r_0$, TDMA has a higher aggregate capacity, and the opposite occurs otherwise. The notion of setting a carrier sensing threshold or range can be viewed as deciding when to *switch* between TDMA and CDMA: use TDMA when the separation is smaller than the carrier sensing range, use CDMA otherwise. Carrier sensing allows at most one link to be active at a time, so the links within carrier sensing range share the wireless channel like TDMA. Partial interference is analogous to CDMA that the aggregate throughput increases smoothly as the link separation increases. We can obtain the behavior in previous Section by setting the carrier sensing range to be close to r_0, and achieve optimal performance in terms of aggregate capacity by setting the carrier sensing range to be r_0.

4.5 Admissible (Stability) Region

As an attempt to obtain the capacity of 802.11 networks under partial interference, we compute the *admissible (stability) region* predicted from our model. The admissible region includes all flow vectors (λ_1, λ_2) such that if (λ_1, λ_2) is located inside the admissible region, then a flow of λ_n can be allocated on and

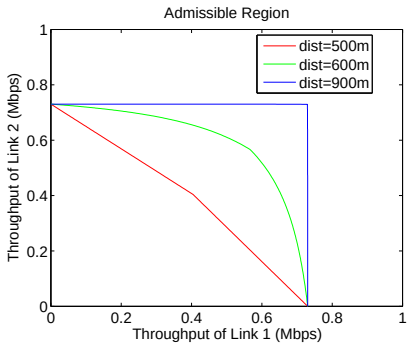

Figure 4.6: Admissible region for various link separations.

achieved by (T_n, R_n), $n = 1, 2$. We use the same settings as above, and choose the carrier sensing threshold to be -78 dBm. The link separations are chosen to be 500, 600 and 900 meters for illustrative purposes, because they correspond to different shapes of the admissible region. Fig. 4.6 shows the admissible region for these three link separations. The link separation of 500 meters represents that the links are in mutual interference, and the admissible region has a triangular shape. When the links are separated by 900 meters, the links do not interfere with each other, and the admissible region is rectangular. For the link separation of 600 meters, partial interference exists and the admissible region becomes convex.

Although we are able to compute the admissible region for a two-link 802.11 network numerically, the closed-form expression for the admissible region is unknown. Also, for an 802.11 network with two links, we have to solve a system of six nonlinear equations to compute the admissible region. When the number of links in the network grows, the number of equations involved will increase and the system of equations will be more difficult to solve. Therefore the computation of the admissible region of general 802.11 networks seems to be forbiddingly intractable.

4.6 Chapter Summary

In this Chapter, we have introduced an analytical framework to characterize partial interference in 802.11 networks. We have also demonstrated that there is a partial interference region, such that when the separation between the links falls in this region, the throughput of each link increases continuously with the link separation. Also, we have computed numerically the stability region of 802.11 networks with two links under partial interference. The computation of the stability region in this case is difficult to generalize when there are more links in the network. Therefore, in next Chapter, we study the stability region of a simpler random access protocol, *i.e.*, slotted ALOHA.

□ **End of chapter.**

Chapter 5

Partial Interference in Slotted ALOHA

5.1 Introduction

In Chapter 4, we attempted to find the stability region of 802.11 networks. When there are two links in the network, we have to solve a system of nonlinear equations. If more links are added to the network, the system of nonlinear equations we need to solve would be increasingly more complicated. Also, the results obtained in Chapter 4 can only be computed numerically but not analytically. From these, the stability region of general 802.11 networks seems to be computationally intractable.

In order to obtain insights in the stability region of general 802.11 networks, in this Chapter, we study the stability of slotted ALOHA, which is a simpler random access protocol, under the assumptions of finite links and infinite buffer. By considering partial interference, for the case of two links, we compute analytically the exact stability region. From this, we observe that there is a *gradual transition* from the collision channel to the orthogonal channel when the link separation increases. The stability region can be either convex or nonconvex, depending on the link separation and the transmission probability vector. A partial characterization on the boundary of the stability re-

gion in *closed form* for the case of general number of links is also given.

5.2 The Finite-Link Slotted ALOHA Model

5.2.1 Assumptions

Let $\mathcal{M} = \{n\}_{n=1}^{M}$ be the set of links in the slotted ALOHA system. Time is slotted. The following assumptions apply to all links $n \in \mathcal{M}$. Let T_n and R_n be the transmitter and the receiver of link n respectively. T_n has an infinite buffer. The packet arrival process at T_n is Bernoulli with mean λ_n and is independent of the arrivals at other transmitters. T_n attempts a *virtual transmission* with probability p_n, *i.e.*, if its buffer is nonempty, T_n attempts an *actual transmission* with probability p_n; otherwise, T_n always remains silent. Also define $\overline{p}_n = 1 - p_n$.

In the system, each time slot is just enough for transmission of one packet. Packets are assumed to have equal lengths. We assume transmission results are independent in each slot. For $n \in \mathcal{A} \subseteq \mathcal{M}$, let $\mathsf{q}_{n,\mathcal{A}}^{\mathcal{M}}$ be the probability that the transmission on link n is successful when $\{T_{n'}\}_{n' \in \mathcal{A}}$ is the set of active transmitters. $\mathsf{q}_{n,\mathcal{A}}^{\mathcal{M}}$ depends on the SNR at the receiver and the modulation scheme used. We also assume the transmitters know immediately the transmission results, so that the transmitters remove successfully transmitted packets and retain only those unsuccessful ones.

5.2.2 Stability of Slotted ALOHA

We let $Q_n(t), t \in \mathbb{N}$ be the queue length in T_n at the beginning of slot t, and use a M-dimensional Markov chain $\mathbf{Q}^{\mathcal{M}}(t) = \big(Q_n(t)\big)_{n \in \mathcal{M}}$ to represent the queue lengths in all transmitters. We denote by $A_n(t)$ the number of packets arrived at T_n in slot t, and $D_n(t)$ the number of packets successfully transmitted in slot

t by T_n when $Q_n(t) > 0$. Then $Q_n(t+1) = [Q_n(t) - D_n(t)]^+ + A_n(t)$, where $[z]^+ = \max\{0, z\}$ is used to account for the case that there is no packet transmitted when $Q_n(t) = 0$. We use the definition of stability in [3, 10, 14].

Definition 5.1. *A M-dimensional stochastic process $\mathbf{Q}^{\mathcal{M}}(t)$ is stable if for $\mathbf{x} \in \mathbb{N}^M$ the following holds:*

$$\lim_{t\to\infty} \Pr\Big\{\mathbf{Q}^{\mathcal{M}}(t) < \mathbf{x}\Big\} = F(\mathbf{x}) \text{ and } \lim_{\mathbf{x}\to\infty} F(\mathbf{x}) = 1.$$

If the following weaker condition holds instead,

$$\lim_{\mathbf{x}\to\infty} \liminf_{t\to\infty} \Pr\Big\{\mathbf{Q}^{\mathcal{M}}(t) < \mathbf{x}\Big\} = 1,$$

then the process is substable. The process is unstable if it is neither stable nor substable.

The stability problem of slotted ALOHA we consider here is to determine whether the slotted ALOHA system with the set of links $\mathcal{M}$ is stable given the parameters $\{\lambda_n\}_{n\in\mathcal{M}}$ and $\{p_n\}_{n\in\mathcal{M}}$. We use the result from [24]: On the assumption that the arrival and the service processes of a queue are stationary, the queue is stable if the average arrival rate is less than the average service rate, and the queue is unstable if the average arrival rate is larger than the average service rate. We also define the slotted ALOHA system to be stable when all queues in the system are stable.

5.3 Stability Region of 2-Link Slotted ALOHA under Partial Interference

We extend the model in [10] to obtain the following results. For $n \in \mathcal{M}$, let P_n and N_n be the transmission power used by T_n and the background noise power at R_n respectively. Assume the signal propagation follows the path loss model $pl(d) = Cd^{-\alpha}$,

where d is the propagation distance, α is the path loss exponent and C is a constant. We let $\gamma_{n,\mathcal{A}}^{\mathcal{M}}$ be the SNR attained at R_n when $\{T_{n'}\}_{n' \in \mathcal{A}}$ is the set of active transmitters. Assume a packet consists of L bits. Let $e(\gamma)$ be the bit error rate when the SNR is γ. In particular, if DBPSK is used in the physical layer, $e(\gamma) = \frac{1}{2}\exp(-\gamma)$. Under binary interference, we let the SNR threshold γ_0 be the case that the packet error rate is ϵ, *i.e.*, $1 - \left[1 - \frac{1}{2}\exp(-\gamma_0)\right]^L = \epsilon$. Consider $M = 2$. When only T_1 is active, the SNR attained at R_1 is $\gamma_{1,\{1\}}^{\mathcal{M}} = \dfrac{P_1 C d_{T_1,R_1}^{-\alpha}}{N_1}$, and

$$\mathsf{q}_{1,\{1\}}^{\mathcal{M}} = \begin{cases} 1, & \gamma_{1,\{1\}}^{\mathcal{M}} \geq \gamma_0 \\ 0, & \gamma_{1,\{1\}}^{\mathcal{M}} < \gamma_0 \end{cases}, \tag{5.1}$$

where $d_{X,Y}$ is the distance between X and Y. When both T_1 and T_2 are active, then $\gamma_{1,\{1,2\}}^{\mathcal{M}} = \dfrac{P_1 C d_{T_1,R_1}^{-\alpha}}{P_2 C d_{T_2,R_1}^{-\alpha} + N_1}$ is the SNR attained at R_1, and

$$\mathsf{q}_{1,\{1,2\}}^{\mathcal{M}} = \begin{cases} 1, & \gamma_{1,\{1,2\}}^{\mathcal{M}} \geq \gamma_0 \\ 0, & \gamma_{1,\{1,2\}}^{\mathcal{M}} < \gamma_0 \end{cases}. \tag{5.2}$$

If we consider partial interference instead, we can calculate $\mathsf{q}_{n,\mathcal{A}}^{\mathcal{M}}$ as follows. When only T_1 is active,

$$\mathsf{q}_{1,\{1\}}^{\mathcal{M}} = \left[1 - e\left(\gamma_{1,\{1\}}^{\mathcal{M}}\right)\right]^L. \tag{5.3}$$

When both T_1 and T_2 are active,

$$\mathsf{q}_{1,\{1,2\}}^{\mathcal{M}} = \left[1 - e\left(\gamma_{1,\{1,2\}}^{\mathcal{M}}\right)\right]^L. \tag{5.4}$$

Similarly, we can derive expressions for $\mathsf{q}_{2,\{2\}}^{\mathcal{M}}$ and $\mathsf{q}_{2,\{1,2\}}^{\mathcal{M}}$ under binary and partial interference.

To evaluate the boundary of the stability region for the 2-link slotted ALOHA system, we use stochastic dominance as introduced in [2]. We use $\mathsf{S}_{\mathcal{P}}$ to represent a *dominant system* of the original system S, with $\mathcal{P}$ being the *persistent* set. The transmitters of the links in this set transmit dummy packets when they decide to transmit but do not have packets queued in their buffer. The remaining transmitters behave identically as those in S. We first consider the dominant system $\mathsf{S}_{\{1\}}$. In this dominant system, the successful transmission probability of link 2 is $p_2\overline{p}_1\mathsf{q}^{\mathcal{M}}_{2,\{2\}} + p_2p_1\mathsf{q}^{\mathcal{M}}_{2,\{1,2\}}$. For link 1, the queue in T_2 is empty with probability $1 - \dfrac{\lambda_2}{p_2\overline{p}_1\mathsf{q}^{\mathcal{M}}_{2,\{2\}} + p_2p_1\mathsf{q}^{\mathcal{M}}_{2,\{1,2\}}}$, in this case the successful transmission probability is $p_1\mathsf{q}^{\mathcal{M}}_{1,\{1\}}$; otherwise, the successful transmission probability is $p_1\overline{p}_2\mathsf{q}^{\mathcal{M}}_{1,\{1\}} + p_1p_2\mathsf{q}^{\mathcal{M}}_{1,\{1,2\}}$. Hence, the average successful transmission probability of link 1 is

$$p_1\mathsf{q}^{\mathcal{M}}_{1,\{1\}}\left(1 - \frac{\lambda_2}{p_2\overline{p}_1\mathsf{q}^{\mathcal{M}}_{2,\{2\}} + p_2p_1\mathsf{q}^{\mathcal{M}}_{2,\{1,2\}}}\right) + \left(p_1\overline{p}_2\mathsf{q}^{\mathcal{M}}_{1,\{1\}} + p_1p_2\mathsf{q}^{\mathcal{M}}_{1,\{1,2\}}\right)\frac{\lambda_2}{p_2\overline{p}_1\mathsf{q}^{\mathcal{M}}_{2,\{2\}} + p_2p_1\mathsf{q}^{\mathcal{M}}_{2,\{1,2\}}}$$

With the following notations,

$$\lambda'_1 = p_1\overline{p}_2\mathsf{q}^{\mathcal{M}}_{1,\{1\}} + p_1p_2\mathsf{q}^{\mathcal{M}}_{1,\{1,2\}}, \mathsf{Q}^{\mathcal{M}}_{1,\{1\},\{2\}} = \mathsf{q}^{\mathcal{M}}_{1,\{1\}} - \mathsf{q}^{\mathcal{M}}_{1,\{1,2\}},$$
$$\lambda'_2 = p_2\overline{p}_1\mathsf{q}^{\mathcal{M}}_{2,\{2\}} + p_2p_1\mathsf{q}^{\mathcal{M}}_{2,\{1,2\}}, \mathsf{Q}^{\mathcal{M}}_{2,\{2\},\{1\}} = \mathsf{q}^{\mathcal{M}}_{2,\{2\}} - \mathsf{q}^{\mathcal{M}}_{2,\{1,2\}},$$

the stability region of $\mathsf{S}_{\{1\}}$ is

$$\lambda_1 < p_1\mathsf{q}^{\mathcal{M}}_{1,\{1\}} - \frac{\lambda_2p_2p_1\mathsf{Q}^{\mathcal{M}}_{1,\{1\},\{2\}}}{\lambda'_2} \text{ and } \lambda_2 < \lambda'_2, \tag{5.5}$$

and by symmetry, the stability region of $\mathsf{S}_{\{2\}}$ is

$$\lambda_2 < p_2\mathsf{q}^{\mathcal{M}}_{2,\{2\}} - \frac{\lambda_1p_1p_2\mathsf{Q}^{\mathcal{M}}_{2,\{2\},\{1\}}}{\lambda'_1} \text{ and } \lambda_1 < \lambda'_1. \tag{5.6}$$

Table 5.1: Parameters used for the analytical results of slotted ALOHA.

P_1, P_2	24.5 dBm	N_1, N_2	-88 dBm
G_T, G_R	1	h_T, h_R	1.5 m
ϵ	0.001	d_{T_1,R_1}, d_{T_2,R_2}	450 m

The union of these two regions constitutes the inner bound on the stability region of the original system S.

The reason for the union of these two regions to be the outer bound on the stability region follows from the indistinguishability argument [2, 10]. Consider the dominant system $\mathsf{S}_{\{1\}}$. With a particular initial condition on the length of the queues, if the queue in T_1 is unstable, it is equivalent to the case that the queue in T_1 never empties with nonzero probability. Then $\mathsf{S}_{\{1\}}$ and S will be indistinguishable, in the sense that the packets transmitted from T_1 in $\mathsf{S}_{\{1\}}$ are always real packets, and S is also unstable. Therefore, the union of the regions defined by (5.5) and (5.6) is the *exact* stability region for $M = 2$.

5.4 Some Illustrations

In this Section, we depict the stability region derived in previous Section by considering the parallel-link topology in Fig. 5.1. We use the two-ray ground reflection model

$$pl(d) = \frac{G_T G_R h_T^2 h_R^2}{d^4}$$

to represent the path loss as in Chapter 3. The values of various parameters are shown in Table 5.1.

We first assume $L = 8192$ bits, $p_1 = p_2 = 0.8$ and vary the link separation, *i.e.*, the perpendicular distance between the links, to obtain the results under binary interference in Fig. 5.2(a). The stability region has only two possible shapes. For the separations of 600, 800 and 1000 meters, the SNR attained

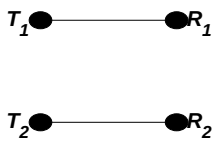

Figure 5.1: A sample topology.

at either receiver when both transmitters are active is smaller than the threshold. Therefore the underlying channel follows the collision channel model and the stability region is nonconvex. When the separation is 1200 meters, the links are separated far enough so that transmissions on both links are independent. The channel can be regarded as the orthogonal channel and the stability region is convex. Therefore, the threshold in binary interference determines when to *switch* between the collision channel and the orthogonal channel.

Fig. 5.2(b) shows the corresponding results under partial interference. When the link separation is small, the amount of interference is so large that partial interference degenerates to the collision channel. As the link separation increases, the stability region expands gradually and changes from nonconvex to convex. At another extreme, when the links are sufficiently far apart, partial interference is identical to the orthogonal channel. Therefore, partial interference can be viewed as a generalization of binary interference that it *interpolates* the transition from the collision channel to the orthogonal channel. Notice that the results here are similar to the case considered in Chapter 4, therefore our results should be applicable to networks with practical random access protocols like 802.11.

Next, we assume the links are separated by 800 meters. We let both links transmit with probability p, and illustrate the effect of p on the convexity of the stability region under binary interference in Fig. 5.3(a). When p is small, *i.e.*, 0.2 and 0.4, the links are too conservative in attempting transmissions. It

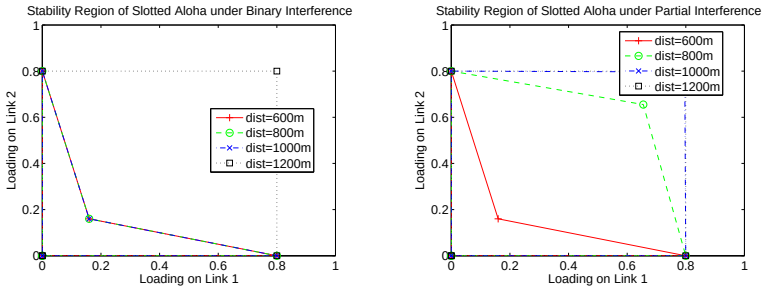

(a) binary interference. (b) partial interference.

Figure 5.2: Stability region for $M = 2$ with transmission probabilities 0.8 under binary and partial interference.

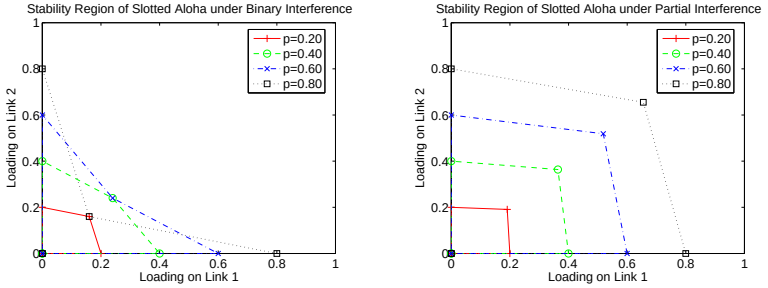

(a) binary interference. (b) partial interference.

Figure 5.3: Stability region for $M = 2$ with link separation 800 meters under binary and partial interference.

leads to better channel utilization by adding one more link to the system, and the stability region is convex. On the other hand, when p is large, *i.e.*, 0.6 and 0.8, the links are too aggressive. When one more link is added to the system, it increases contention and hence reduces the loading supported by each link drastically. As a result, the stability region is nonconvex. The convexity of the stability region can therefore be regarded as a measure of the contention level in a network.

Fig. 5.3(b) illustrates the stability region when partial interference is considered instead, under the same settings. Although the SNR attained at a receiver when both transmitters are active is smaller than the threshold, the SNR is large enough to support a sustainable throughput probabilistically. Therefore, it is

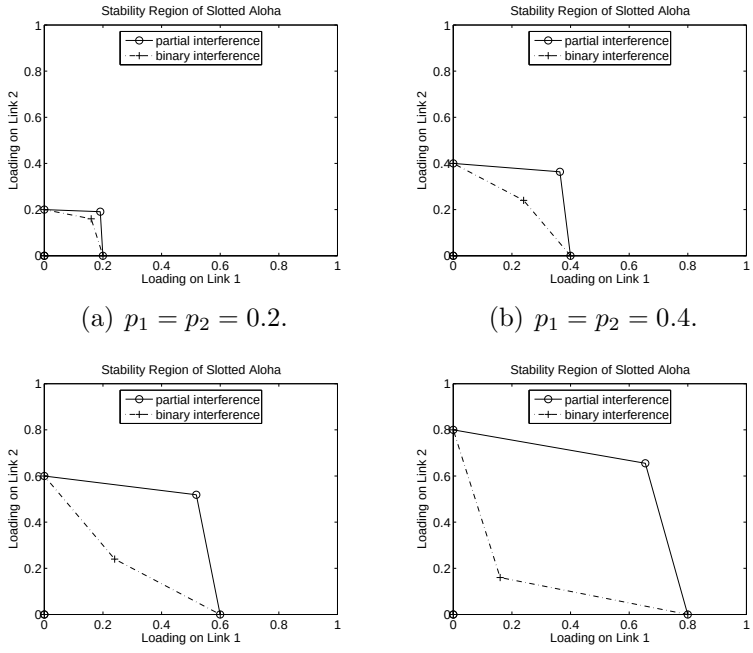

(a) $p_1 = p_2 = 0.2$. (b) $p_1 = p_2 = 0.4$.

(c) $p_1 = p_2 = 0.6$. (d) $p_1 = p_2 = 0.8$.

Figure 5.4: Stability region for $M = 2$ under binary interference and partial interference with various transmission probabilities.

possible to receive more packets opportunistically by exploiting partial interference, thereby increasing the loading supported by each link and allowing the stability region to be convex. If we compare the stability region under binary and partial interference in identical settings, as shown in Figs. 5.4(a)-5.4(d), the stability region under partial interference is always larger than that under binary interference. This implies that by considering partial interference, more combinations of flows on the links can be admitted, and the capacity of a wireless network can be potentially increased.

5.5 Generalization to the M-Link Case

In this Section, we give in closed form a partial characterization on the boundary of the stability region of M-link slotted

ALOHA under partial interference. First, for $n \in \mathcal{A} \subseteq \mathcal{M}$, $\gamma_{n,\mathcal{A}}^{\mathcal{M}} = \dfrac{P_n C d_{T_n,R_n}^{-\alpha}}{\sum\limits_{n' \in \mathcal{A}\setminus\{n\}} P_{n'} C d_{T_{n'},R_n}^{-\alpha} + N_n}$. Therefore, under binary interference,

$$\mathsf{q}_{n,\mathcal{A}}^{\mathcal{M}} = \begin{cases} 1, & \gamma_{n,\mathcal{A}}^{\mathcal{M}} \geq \gamma_0 \\ 0, & \gamma_{n,\mathcal{A}}^{\mathcal{M}} < \gamma_0 \end{cases}, \tag{5.7}$$

while under partial interference,

$$\mathsf{q}_{n,\mathcal{A}}^{\mathcal{M}} = \left[1 - e\left(\gamma_{n,\mathcal{A}}^{\mathcal{M}}\right)\right]^L. \tag{5.8}$$

For each $\mathcal{M}' \subseteq \mathcal{M}$, let $\mathsf{p}^{\mathcal{M}}(\mathcal{M}') = \left(\mathsf{p}_n^{\mathcal{M}}(\mathcal{M}')\right)_{n\in\mathcal{M}}$ be a M-dimensional 0-1 vector such that

$$\mathsf{p}_n^{\mathcal{M}}(\mathcal{M}') = \begin{cases} 1, & n \in \mathcal{M}' \\ 0, & n \notin \mathcal{M}' \end{cases},$$

where $\mathcal{M}'$ is a set of persistent links and all other links are empty. Define $\Pi^{\mathsf{p}^{\mathcal{M}}(\mathcal{M}')} = \left(\Pi_n^{\mathsf{p}^{\mathcal{M}}(\mathcal{M}')}\right)_{n\in\mathcal{M}}$, where

$$\Pi_n^{\mathsf{p}^{\mathcal{M}}(\mathcal{M}')} = \sum_{\mathcal{A}:\, n\in\mathcal{A}\subseteq\mathcal{M}'} \prod_{n'\in\mathcal{A}} p_{n'} \prod_{n''\in\mathcal{M}'\setminus\mathcal{A}} \overline{p}_{n''} \mathsf{q}_{n,\mathcal{A}}^{\mathcal{M}}, \tag{5.9}$$

to be a *corner point* corresponding to the case that $\mathcal{M}'$ is the set of persistent links. Notice RHS of (5.9) is zero when $n \notin \mathcal{M}'$. Then we obtain the following Theorem.

Theorem 5.1. *All corner points lie on the boundary of the stability region.*

Proof. When $\mathcal{M}' = \emptyset$, (5.9) becomes $\Pi^{\mathsf{p}^{\mathcal{M}}(\mathcal{M}')} = \mathbf{0}$, which is obviously on the boundary. If $\mathcal{M}' \neq \emptyset$, each link $n \in \mathcal{M}'$ operates as *M/M/1*. If at a certain instant, only the links in $\mathcal{A} \subseteq \mathcal{M}'$ are active, which occurs with probability $\prod\limits_{n'\in\mathcal{A}} p_{n'} \prod\limits_{n''\in\mathcal{M}'\setminus\mathcal{A}} \overline{p}_{n''}$, the

probability of successful transmission of link n is $\mathsf{q}^{\mathcal{M}}_{n,\mathcal{A}}$. Therefore, by unconditioning on $\mathcal{A}$ while noticing $\mathsf{q}^{\mathcal{M}}_{n,\mathcal{A}} = 0$ if $n \notin \mathcal{A}$, the successful transmission probability of link n is

$$\sum_{\mathcal{A}\colon\, n\in\mathcal{A}\subseteq\mathcal{M}'} \prod_{n'\in\mathcal{A}} p_{n'} \prod_{n''\in\mathcal{M}'\setminus\mathcal{A}} \overline{p}_{n''} \mathsf{q}^{\mathcal{M}}_{n,\mathcal{A}}.$$

Therefore $\Pi^{\mathsf{p}^{\mathcal{M}}(\mathcal{M}')}$ lies on the boundary. □

By using stochastic dominance and the indistinguishability argument, we obtain the following Theorem.

Theorem 5.2. *Let $\Pi^{\mathsf{p}^{\mathcal{M}}(\mathcal{P})}, \Pi^{\mathsf{p}^{\mathcal{M}}(\mathcal{P}\cup\mathcal{D})}$ be two corner points such that $\mathcal{D} = \{\bar{n}\} \subseteq \mathcal{M} \setminus \mathcal{P}$. Then the line segment joining these two points lies on the boundary of the stability region. This line segment represents the case that $\mathcal{P}$ is the set of persistent links while $\bar{n}$ is the only non-empty non-persistent link in the system.*

Proof. When $|\mathcal{P}| = 0$, it is trivial that the line segment between $\Pi^{\mathsf{p}^{\mathcal{M}}(\mathcal{P})}$ and $\Pi^{\mathsf{p}^{\mathcal{M}}(\mathcal{P}\cup\mathcal{D})}$ lies on the boundary because it is part of the positive $\lambda_{\bar{n}}$-axis. Assume $|\mathcal{P}| > 0$. We prove

$$\begin{aligned}
&\lambda_{\bar{n}} < \lambda'_{\bar{n}}, \bar{n} \in \mathcal{D},\\
&\lambda_n < \sum_{\mathcal{A}\colon\, n\in\mathcal{A}\subseteq\mathcal{P}} \prod_{n'\in\mathcal{A}} p_{n'} \prod_{n''\in\mathcal{P}\setminus\mathcal{A}} \overline{p}_{n''} \mathsf{q}^{\mathcal{M}}_{n,\mathcal{A}}\\
&\qquad -\frac{\lambda_{\bar{n}}}{\lambda'_{\bar{n}}} p_{\bar{n}} \sum_{\mathcal{A}\colon\, n\in\mathcal{A}\subseteq\mathcal{P}} \prod_{n'\in\mathcal{A}} p_{n'} \prod_{n''\in\mathcal{P}\setminus\mathcal{A}} \overline{p}_{n''} \mathsf{Q}^{\mathcal{M}}_{n,\mathcal{A},\mathcal{D}}, n \in \mathcal{P},\\
&\lambda_{\tilde{n}} = 0, \tilde{n} \in \mathcal{M} \setminus (\mathcal{P} \cup \mathcal{D})
\end{aligned} \tag{5.10}$$

with

$$\begin{aligned}
\lambda'_{\bar{n}} &= \sum_{\mathcal{A}\colon\, \bar{n}\in\mathcal{A}\subseteq(\mathcal{P}\cup\mathcal{D})} \prod_{n'\in\mathcal{A}} p_{n'} \prod_{n''\in(\mathcal{P}\cup\mathcal{D})\setminus\mathcal{A}} \overline{p}_{n''} \mathsf{q}^{\mathcal{M}}_{\bar{n},\mathcal{A}},\\
\mathsf{Q}^{\mathcal{M}}_{n,\mathcal{A},\mathcal{D}} &= \mathsf{q}^{\mathcal{M}}_{n,\mathcal{A}} - \mathsf{q}^{\mathcal{M}}_{n,\mathcal{A}\cup\mathcal{D}}, \mathcal{A}\colon\, n \in \mathcal{A} \subseteq \mathcal{P}.
\end{aligned}$$

lies on the boundary of the stability region. For any $\tilde{n} \notin \mathcal{P} \cup \mathcal{D}$, $T_{\tilde{n}}$ has no packet, hence $\lambda_{\tilde{n}} = 0$. Therefore we consider the

dominant system $\mathsf{S}_{\mathcal{P}}$, assuming the system contains only the links in $\mathcal{P} \cup \mathcal{D}$. For the sufficiency part, the queue in $T_{\bar{n}}$ in $\mathsf{S}_{\mathcal{P}}$ is stable if

$$\begin{aligned}\lambda_{\bar{n}} &< p_{\bar{n}} \sum_{\mathcal{A} \subseteq \mathcal{P}} \prod_{n' \in \mathcal{A}} p_{n'} \prod_{n'' \in \mathcal{P} \setminus \mathcal{A}} \overline{p}_{n''} \mathsf{q}^{\mathcal{M}}_{\bar{n}, \mathcal{A} \cup \mathcal{D}} \\ &= \sum_{\mathcal{A}\colon\, \bar{n} \in \mathcal{A} \subseteq (\mathcal{P} \cup \mathcal{D})} \prod_{n' \in \mathcal{A}} p_{n'} \prod_{n'' \in (\mathcal{P} \cup \mathcal{D}) \setminus \mathcal{A}} \overline{p}_{n''} \mathsf{q}^{\mathcal{M}}_{\bar{n}, \mathcal{A}} = \lambda'_{\bar{n}}\end{aligned}$$

For any $n \in \mathcal{P}$, the queue in T_n in $\mathsf{S}_{\mathcal{P}}$ is stable if

$$\begin{aligned}\lambda_n &< \left(1 - \frac{\lambda_{\bar{n}}}{\lambda'_{\bar{n}}}\right) \sum_{\mathcal{A}\colon\, n \in \mathcal{A} \subseteq \mathcal{P}} \prod_{n' \in \mathcal{A}} p_{n'} \prod_{n'' \in \mathcal{P} \setminus \mathcal{A}} \overline{p}_{n''} \mathsf{q}^{\mathcal{M}}_{n, \mathcal{A}} \\ &\quad + \frac{\lambda_{\bar{n}}}{\lambda'_{\bar{n}}} \sum_{\mathcal{A}\colon\, n \in \mathcal{A} \subseteq (\mathcal{P} \cup \mathcal{D})} \prod_{n' \in \mathcal{A}} p_{n'} \prod_{n'' \in (\mathcal{P} \cup \mathcal{D}) \setminus \mathcal{A}} \overline{p}_{n''} \mathsf{q}^{\mathcal{M}}_{n, \mathcal{A}} \\ &= \left(1 - \frac{\lambda_{\bar{n}}}{\lambda'_{\bar{n}}}\right) \sum_{\mathcal{A}\colon\, n \in \mathcal{A} \subseteq \mathcal{P}} \prod_{n' \in \mathcal{A}} p_{n'} \prod_{n'' \in \mathcal{P} \setminus \mathcal{A}} \overline{p}_{n''} \mathsf{q}^{\mathcal{M}}_{n, \mathcal{A}} \\ &\quad + \frac{\lambda_{\bar{n}}}{\lambda'_{\bar{n}}} \Bigg(\overline{p}_{\bar{n}} \sum_{\mathcal{A}\colon\, n \in \mathcal{A} \subseteq \mathcal{P}} \prod_{n' \in \mathcal{A}} p_{n'} \prod_{n'' \in \mathcal{P} \setminus \mathcal{A}} \overline{p}_{n''} \mathsf{q}^{\mathcal{M}}_{n, \mathcal{A}} \\ &\quad + p_{\bar{n}} \sum_{\mathcal{A}\colon\, n \in \mathcal{A} \subseteq \mathcal{P}} \prod_{n' \in \mathcal{A}} p_{n'} \prod_{n'' \in \mathcal{P} \setminus \mathcal{A}} \overline{p}_{n''} \mathsf{q}^{\mathcal{M}}_{n, \mathcal{A} \cup \mathcal{D}} \Bigg) \\ &= \sum_{\mathcal{A}\colon\, n \in \mathcal{A} \subseteq \mathcal{P}} \prod_{n' \in \mathcal{A}} p_{n'} \prod_{n'' \in \mathcal{P} \setminus \mathcal{A}} \overline{p}_{n''} \mathsf{q}^{\mathcal{M}}_{n, \mathcal{A}} \\ &\quad - \frac{\lambda_{\bar{n}}}{\lambda'_{\bar{n}}} p_{\bar{n}} \sum_{\mathcal{A}\colon\, n \in \mathcal{A} \subseteq \mathcal{P}} \prod_{n' \in \mathcal{A}} p_{n'} \prod_{n'' \in \mathcal{P} \setminus \mathcal{A}} \overline{p}_{n''} \mathsf{Q}^{\mathcal{M}}_{n, \mathcal{A}, \mathcal{D}}\end{aligned}$$

The necessity follows directly from the indistinguishability argument. We observe that λ_n varies linearly with $\lambda_{\bar{n}}$ on the boundary, $\forall n \notin \mathcal{D}$. It is trivial that $\lambda_{\bar{n}} = 0$ and $\lambda_{\bar{n}} = \lambda'_{\bar{n}}$ correspond to $\Pi^{\mathsf{p}^{\mathcal{M}}(\mathcal{P})}$ and $\Pi^{\mathsf{p}^{\mathcal{M}}(\mathcal{P} \cup \mathcal{D})}$ respectively. □

We illustrate the results of these Theorems by considering

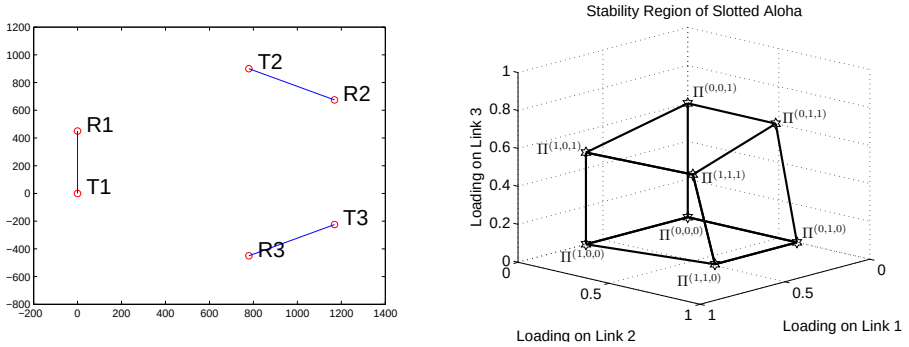

(a) A sample topology. (b) Part of the exact boundary.

Figure 5.5: Stability region with $M = 3$.

$M = 3$ with the ring topology in Fig. 5.5(a). The distance between a receiver and the nearest interfering transmitter is 900 meters. Each link transmits with probability 0.6. Other parameters are the same as in Table 5.1. From Theorem 5.1, each of the eight 3-dimensional 0-1 vector corresponds to a corner point shown in Fig. 5.5(b), and their coordinates can be obtained from (5.9). By Theorem 5.2, the solid lines in Fig. 5.5(b) are part of the boundary of the stability region. As another example, for $M = 2$, notice that (5.5) and (5.6) are special cases of (5.10). As a direct consequence of our Theorems 5.1 and 5.2, the stability region of slotted ALOHA with two links under partial interference is piecewise linear.

Theorems 5.1 and 5.2 cover all cases with zero or one non-empty non-persistent link in the system respectively. However, if there are at least two non-empty non-persistent links, the stationary joint queue statistics must be involved in calculating the boundary. Hence, the results here are the best we can obtain without the stationary joint queue statistics. Unless we are able to compute the stationary joint queue statistics in closed-form, we are unable to solve the capacity-finding problem, even assuming the simplest random access protocol, *i.e.*, slotted ALOHA.

5.6 Chapter Summary

We have studied the stability problem of finite-link infinite-buffer slotted ALOHA and derived the exact stability region when there are two links in the network under partial interference. We illustrated that under partial interference, there is one common property for the stability regions of 802.11 and slotted ALOHA: the stability region expands gradually as the separation between the links increases. When there are more than two links in the network, we only obtained part of the boundary of the stability region. Even for the case of collision channel, we still cannot obtain the exact stability region, because it involves the stationary joint queue statistics which do not have closed form to date. Therefore, for both 802.11 and slotted ALOHA, we cannot analytically establish the boundary of the stability region.

□ **End of chapter.**

Chapter 6

FRASA

6.1 Introduction

In previous two Chapters, we attempted to find the boundary of the stability regions of 802.11 and slotted ALOHA networks respectively. However, there is only limited success for both tasks. For 802.11, the boundary of the stability region is computed numerically; while for slotted ALOHA, only part of the boundary can be obtained analytically. Therefore, instead of finding an analytically tractable boundary of the stability region of wireless random access networks, we have to resort to approximation.

In this Chapter, we propose FRASA, *Feedback Retransmission Approximation for Slotted ALOHA*, to study the stability region of finite-link slotted ALOHA under collision channel. With FRASA, we derive in *closed form* the boundary of the stability region for *any* number of links in the system. The result derived from FRASA is identical to the analytical result of finite-link slotted ALOHA when there are two links in the system. Simulation shows that the stability region obtained from FRASA is a good *approximation* to the stability region of finite-link slotted ALOHA. FRASA also has a wider range of applicability than the bounds derived in previous researches. We provide a *convex hull bound*, which is convex, piecewise linear and

outer-bounds the stability region of FRASA. This bound can be computed by using the transmission probability vector only. We also characterize **p**-*convexity*, an essential property that the stability region of FRASA should have to ensure the convex hull bound to be close to the boundary. From this, we derive that the stability region of FRASA can never be convex when there are more than two links in the system. A convex and piecewise linear inner bound on the stability region of FRASA, called the *supporting hyperplane bound*, is also given. Furthermore, we extend the results of FRASA to include other interference models like binary and partial interference. The analytical findings with FRASA can also provide more insights on the characterization of the capacity region of other types of wireless random access networks.

6.2 The FRASA Model

In slotted ALOHA, there is a queue of infinite buffer at each transmitter. Packet arrivals are assumed to be Bernoulli. When a packet arrives, it joins the end of the queue. The head-of-line packet is transmitted when the transmitter decides to transmit, and it remains at head-of-line until it is successfully transmitted. This is depicted in the upper part of Fig. 6.1.

Due to the complexity introduced by the queues, we propose FRASA, *Feedback Retransmission Approximation for Slotted ALOHA*, as a surrogate to approximate finite-link slotted ALOHA. In FRASA, the buffer in each transmitter can hold one packet only. Whenever there is a packet in the buffer, if the transmitter decides not to transmit the packet, or the transmitter cannot successfully transmit the packet due to collision, the packet will be removed from the buffer and put back in the buffer again after a random delay which is geometrically distributed. Therefore, the *aggregate arrival* of packets to the buffer, which

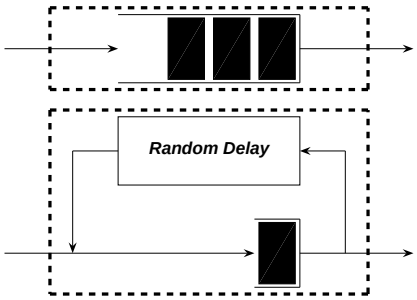

Figure 6.1: Slotted ALOHA model: (Upper) Original; (Lower) FRASA.

is defined as the sum of the new arrivals and the retransmissions, is assumed to be Bernoulli or memoryless. Similar approximation was introduced by [25]. FRASA is shown in the lower part of Fig. 6.1.

Assume there are M links in the network, and the set of links is denoted by $\mathcal{M} = \{n\}_{n=1}^{M}$. Denote this FRASA system by $\overline{\mathsf{S}}$. Let $\mathbf{p} = (p_n)_{n\in\mathcal{M}}$ be the transmission probability vector. Define $\overline{p}_n = 1 - p_n$ for all $n \in \mathcal{M}$. We first consider a *reduced FRASA system*, in which we let $M - 1$ of the links have fixed aggregate arrival rates and the remaining link is assumed with infinite backlog. Take $\hat{n} \in \mathcal{M}$ to be the link with infinite backlog and denote this reduced FRASA system by $\overline{\mathsf{S}}_{\hat{n}}$. Let χ_n be the aggregate arrival rate of link $n \in \mathcal{M} \setminus \{\hat{n}\}$ where χ_n is between zero and one. Hence, link $\hat{n}$ is active with probability $p_{\hat{n}}$, while for $n \neq \hat{n}$, link n is active with probability $\chi_n p_n$. Therefore, $\overline{\boldsymbol{\lambda}} = \left(\overline{\lambda}_n\right)_{n\in\mathcal{M}}$ is the successful transmission probability vector and

$$\overline{\lambda}_n = \begin{cases} \chi_n p_n (1 - p_{\hat{n}}) \displaystyle\prod_{n'\in\mathcal{M}\setminus\{n,\hat{n}\}} (1 - \chi_{n'} p_{n'}), & n \neq \hat{n} \\ p_{\hat{n}} \displaystyle\prod_{n'\in\mathcal{M}\setminus\{\hat{n}\}} (1 - \chi_{n'} p_{n'}), & n = \hat{n} \end{cases}, \tag{6.1}$$

with $\overline{\lambda}_{\hat{n}} > 0$. We use the results from [24] to determine when $\overline{\mathsf{S}}_{\hat{n}}$ is stable as in Chapter 5: on the assumption that the arrival

and the service processes of a queue are stationary, the queue is stable if the average arrival rate is less than the average service rate, and the queue is unstable if the average arrival rate is larger than the average service rate. Then, $\lambda_n = \overline{\lambda}_n, \forall n \in \mathcal{M}$ is the *parametric form* of the boundary of the stability region of $\overline{\mathsf{S}}_{\hat{n}}$. We can obtain a non-parametric version by using (6.1) as follows.

Lemma 6.1. *Consider* $\overline{\mathsf{S}}_{\hat{n}}$. *When*

$$\frac{\lambda_{\hat{n}}(1-p_{\hat{n}})}{p_{\hat{n}}} \geq \frac{\lambda_n(1-p_n)}{p_n} \geq 0 \tag{6.2}$$

is satisfied for all $n \in \mathcal{M} \setminus \{\hat{n}\}$, *the hypersurface* $\mathsf{F}_{\hat{n}}$, *i.e.,*

$$\prod_{n' \in \mathcal{M}} [\lambda_{\hat{n}}(1-p_{\hat{n}}) + \lambda_{n'} p_{\hat{n}}] = p_{\hat{n}}[\lambda_{\hat{n}}(1-p_{\hat{n}})]^{M-1} \tag{6.3}$$

is the non-parametric form of the boundary of the stability region of $\overline{\mathsf{S}}_{\hat{n}}$.

Proof. Starting from the parametric form (6.1), for $n \in \mathcal{M}\setminus\{\hat{n}\}$,

$$\begin{aligned}\frac{\lambda_n}{\lambda_{\hat{n}}} &= \frac{\chi_n p_n (1-p_{\hat{n}}) \displaystyle\prod_{n' \in \mathcal{M}\setminus\{n,\hat{n}\}} (1-\chi_{n'}p_{n'})}{p_{\hat{n}} \displaystyle\prod_{n' \in \mathcal{M}\setminus\{\hat{n}\}} (1-\chi_{n'}p_{n'})} \\ &= \frac{\chi_n p_n (1-p_{\hat{n}})}{p_{\hat{n}}(1-\chi_n p_n)}\end{aligned}$$

Therefore,

$$\chi_n = \frac{\lambda_n p_{\hat{n}}}{\lambda_{\hat{n}}(1-p_{\hat{n}})p_n + \lambda_n p_{\hat{n}} p_n}$$

and the condition $0 \leq \chi_n \leq 1$ is translated into

$$\frac{\lambda_{\hat{n}}(1-p_{\hat{n}})}{p_{\hat{n}}} \geq \frac{\lambda_n(1-p_n)}{p_n} \geq 0.$$

Combining these results,

$$\begin{aligned}\lambda_{\hat{n}} &= p_{\hat{n}} \prod_{n' \in \mathcal{M} \setminus \{\hat{n}\}} (1 - \chi_{n'} p_{n'}) \\ &= p_{\hat{n}} \prod_{n' \in \mathcal{M} \setminus \{\hat{n}\}} \left[1 - \frac{\lambda_{n'} p_{\hat{n}} p_{n'}}{\lambda_{\hat{n}}(1 - p_{\hat{n}}) p_{n'} + \lambda_{n'} p_{\hat{n}} p_{n'}} \right] \\ &= p_{\hat{n}} \prod_{n' \in \mathcal{M} \setminus \{\hat{n}\}} \frac{\lambda_{\hat{n}}(1 - p_{\hat{n}})}{\lambda_{\hat{n}}(1 - p_{\hat{n}}) + \lambda_{n'} p_{\hat{n}}},\end{aligned}$$

we obtain

$$\prod_{n' \in \mathcal{M}} [\lambda_{\hat{n}}(1 - p_{\hat{n}}) + \lambda_{n'} p_{\hat{n}}] = p_{\hat{n}} [\lambda_{\hat{n}}(1 - p_{\hat{n}})]^{M-1}$$

as the boundary of the stability region of $\overline{\mathsf{S}}_{\hat{n}}$. □

Recall the system is stable if all queues in the system are stable [3, 10, 14], and notice the expression $\frac{\lambda_n(1-p_n)}{p_n}$ in (6.2) is identical to the *instability rank* introduced in [3]. When $\max_{n \in \mathcal{M}} \frac{\lambda_n(1-p_n)}{p_n} = \frac{\lambda_{\hat{n}}(1-p_{\hat{n}})}{p_{\hat{n}}}$ holds as in (6.2), link $\hat{n}$ is the most probable one to be the first unstable link. Hence, we let link $\hat{n}$ to be infinitely backlogged and use Lemma 6.1 to obtain the stability region of FRASA as in the following Theorem.

Theorem 6.1. $\overline{\mathcal{R}} = \bigcup_{\hat{n} \in \mathcal{M}} \overline{\mathcal{R}}_{\hat{n}}$ *is the stability region of FRASA, where* $\overline{\mathcal{R}}_{\hat{n}}$ *is represented by:*

$$\frac{\lambda_{\hat{n}}(1 - p_{\hat{n}})}{p_{\hat{n}}} \geq \frac{\lambda_n(1 - p_n)}{p_n} \geq 0, \forall n \in \mathcal{M} \setminus \{\hat{n}\}, \tag{6.4}$$

$$\prod_{n' \in \mathcal{M}} [\lambda_{\hat{n}}(1 - p_{\hat{n}}) + \lambda_{n'} p_{\hat{n}}] < p_{\hat{n}} [\lambda_{\hat{n}}(1 - p_{\hat{n}})]^{M-1}. \tag{6.5}$$

The union here is actually a disjoint union.

Proof. By (6.4), the positive orthant is partitioned into M regions. In the region that $\max_{n\in\mathcal{M}} \frac{\lambda_n(1-p_n)}{p_n} = \frac{\lambda_{\hat{n}}(1-p_{\hat{n}})}{p_{\hat{n}}}$, link $\hat{n}$ is the most probable one to be the first link to become unstable, therefore we let link $\hat{n}$ be the only link with infinite backlog (in case there are more than one n that maximize the instability rank, choose one of them to be $\hat{n}$ arbitrarily). Then from Lemma 6.1,

$$\prod_{n'\in\mathcal{M}} [\lambda_{\hat{n}}(1-p_{\hat{n}}) + \lambda_{n'}p_{\hat{n}}] = p_{\hat{n}}[\lambda_{\hat{n}}(1-p_{\hat{n}})]^{M-1}$$

is the boundary of the stability region of FRASA. Consider a point $\boldsymbol{\lambda} = (\lambda_n)_{n\in\mathcal{M}}$ in M-dimensional space where $\lambda_{\hat{n}} < p_{\hat{n}}$ and $\lambda_n = 0, \forall n \in \mathcal{M} \setminus \{\hat{n}\}$. This point lies inside the stability region of FRASA. Substituting into the above equation, we get $\lambda_{\hat{n}}[\lambda_{\hat{n}}(1-p_{\hat{n}})]^{M-1}$ on LHS and $p_{\hat{n}}[\lambda_{\hat{n}}(1-p_{\hat{n}})]^{M-1}$ on RHS. Therefore, when (6.4) holds,

$$\prod_{n'\in\mathcal{M}} [\lambda_{\hat{n}}(1-p_{\hat{n}}) + \lambda_{n'}p_{\hat{n}}] < p_{\hat{n}}[\lambda_{\hat{n}}(1-p_{\hat{n}})]^{M-1}$$

is the condition for the reduced FRASA system $\overline{\mathsf{S}}_{\hat{n}}$ to be stable. Thus, the region formed by (6.4) and (6.5) is part of the stability region of $\overline{\mathsf{S}}$. By taking the union over all possible values of $\hat{n}$, we obtain the stability region of FRASA. □

We first illustrate our results for $M = 2$. When

$$\frac{\lambda_1(1-p_1)}{p_1} \geq \frac{\lambda_2(1-p_2)}{p_2} \geq 0$$

holds, the boundary of the stability region of FRASA is

$$\lambda_1[\lambda_1(1-p_1) + \lambda_2 p_1] = p_1\lambda_1(1-p_1),$$

which is reduced to

$$\lambda_1 = p_1\left(1 - \frac{\lambda_2}{1-p_1}\right)$$

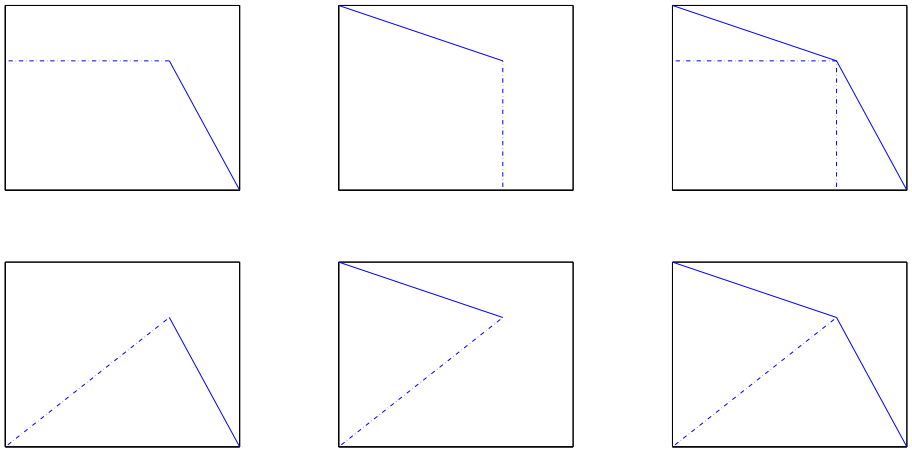

Figure 6.2: Stability region with $M = 2$: (Upper) From [2]; (Lower) From FRASA.

after simplification. Geometrically, it is a straight line joining the points $(p_1, 0)$ and $(p_1\overline{p}_2, p_2\overline{p}_1)$. This is depicted in the bottom left of Fig. 6.2. By symmetry, we also get

$$\lambda_2 = p_2\left(1 - \frac{\lambda_1}{1-p_2}\right)$$

as the boundary of the stability region of FRASA when

$$\frac{\lambda_2(1-p_2)}{p_2} \geq \frac{\lambda_1(1-p_1)}{p_1} \geq 0$$

holds. This is a straight line joining the points $(0, p_2)$ and $(p_1\overline{p}_2, p_2\overline{p}_1)$. This is shown in the bottom center of Fig. 6.2. The bottom right of Fig. 6.2 contains the final result of the stability region obtained from FRASA. The stability region derived in [2] is illustrated in the top row of Fig. 6.2 for comparison. We see that the final results are identical to each other.

Next we consider the case of $M = 3$ and each link has a transmission probability of 0.3. Figs. 6.3(a), 6.3(b) and 6.3(c) illustrate the results of Lemma 6.1 for $\overline{\mathsf{S}}_1$, $\overline{\mathsf{S}}_2$ and $\overline{\mathsf{S}}_3$ respectively. The single-colored hyperplanes in Figs. 6.3(a), 6.3(b)

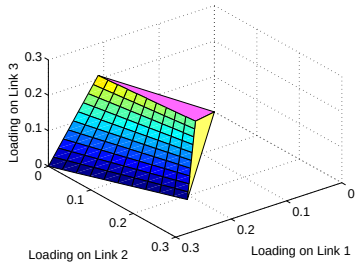

(a) $\overline{\mathcal{R}}_1$, stability region with link 1 having maximum instability rank.

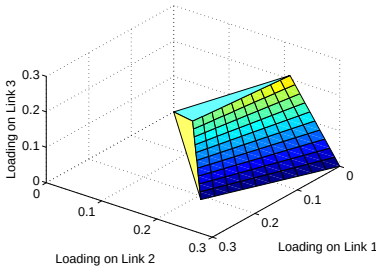

(b) $\overline{\mathcal{R}}_2$, stability region with link 2 having maximum instability rank.

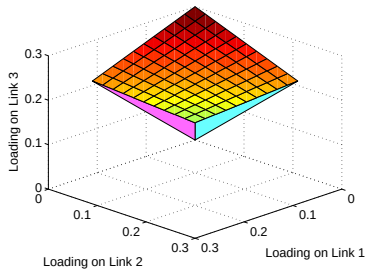

(c) $\overline{\mathcal{R}}_3$, stability region with link 3 having maximum instability rank.

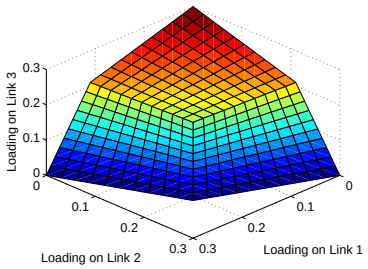

(d) $\overline{\mathcal{R}}$, the whole stability region.

Figure 6.3: Stability region of FRASA with $M = 3$ and transmission probabilities 0.3 by Lemma 6.1 and Theorem 6.1.

and 6.3(c) form the partition of the positive orthant generated by (6.2), while the multi-colored hypersurfaces come from (6.3). The union of these regions constitutes the stability region in Fig. 6.3(d) as stated in Theorem 6.1. Another example is shown in Figs. 6.4(a)-6.4(d), in which each link transmits with probability 0.6.

6.3 Validation of the FRASA Model

6.3.1 Simulation Results

In this Section, we first use simulation to verify if FRASA is a good approximation to finite-link slotted ALOHA. Since when $M = 2$, we obtain identical results for both FRASA and finite-

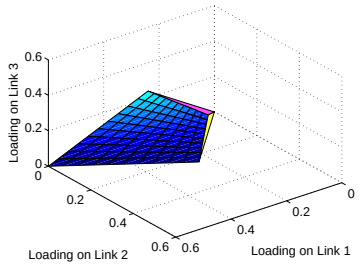

(a) $\overline{\mathcal{R}}_1$, stability region with link 1 having maximum instability rank.

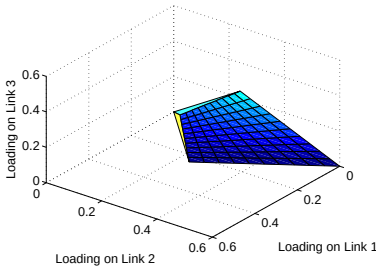

(b) $\overline{\mathcal{R}}_2$, stability region with link 2 having maximum instability rank.

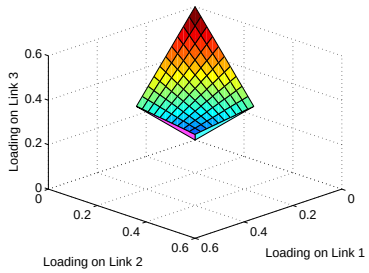

(c) $\overline{\mathcal{R}}_3$, stability region with link 3 having maximum instability rank.

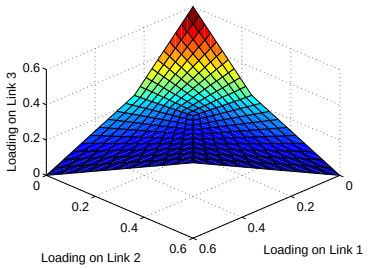

(d) $\overline{\mathcal{R}}$, the whole stability region.

Figure 6.4: Stability region of FRASA with $M = 3$ and transmission probabilities 0.6 by Lemma 6.1 and Theorem 6.1.

link slotted ALOHA, we consider $M = 3$ here.

First, to check whether the slotted ALOHA system is stable or not by simulation, we extend the algorithm proposed in [26]. This is stated as Algorithm 1.

In this algorithm, for each simulation run, we partition the simulation time into $\mathcal{N}$ batches, where $\mathcal{N} \geq 2$. We calculate the average queue lengths for each batch, $\overline{Q}_{n,w}(b)$, starting from the second batch (Line 2). We discard the first batch to remove any transient behavior in the system. Then we compute the sample mean and sample variance of the average queue length, *i.e.*, $E\left[\overline{Q}_{n,w}\right]$ and $Var\left(\overline{Q}_{n,w}\right)$, respectively (Lines 3-4). We use the difference between the last and the second observation, *i.e.*,

Algorithm 1 Stability Checking

Require: number of batches: $\mathcal{N} \geq 2$
Require: probability of type I error: a
Require: number of slots: $\mathcal{T}$
Require: simulation runs: $\mathcal{W}$ odd
Require: queue lengths: $Q_{n,w}(t), t \leq \mathcal{T}, n \in \mathcal{M}, 1 \leq w \leq \mathcal{W}$

$\mathcal{B} \leftarrow \dfrac{\mathcal{T}}{\mathcal{N}}$

$\overline{Q}_{n,w}(b) \leftarrow \dfrac{1}{\mathcal{B}} \displaystyle\sum_{t=(b-1)\mathcal{B}+1}^{b\mathcal{B}} Q_{n,w}(t), 2 \leq b \leq \mathcal{N}, n \in \mathcal{M}, 1 \leq w \leq \mathcal{W}$

$E\big[\overline{Q}_{n,w}\big] \leftarrow \dfrac{1}{\mathcal{N}-1} \displaystyle\sum_{b=2}^{\mathcal{N}} \overline{Q}_{n,w}(b), n \in \mathcal{M}, 1 \leq w \leq \mathcal{W}$

$Var\big(\overline{Q}_{n,w}\big) \leftarrow \dfrac{1}{\mathcal{N}-2} \displaystyle\sum_{b=2}^{\mathcal{N}} \Big\{\overline{Q}_{n,w}(b) - E\big[\overline{Q}_{n,w}\big]\Big\}^2, n \in \mathcal{M}, 1 \leq w \leq \mathcal{W}$

$\hat{Q}_{n,w} \leftarrow \overline{Q}_{n,w}(\mathcal{N}) - \overline{Q}_{n,w}(2), n \in \mathcal{M}, 1 \leq w \leq \mathcal{W}$

for $w = 1$ to $\mathcal{W}$ **do**
  if $\dfrac{\hat{Q}_{n,w}}{\sqrt{2Var\big(\overline{Q}_{n,w}\big)}} > t_{1-\mathsf{a},\mathcal{N}-2}, \exists n \in \mathcal{M}$ **then**
    $X_w = 0$
  else
    $X_w = 1$
  end if
end for
if $\displaystyle\sum_{w=1}^{\mathcal{W}} X_w > \frac{\mathcal{W}}{2}$ **then**
  output STABLE
else
  output UNSTABLE
end if

$\hat{Q}_{n,w}$, in the hypothesis testing (Line 5). If,

$$\frac{\hat{Q}_{n,w}}{\sqrt{2Var(\overline{Q}_{n,w})}} > t_{1-\mathsf{a},\mathcal{N}-2}, \exists n \in \mathcal{M}, \tag{6.6}$$

where $t_{1-\mathsf{a},\mathcal{N}-2}$ is the (1-a)-percentile of t-distribution with $\mathcal{N}-2$ degrees of freedom, is satisfied, we assume the system is unstable; otherwise all queues in the slotted ALOHA system is stable and so does the system (Lines 7-11). If the system is unstable, there must exist $\hat{n} \in \mathcal{M}$ such that the length of queue $\hat{n}$ has positive linear growth rate, making the hypothesis (6.6) satisfied with high probability. Otherwise, the expectation of $\hat{Q}_{n,w}$ would be zero for all $n \in \mathcal{M}$, and with high probability (6.6) would be false. We perform $\mathcal{W}$ simulation runs and then use majority vote to determine whether the system is stable (Line 13-17), therefore we require $\mathcal{W}$ to be odd. More than one simulation runs are performed in order to reduce the error in simulations.

Using Algorithm 1 as a subroutine, we use the following approach to find the boundary of the stability region, which is stated as Algorithm 2.

This algorithm is based on bisection method [22]. We let λ_1 and λ_2 increase from zero to one (Line 1-2). Given any $\mathbf{p} = (p_1, p_2, p_3)$, for any λ_1 and λ_2 between zero and one, let the initial search range of λ_3 be $[0, 1]$ and set λ_3 to be the midpoint of the search range. Then we let $\boldsymbol{\lambda} = (\lambda_1, \lambda_2, \lambda_3)$ be the arrival probabilities of the links and simulate the slotted ALOHA system (Line 6). We use Algorithm 1 to check the stability of the queues in the system and conclude the stability of the system. If Algorithm 1 indicates that the system is stable, we set the next search range of λ_3 to be the upper half of the original one (Line 8); otherwise, we use the lower half as the next search range (Line 10). We iterate until the search range is sufficiently small (Line 5). Then we take the midpoint of the final search range to be the boundary value of λ_3 for the given values of λ_1 and

Algorithm 2 Stability Region Boundary Generation

Require: $0 \leq p_1, p_2, p_3 \leq 1$
Require: $\overline{\delta} > 0$
for $\lambda_1 = 0$ to 1 in step 0.01 **do**
  for $\lambda_2 = 0$ to 1 in step 0.01 **do**
    $\lambda_3 \leftarrow 0.5$
    $\delta \leftarrow 0.25$
    while $\delta \geq \overline{\delta}$ **do**
      perform $\mathcal{W}$ simulation runs
      if Algorithm 1 returns STABLE **then**
        $\lambda_3 \leftarrow \lambda_3 + \delta$
      else
        $\lambda_3 \leftarrow \lambda_3 - \delta$
      end if
      $\delta \leftarrow \frac{\delta}{2}$
    end while
  end for
end for

Table 6.1: Parameters used for the simulations.

$\mathcal{N}$	2	a	0.05
$\mathcal{T}$	4000	$\mathcal{W}$	3
$t_{1-\mathsf{a},\mathcal{N}-2}$	1.8595	$\overline{\delta}$	0.001

λ_2. We repeat this procedure for any combination of λ_1 and λ_2 to get the boundary of the stability region. The values of the parameters used in these algorithms are shown in Table 6.1.

For illustrative purposes, we only show the cross-sections of the stability regions. We first let all links transmit with probability 0.3. In Fig. 6.5(a) we depict the cross-sections of the stability region by fixing λ_2, while in Fig. 6.5(b) the cross-sections of the stability region are obtained by fixing λ_1. The solid lines represent the simulation results while the dash-dot lines are obtained from FRASA. In Figs. 6.6(a) and 6.6(b) we show the corresponding results by changing the transmission probabilities of all links to 0.6. We observe that there is a close match between

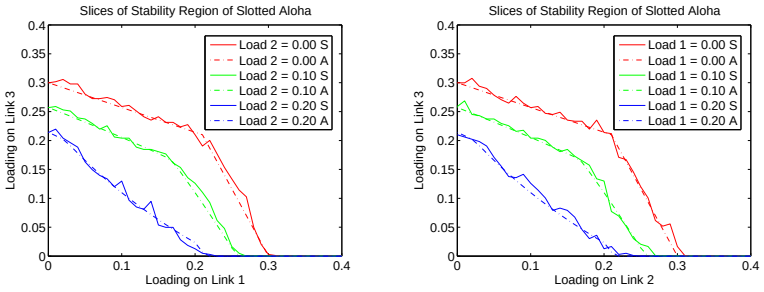

(a) λ_2 fixed. (b) λ_1 fixed.

Figure 6.5: Cross-section of stability region with $M = 3$ and transmission probabilities 0.3.

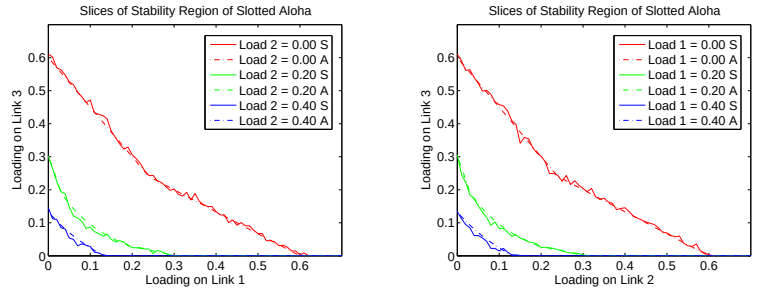

(a) λ_2 fixed. (b) λ_1 fixed.

Figure 6.6: Cross-section of stability region with $M = 3$ and transmission probabilities 0.6.

the stability region of FRASA and the stability region of slotted ALOHA. In FRASA, we introduce the parameter $\{\chi_n\}_{n\in\mathcal{M}\setminus\{\hat{n}\}}$ to compute the boundary of the stability region. $\{\chi_n\}_{n\in\mathcal{M}\setminus\{\hat{n}\}}$ in FRASA can be regarded as the stationary joint queue statistics, which are essential for computing the boundary of the stability region of slotted ALOHA as stated in Chapter 5. Therefore, the stability region of FRASA is a good approximation to the stability region of slotted ALOHA, in the sense that we compute the stability region of slotted ALOHA by assuming we know the stationary joint queue statistics.

6.3.2 Comparison to Previous Bounds

Here, we demonstrate that FRASA is a good approximation to finite-link slotted ALOHA by showing the boundary values obtained from FRASA lie inside the upper and lower bounds in [3]. We fix the loading of the first $M-1$ links, evaluate the "FRASA" value of λ_M, and evaluate the "Upper" bound and "Lower" bound of λ_M by using Theorems 3 and 5 in [3] respectively. Before showing this, we point out that the bounds in [3] are applicable only when the instability rank assumption, *i.e.*, link M has the highest instability rank, holds. This is best illustrated by the following examples. Consider a slotted ALOHA system with two links. We let both links transmit with probability 0.6. We keep increasing λ_1 while assuming $\frac{\lambda_1(1-p_1)}{p_1} \leq \frac{\lambda_2(1-p_2)}{p_2}$, and evaluate the upper bound on λ_2 by using Theorem 3 in [3]. When $\lambda_1 > p_1\overline{p}_2$, the upper bound, *i.e.*, $\lambda_{2,\max}$, satisfies $\frac{\lambda_2(1-p_2)}{p_2} \leq \frac{\lambda_{2,\max}(1-p_2)}{p_2} < \frac{\lambda_1(1-p_1)}{p_1}$, showing that the instability rank assumption does not hold. We change the transmission probabilities of both links to 0.3 and repeat the whole process, but evaluate the lower bound on λ_2 by using Theorem 5 in [3]. It is found that when $\lambda_1 > p_1\overline{p}_2$, the lower bound, *i.e.*, $\lambda_{2,\min}$, satisfies $\frac{\lambda_{2,\min}(1-p_2)}{p_2} < \frac{\lambda_1(1-p_1)}{p_1}$, and we cannot conclude whether the instability rank assumption is valid or not. These results are depicted in Figs. 6.7(a) and 6.7(b) respectively. In the case of $M=2$, we already have the complete characterization on the boundary of the stability region, therefore we can explicitly evaluate λ_2 and show that when $\lambda_1 > p_1\overline{p}_2$, the instability rank assumption does not hold, and the Theorems in [3] are not applicable. When $M > 2$, if there are some λ_n satisfying $\lambda_n > p_n \prod_{n' \in \mathcal{M}\setminus\{n\}} \overline{p}_{n'}$, it is difficult

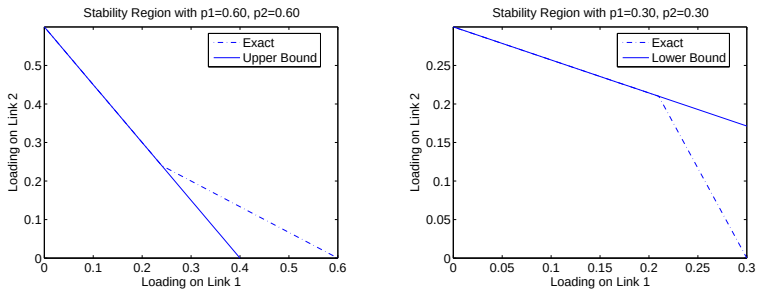

(a) (b)

Figure 6.7: Restricted application of the upper and lower bounds in [3].

to predict whether the instability rank assumption is valid or not. When the instability rank assumption is not valid, one may tempt to switch the order of the links to keep the validity of the assumption. But in this case, we even cannot determine the stability of the links with instability ranks higher than that of link M, because the bounds on link n depend on the loadings on the links having smaller instability ranks than link n [3]. Therefore, when using the bounds in [3], we cannot set the loadings on the first $M-1$ links too large in order to maintain the instability rank assumption.

However, such restriction does not exist in computing the "FRASA" value of λ_M. We first let link M be the link with the highest instability rank, *i.e.*, $\hat{n} = M$. Then we solve (6.3) for λ_M, which is an equation of degree $M-1$, and get $M-1$ values of λ_M. Exactly one of them is the desired value, which makes the instability rank of link M the highest. Otherwise, we find the link with the highest instability rank among the first $M-1$ links. We let it equals $\hat{n}$ and solve (6.3) for λ_M, which is an equation of degree one. In this case, we get a nonnegative value which is the desired value of λ_M. Otherwise, we conclude that with the loadings on the first $M-1$ links, it is impossible to keep the system stable no matter how small λ_M is.

To compare the numerical values computed from FRASA

against the bounds in [3], we consider the numerical examples in [2] and [3]. The examples are reproduced in Tables 6.2-6.15. The values of the loadings are classified into four groups in each table. In G1, one or more values of λ_n are zero. In G2, all λ_n are approximately equal to $\frac{1}{2}p_n \prod_{n' \in \mathcal{M}\setminus\{n\}} \overline{p}_{n'}$. In G3, all λ_n are close to $p_n \prod_{n' \in \mathcal{M}\setminus\{n\}} \overline{p}_{n'}$. In G4, one or more λ_n satisfy $\lambda_n > p_n \prod_{n' \in \mathcal{M}\setminus\{n\}} \overline{p}_{n'}$, and these λ_n are marked with asterisks in the tables. In all cases, the values predicted from FRASA lie inside the upper and lower bounds in [3]. Simulations are also performed for all examples in [2] and [3], and the results are shown in brackets in the tables. While the difference between the simulation result and the corresponding "FRASA" value can be as large as 40% (the first case of G4 in Table 6.3), for most cases, 82 (resp. 90) out of 96, the simulation results deviate from the corresponding "FRASA" values by at most $\pm 2\%$ (resp. $\pm 10\%$). The examples also show that the bounds in [3] may not be always applicable, as in the case of G4 in Table 6.5.

For the first case of G4 in Table 6.3, we plot the contour of the stability region of FRASA in Fig. 6.8 to investigate the reason for such a large discrepancy between the stability region of slotted ALOHA and FRASA. This contour plot shows that when λ_1 and λ_2 are approximately equal to 0.035 and 0.0561 respectively, the contour lines are very close together, meaning that the boundary of the stability region at $\lambda_1 = 0.035$ and $\lambda_2 = 0.0561$ is almost parallel to the λ_3-axis, *i.e.*, the boundary is very sensitive to small changes in λ_1 and λ_2. Therefore, in this situation, it is difficult to obtain the boundary of the stability region of slotted ALOHA by simulations.

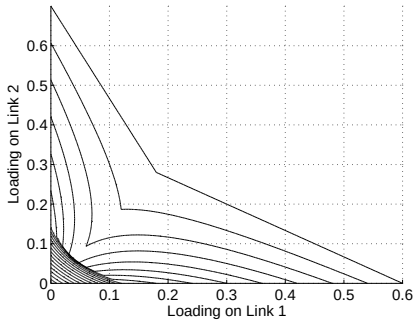

Figure 6.8: Contour plot of the stability region of FRASA for the first case of G4 in Table 6.3.

6.4 Convex Hull Bound

Although Theorem 6.1 gives us a closed-form expression for the stability region of FRASA, this stability region is not convex when $M > 2$ (as shown in the next Section). Therefore we are motivated to derive outer and inner bounds on the stability region of FRASA that are convex and piecewise linear, which can be used to find the upper and lower bounds on network capacity respectively. In this Section, we first develop an outer bound on the stability region of FRASA that is guaranteed to be convex and piecewise linear by using *corner points* of the stability region of FRASA. For each $\mathcal{M}' \subseteq \mathcal{M}$, we obtain a corner point $\Pi^{\mathsf{p}^{\mathcal{M}}(\mathcal{M}')} = \left(\Pi_n^{\mathsf{p}^{\mathcal{M}}(\mathcal{M}')}\right)_{n\in\mathcal{M}}$, where

$$\Pi_n^{\mathsf{p}^{\mathcal{M}}(\mathcal{M}')} = \begin{cases} p_n \prod_{n'\in\mathcal{M}'\setminus\{n\}} \overline{p}_{n'}, & n \in \mathcal{M}' \\ 0, & n \in \mathcal{M}\setminus\mathcal{M}' \end{cases}. \tag{6.7}$$

These corner points, by construction, lie on the boundary of the stability region of FRASA because they satisfy the parametric form (6.1). We first obtain the following Lemma, stating the relationship between the boundary of the stability region of FRASA and the corner points.

Lemma 6.2. *The boundary of the stability region of $\overline{\mathsf{S}}_{\hat{n}}$, i.e., the hypersurface $\mathsf{F}_{\hat{n}}$, is contained in the convex hull $\mathsf{H}_{\hat{n}}$ generated by the corner points $\Pi^{\mathsf{p}^{\mathcal{M}}(\mathcal{M}'\cup\{\hat{n}\})}$ for all $\mathcal{M}' \subseteq \mathcal{M} \setminus \{\hat{n}\}$, i.e., every point satisfying (6.3) is a convex combination of the corner points $\Pi^{\mathsf{p}^{\mathcal{M}}(\mathcal{M}'\cup\{\hat{n}\})}$ for all $\mathcal{M}' \subseteq \mathcal{M} \setminus \{\hat{n}\}$.*

Proof. Let $\Pi = (\Pi_n)_{n\in\mathcal{M}}$ be a point satisfying (6.3). Then, from the parametric form (6.1),

$$\Pi_n = \begin{cases} \chi_n p_n (1-p_{\hat{n}}) \displaystyle\prod_{n'\in\mathcal{M}\setminus\{n,\hat{n}\}} (1-\chi_{n'}p_{n'}), & n \neq \hat{n} \\ p_{\hat{n}} \displaystyle\prod_{n'\in\mathcal{M}\setminus\{\hat{n}\}} (1-\chi_{n'}p_{n'}), & n = \hat{n} \end{cases}. \tag{6.8}$$

If Π is a convex combination of $\Pi^{\mathsf{p}^{\mathcal{M}}(\mathcal{M}'\cup\{\hat{n}\})}$ for all $\mathcal{M}' \subseteq \mathcal{M} \setminus \{\hat{n}\}$, then

$$\Pi_n = \begin{cases} p_n \overline{p}_{\hat{n}} \displaystyle\sum_{\mathcal{M}':\, n\in\mathcal{M}'\subseteq\mathcal{M}\setminus\{\hat{n}\}} \phi_{\mathcal{M}'} \prod_{n'\in\mathcal{M}'\setminus\{n\}} \overline{p}_{n'}, & n \neq \hat{n} \\ p_{\hat{n}} \displaystyle\sum_{\mathcal{M}'\subseteq\mathcal{M}\setminus\{\hat{n}\}} \phi_{\mathcal{M}'} \prod_{n'\in\mathcal{M}'} \overline{p}_{n'}, & n = \hat{n} \end{cases} \tag{6.9}$$

where

$$\sum_{\mathcal{M}'\subseteq\mathcal{M}\setminus\{\hat{n}\}} \phi_{\mathcal{M}'} = 1 \text{ and } \phi_{\mathcal{M}'} \geq 0, \forall \mathcal{M}' \subseteq \mathcal{M} \setminus \{\hat{n}\}.$$

We will show that $\{\phi_{\mathcal{M}'}\}_{\mathcal{M}'\subseteq\mathcal{M}\setminus\{\hat{n}\}}$ always exists. When $n = \hat{n}$, we get

$$\sum_{\mathcal{M}'\subseteq\mathcal{M}\setminus\{\hat{n}\}} \phi_{\mathcal{M}'} \prod_{n'\in\mathcal{M}'} \overline{p}_{n'} = \prod_{n'\in\mathcal{M}\setminus\{\hat{n}\}} (1-\chi_{n'}p_{n'}).$$

Consider this as a multinomial in $\{p_n\}_{n\in\mathcal{M}\setminus\{\hat{n}\}}$. By equating the coefficient of $\displaystyle\prod_{n'\in\mathcal{M}''} p_{n'}$ for all $\mathcal{M}'' \subseteq \mathcal{M} \setminus \{\hat{n}\}$, we get

$$\sum_{\mathcal{M}':\, \mathcal{M}''\subseteq\mathcal{M}'\subseteq\mathcal{M}\setminus\{\hat{n}\}} \phi_{\mathcal{M}'} = \prod_{n'\in\mathcal{M}''} \chi_{n'}. \tag{6.10}$$

Also by equating the coefficient of $\prod_{n' \in \mathcal{M}''} p_{n'}$ for all $\mathcal{M}'' \subseteq \mathcal{M} \setminus \{n, \hat{n}\}$ with $n \neq \hat{n}$, we get

$$\sum_{\mathcal{M}' \colon \mathcal{M}'' \cup \{n\} \subseteq \mathcal{M}' \subseteq \mathcal{M} \setminus \{\hat{n}\}} \phi_{\mathcal{M}'} = \chi_n \prod_{n' \in \mathcal{M}''} \chi_{n'}.$$

Observe that this is only a special case of (6.10), it suffices to consider (6.10) only. Notice that (6.10) is a system of linear equations. By Gaussian elimination, we see that for all $\mathcal{M}'' \subseteq \mathcal{M} \setminus \{\hat{n}\}$,

$$\begin{aligned} \phi_{\mathcal{M}''} &= \sum_{\mathcal{M}' \colon \mathcal{M}'' \subseteq \mathcal{M}' \subseteq \mathcal{M} \setminus \{\hat{n}\}} (-1)^{|\mathcal{M}'| - |\mathcal{M}''|} \prod_{n' \in \mathcal{M}''} \chi_{n'} \\ &= \prod_{n' \in \mathcal{M}''} \chi_{n'} \prod_{n'' \in \mathcal{M} \setminus (\mathcal{M}'' \cup \{\hat{n}\})} (1 - \chi_{n''}) \geq 0. \end{aligned}$$

Also, by considering $\mathcal{M}'' = \emptyset$ in (6.10), we obtain

$$\sum_{\mathcal{M}' \subseteq \mathcal{M} \setminus \{\hat{n}\}} \phi_{\mathcal{M}'} = 1.$$

Therefore, every point satisfying (6.3) is a convex combination of $\Pi^{\mathsf{p}^{\mathcal{M}}(\mathcal{M}' \cup \{\hat{n}\})}$ for all $\mathcal{M}' \subseteq \mathcal{M} \setminus \{\hat{n}\}$. □

By using Lemma 6.2 and Theorem 6.1, we obtain the following Theorems about using convex hulls to bound the stability region of FRASA. To obtain the bounds from these Theorems, we only have to know the coordinates of all corner points, which can be computed from (6.7) based on the transmission probability vector only.

Theorem 6.2 (Bound of Convex-Hull Union)**.** *The convex hull generated by $\Pi^{\mathsf{p}^{\mathcal{M}}(\mathcal{M}' \cup \{\hat{n}\})}$ for all $\mathcal{M}' \subseteq \mathcal{M} \setminus \{\hat{n}\}$ together with $\mathbf{0}$, i.e., the origin, is a piecewise linear outer bound on $\overline{\mathcal{R}}_{\hat{n}}$. Denote this convex hull by $\mathcal{H}_{\hat{n}}$. Therefore, the union of these $\mathcal{H}_{\hat{n}}$ for all $\hat{n} \in \mathcal{M}$, i.e., $\overline{\mathcal{H}} = \bigcup_{\hat{n} \in \mathcal{M}} \mathcal{H}_{\hat{n}}$, is a piecewise linear outer bound on the stability region of FRASA. The union here is also disjoint.*

Proof. Consider the reduced FRASA system $\overline{\mathsf{S}}_{\hat{n}}$ and let $\mathcal{M}' \subseteq \mathcal{M} \setminus \{\hat{n}\}$. From (6.7), for every $n \in \mathcal{M} \setminus \{\hat{n}\}$, all corner points $\Pi^{\mathsf{p}^{\mathcal{M}}(\mathcal{M}' \cup \{\hat{n}\})}$ with $n \in \mathcal{M}'$ and $\mathbf{0}$ lie on the boundary $\frac{\lambda_{\hat{n}}(1-p_{\hat{n}})}{p_{\hat{n}}} = \frac{\lambda_n(1-p_n)}{p_n}$, all corner points $\Pi^{\mathsf{p}^{\mathcal{M}}(\mathcal{M}' \cup \{\hat{n}\})}$ with $n \notin \mathcal{M}' \cup \{\hat{n}\}$ and $\mathbf{0}$ lie on the boundary $\frac{\lambda_n(1-p_n)}{p_n} = 0$. Also, for all $n \in \mathcal{M} \setminus \{\hat{n}\}$, the condition $0 \leq \chi_n \leq 1$ implies none of the corner points lie outside the region $\frac{\lambda_{\hat{n}}(1-p_{\hat{n}})}{p_{\hat{n}}} \geq \frac{\lambda_n(1-p_n)}{p_n} \geq 0$. Hence, for all $n \in \mathcal{M} \setminus \{\hat{n}\}$, $\frac{\lambda_{\hat{n}}(1-p_{\hat{n}})}{p_{\hat{n}}} = \frac{\lambda_n(1-p_n)}{p_n}$ and $\frac{\lambda_n(1-p_n)}{p_n} = 0$ are the boundaries of both $\overline{R}_{\hat{n}}$ and $\mathcal{H}_{\hat{n}}$. Therefore, from Lemma 6.2, $\overline{\mathcal{R}}_{\hat{n}} \subseteq \mathcal{H}_{\hat{n}}$, and $\overline{\mathcal{R}} = \bigcup_{\hat{n} \in \mathcal{M}} \overline{\mathcal{R}}_{\hat{n}} \subseteq \bigcup_{\hat{n} \in \mathcal{M}} \mathcal{H}_{\hat{n}} = \overline{\mathcal{H}}$. Since the boundaries $\frac{\lambda_{\hat{n}}(1-p_{\hat{n}})}{p_{\hat{n}}} = \frac{\lambda_n(1-p_n)}{p_n}$ and $\frac{\lambda_n(1-p_n)}{p_n} = 0$ are linear and the convex hull generated by a set of points is piecewise linear, $\overline{\mathcal{H}}$ is piecewise linear. □

Theorem 6.3 (Convex Hull Bound)**.** *$\mathcal{H}$, the convex hull generated by $\Pi^{\mathsf{p}^{\mathcal{M}}(\mathcal{M}')}$ for all $\mathcal{M}' \subseteq \mathcal{M}$, is a convex and piecewise linear outer bound on the stability region of FRASA.*

Proof. Notice that $\mathcal{H}$ is the convex hull of $\overline{\mathcal{H}}$. Since the union of convex sets need not be convex, it is trivial to see that $\overline{\mathcal{H}} \subseteq \mathcal{H}$. Therefore from Theorem 6.2, $\overline{\mathcal{R}} \subseteq \mathcal{H}$. By the same reason as in proving Theorem 6.2, $\mathcal{H}$ is also piecewise linear. □

In finding the bounds on λ_M given the loadings on the other links, we do not have to rely on the instability rank assumption as in [3]. To apply Theorem 6.2, we first assume link M to have the highest instability rank, and generate the corresponding convex hull. If the assumption is valid, we can find a lower bound and an upper bound from the convex hull. Otherwise, we

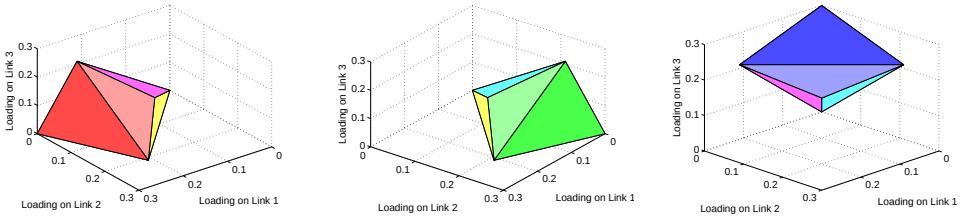

(a) $\mathcal{H}_1$, convex hull of $\overline{\mathcal{R}}_1$. (b) $\mathcal{H}_2$, convex hull of $\overline{\mathcal{R}}_2$. (c) $\mathcal{H}_3$, convex hull of $\overline{\mathcal{R}}_3$.

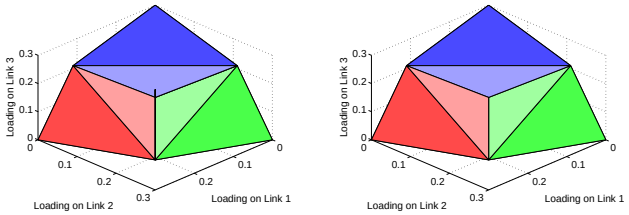

(d) $\overline{\mathcal{H}}$, bound of convex-hull union. (e) $\mathcal{H}$, convex hull bound.

Figure 6.9: Convex hull bound on the stability region of FRASA with $M = 3$ and transmission probabilities 0.3 by Theorems 6.2 and 6.3.

choose from the remaining links the link with the highest instability rank and repeat the process. Theorem 6.3 can be applied in any case in finding the upper bound.

We demonstrate the results from these Theorems in the following examples. Figs. 6.9(a), 6.9(b) and 6.9(c) illustrate the results of Theorem 6.2, assuming the transmission probabilities of all links are 0.3. The polytopes shown in these figures are the convex hulls $\mathcal{H}_1$, $\mathcal{H}_2$ and $\mathcal{H}_3$ generated by the corresponding corner points respectively. Fig. 6.9(d) shows $\overline{\mathcal{H}}$, the union of the convex hulls in Figs. 6.9(a), 6.9(b) and 6.9(c). Fig. 6.9(e) depicts $\mathcal{H}$, the convex hull generated by all corner points. The polytopes in Figs. 6.9(d) and 6.9(e) are identical. To show that this is not necessarily true, we give another example in which the transmission probabilities of all links are 0.6. In this example, $\overline{\mathcal{H}}$ in Fig. 6.10(d) is contained inside $\mathcal{H}$ in Fig. 6.10(e).

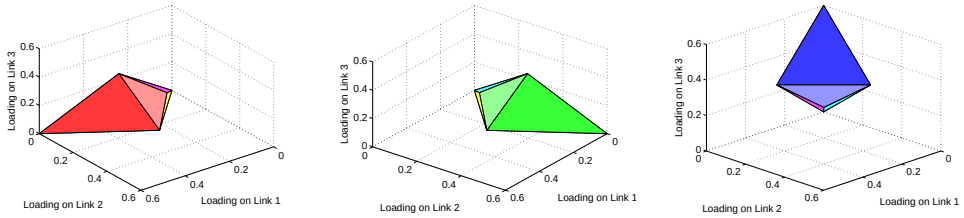

(a) $\mathcal{H}_1$, convex hull of $\overline{\mathcal{R}}_1$. (b) $\mathcal{H}_2$, convex hull of $\overline{\mathcal{R}}_2$. (c) $\mathcal{H}_3$, convex hull of $\overline{\mathcal{R}}_3$.

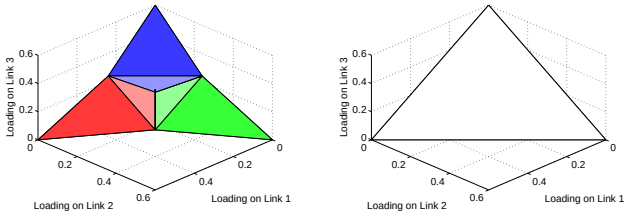

(d) $\overline{\mathcal{H}}$, bound of convex-hull union. (e) $\mathcal{H}$, convex hull bound.

Figure 6.10: Convex hull bound on the stability region of FRASA with $M = 3$ and transmission probabilities 0.6 by Theorems 6.2 and 6.3.

6.5 p-Convexity

From the examples shown in previous Section, the bounds on the stability region of FRASA obtained from Theorems 6.2 and 6.3, *i.e.*, $\overline{\mathcal{H}}$ and $\mathcal{H}$ respectively, need not be identical. Recall that both $\overline{\mathcal{H}}$ and $\mathcal{H}$ are completely characterized by the transmission probability vector only. Intuitively, for $\overline{\mathcal{H}} = \mathcal{H}$, we require $\overline{\mathcal{H}}$ to be a convex set, which means the transmission probability vector may need to satisfy some "convexity" conditions. In this Section, we formalize these ideas and investigate the necessary and sufficient condition for $\overline{\mathcal{H}}$ and $\mathcal{H}$ to be identical.

We first define **p**-convexity, and characterize the condition on the transmission probability vector for **p**-convexity to hold.

Definition 6.1. *We use the corner points* $\Pi^{\mathsf{p}^{\mathcal{M}}(\mathcal{M}\backslash\{\bar{n}\})}$ *for each* $\bar{n} \in \mathcal{M}$ *to form a hyperplane* $\Omega^{\mathcal{M}}$. *If the corner points* $\Pi^{\mathsf{p}^{\mathcal{M}}(\mathcal{M})}$ *and* $\mathbf{0}$ *lie on opposite sides of* $\Omega^{\mathcal{M}}$, *or* $\Pi^{\mathsf{p}^{\mathcal{M}}(\mathcal{M})}$ *lies on* $\Omega^{\mathcal{M}}$, *the stability region of FRASA is said to be* **p***-convex.*

Theorem 6.4. *The stability region of FRASA is* **p***-convex if and only if*

$$\sum_{n\in\mathcal{M}} p_n \leq 1. \tag{6.11}$$

Proof. Introduce the following notations:

$$p^{\mathcal{M}}_{(x,y)} = \prod_{n'\in\mathcal{M}\setminus\{x,y\}} \overline{p}_{n'},$$
$$p^{\mathcal{M}}_{(x)} = \prod_{n'\in\mathcal{M}\setminus\{x\}} \overline{p}_{n'}.$$

Then, for each $\bar{n} \in \mathcal{M}$, $\Pi^{\mathsf{p}^{\mathcal{M}}(\mathcal{M}\setminus\{\bar{n}\})} = \left(\Pi_n^{\mathsf{p}^{\mathcal{M}}(\mathcal{M}\setminus\{\bar{n}\})}\right)_{n\in\mathcal{M}}$ is a point in M-dimensional space with

$$\Pi_n^{\mathsf{p}^{\mathcal{M}}(\mathcal{M}\setminus\{\bar{n}\})} = \begin{cases} p_n p^{\mathcal{M}}_{(n,\bar{n})}, & n \neq \bar{n} \\ 0, & n = \bar{n} \end{cases},$$

and $\Pi^{\mathsf{p}^{\mathcal{M}}(\mathcal{M})} = \left(\Pi_n^{\mathsf{p}^{\mathcal{M}}(\mathcal{M})}\right)_{n\in\mathcal{M}}$ is another point with

$$\Pi_n^{\mathsf{p}^{\mathcal{M}}(\mathcal{M})} = p_n p^{\mathcal{M}}_{(n)}, \forall n \in \mathcal{M}.$$

To determine whether the stability region of FRASA is **p**-convex, we need the following two Lemmas.

Lemma 6.3. *Let $\mathcal{X}_{\mathcal{M}}$ be a $M \times M$ matrix, with the first row equals $\mathbf{0} - \Pi^{\mathsf{p}^{\mathcal{M}}(\mathcal{M}\setminus\{1\})}$, and for $n \in \mathcal{M}\setminus\{1\}$, the n-th row is $\Pi^{\mathsf{p}^{\mathcal{M}}(\mathcal{M}\setminus\{n\})} - \Pi^{\mathsf{p}^{\mathcal{M}}(\mathcal{M}\setminus\{1\})}$. Then*

$$\left|\mathcal{X}_{\mathcal{M}}\right| = (-1)^M (M-1) \prod_{n'\in\mathcal{M}} p_{n'} \prod_{n''\in\mathcal{M}} \overline{p}_{n''}^{M-2}. \tag{6.12}$$

Lemma 6.4. *Let $\mathcal{Y}_{\mathcal{M}}$ be a $M \times M$ matrix, with the first row equals $\Pi^{\mathsf{p}^{\mathcal{M}}(\mathcal{M})} - \Pi^{\mathsf{p}^{\mathcal{M}}(\mathcal{M}\setminus\{1\})}$, and for $n \in \mathcal{M}\setminus\{1\}$, the n-th row is $\Pi^{\mathsf{p}^{\mathcal{M}}(\mathcal{M}\setminus\{n\})} - \Pi^{\mathsf{p}^{\mathcal{M}}(\mathcal{M}\setminus\{1\})}$. Then*

$$\left|\mathcal{Y}_{\mathcal{M}}\right| = (-1)^M \left(\sum_{n\in\mathcal{M}} p_n - 1\right) \prod_{n'\in\mathcal{M}} p_{n'} \prod_{n''\in\mathcal{M}} \overline{p}_{n''}^{M-2}. \tag{6.13}$$

$\left|\mathcal{X}_{\mathcal{M}}\right|$ is calculated as follows:

$$\begin{aligned}
\left|\mathcal{X}_{\mathcal{M}}\right| &= -\begin{vmatrix} 0 & p_2 p^{\mathcal{M}}_{(2,1)} & \cdots & p_M p^{\mathcal{M}}_{(M,1)} \\ p_1 p^{\mathcal{M}}_{(1,2)} & 0 & \cdots & p_M p^{\mathcal{M}}_{(M,2)} \\ \vdots & \vdots & \ddots & \vdots \\ p_1 p^{\mathcal{M}}_{(1,M)} & p_2 p^{\mathcal{M}}_{(2,M)} & \cdots & 0 \end{vmatrix} \\
&= -\prod_{n'\in\mathcal{M}} p_{n'} \prod_{n''\in\mathcal{M}} \overline{p}_{n''}^{M-2} \begin{vmatrix} 0 & 1 & \cdots & 1 \\ 1 & 0 & \cdots & 1 \\ \vdots & \vdots & \ddots & \vdots \\ 1 & 1 & \cdots & 0 \end{vmatrix} \\
&= (-1)^M (M-1) \prod_{n'\in\mathcal{M}} p_{n'} \prod_{n''\in\mathcal{M}} \overline{p}_{n''}^{M-2}
\end{aligned}$$

The first equality is obtained by subtracting the first row of $\mathcal{X}_{\mathcal{M}}$ from all other rows in $\mathcal{X}_{\mathcal{M}}$. The second equality results from the observation that if for all $n'' \in \mathcal{M}$ we multiply $\overline{p}_{n''}$ to both the n''-th row and column, then we have a factor of $\prod_{n''\in\mathcal{M}} \overline{p}_{n''}$ from each element in $\mathcal{X}_{\mathcal{M}}$. $\left|\mathcal{Y}_{\mathcal{M}}\right|$ is obtained similarly as shown below:

$$\begin{aligned}
\left|\mathcal{Y}_{\mathcal{M}}\right| &= -\begin{vmatrix} -p_1 p^{\mathcal{M}}_{(1)} & p_1 p_2 p^{\mathcal{M}}_{(2,1)} & \cdots & p_1 p_M p^{\mathcal{M}}_{(M,1)} \\ p_2 p_1 p^{\mathcal{M}}_{(1,2)} & -p_2 p^{\mathcal{M}}_{(2)} & \cdots & p_2 p_M p^{\mathcal{M}}_{(M,2)} \\ \vdots & \vdots & \ddots & \vdots \\ p_M p_1 p^{\mathcal{M}}_{(1,M)} & p_M p_2 p^{\mathcal{M}}_{(2,M)} & \cdots & -p_M p^{\mathcal{M}}_{(M)} \end{vmatrix} \\
&= -\prod_{n'\in\mathcal{M}} p_{n'} \prod_{n''\in\mathcal{M}} \overline{p}_{n''}^{M-2} \begin{vmatrix} -\overline{p}_1 & p_1 & \cdots & p_1 \\ p_2 & -\overline{p}_2 & \cdots & p_2 \\ \vdots & \vdots & \ddots & \vdots \\ p_M & p_M & \cdots & -\overline{p}_M \end{vmatrix} \\
&= (-1)^M \left(\sum_{n\in\mathcal{M}} p_n - 1\right) \prod_{n'\in\mathcal{M}} p_{n'} \prod_{n''\in\mathcal{M}} \overline{p}_{n''}^{M-2}
\end{aligned}$$

The proof of Theorem 6.4 goes as follows. We first construct a normal vector perpendicular to the hyperplane $\Omega^{\mathcal{M}}$. If we let $\{\mathbf{e}_n\}_{n\in\mathcal{M}}$ be the set of basis vector where $\mathbf{e}_n$ is a unit vector in the direction of increasing λ_n, then

$$\mathbf{n} = \begin{vmatrix} \mathbf{e}_1 & \mathbf{e}_2 & \cdots & \mathbf{e}_n \\ \mathtt{N}_1^2 & \mathtt{N}_2^2 & \cdots & \mathtt{N}_M^2 \\ \vdots & \vdots & \ddots & \vdots \\ \mathtt{N}_1^M & \mathtt{N}_2^M & \cdots & \mathtt{N}_M^M \end{vmatrix}$$

with

$$\mathtt{N}_n^{\bar{n}} = \Pi_n^{\mathtt{p}^{\mathcal{M}}(\mathcal{M}\setminus\{\bar{n}\})} - \Pi_n^{\mathtt{p}^{\mathcal{M}}(\mathcal{M}\setminus\{1\})}$$

will be a normal vector of $\Omega^{\mathcal{M}}$. Therefore, $\left|\mathcal{X}_{\mathcal{M}}\right|$ is the inner product of $\mathbf{0}-\Pi^{\mathtt{p}^{\mathcal{M}}(\mathcal{M}\setminus\{1\})}$ and $\mathbf{n}$, while $\left|\mathcal{Y}_{\mathcal{M}}\right|$ is the inner product of $\Pi^{\mathtt{p}^{\mathcal{M}}(\mathcal{M})} - \Pi^{\mathtt{p}^{\mathcal{M}}(\mathcal{M}\setminus\{1\})}$ and $\mathbf{n}$. $\Pi^{\mathtt{p}^{\mathcal{M}}(\mathcal{M})}$ lies on $\Omega^{\mathcal{M}}$ is equivalent to $\left|\mathcal{Y}_{\mathcal{M}}\right| = 0$. $\Pi^{\mathtt{p}^{\mathcal{M}}(\mathcal{M})}$ and $\mathbf{0}$ lie on opposite sides of $\Omega^{\mathcal{M}}$ is equivalent to that $\left|\mathcal{X}_{\mathcal{M}}\right|$ and $\left|\mathcal{Y}_{\mathcal{M}}\right|$ have opposite signs. With the condition that $\mathbf{0}$ never lies on $\Omega^{\mathcal{M}}$, $\mathbf{p}$-convexity is achieved if and only if $\left|\mathcal{X}_{\mathcal{M}}\right|\left|\mathcal{Y}_{\mathcal{M}}\right| \leq 0$. From Lemmas 6.3 and 6.4, the condition is equivalent to

$$(-1)^{2M}(M-1)\left(\sum_{n\in\mathcal{M}} p_n - 1\right)\prod_{n'\in\mathcal{M}} p_{n'}^2 \prod_{n''\in\mathcal{M}} \overline{p}_{n''}^{2(M-2)} \leq 0.$$

After simplification, it reduces to (6.11). □

The $\mathbf{p}$-convexity of the stability region of FRASA can be regarded as a measure of contention level in the system. p_n can be viewed as the proportion of time that link n is active. $\sum_{n\in\mathcal{M}} p_n \leq 1$ represents the case that the increase in channel utilization outweighs the increase in contention due to addition of one more

link to the system. This is possible because when the channel utilization is small, the probability that a new link choose an idle time slot to transmit is large, therefore the contention introduced by this new link will be small and the stability region of FRASA will be **p**-convex. On the other hand, if $\sum_{n\in\mathcal{M}} p_n > 1$, the contention level will be so large that it is not beneficial to introduce one more link to the system. Even in the ideal case, *i.e.*, TDMA with perfect scheduling, it is impossible to assign time slots to the links such that there is no contention. Hence, contention is inevitable in this situation, and the stability region of FRASA will not be **p**-convex. Consequently, it is undesirable to allow the links to be active with transmission probability vector $(p_n)_{n\in\mathcal{M}}$.

From (6.11), we observe that to make the stability region to be **p**-convex, the transmission probabilities of all links should be set according to the number of neighboring links in proximity. For example, if we assume all links have the same priority, we may set each p_n to be $\frac{1}{M}$.

From Theorem 6.3, we know $\overline{\mathcal{H}} \subseteq \mathcal{H}$. We observe that if the stability region of FRASA with link set $\mathcal{M}$ is **p**-convex, then the stability region of FRASA with link set $\mathcal{M}'$, where $\mathcal{M}' \subseteq \mathcal{M}$ and $|\mathcal{M}'| \geq 2$, is also **p**-convex. It is because if (6.11) is satisfied, then $\sum_{n\in\mathcal{M}'} p_n \leq 1$ must be satisfied also. We now give a necessary and sufficient condition for the equality of $\overline{\mathcal{H}}$ and $\mathcal{H}$ based on this observation.

Theorem 6.5. *$\overline{\mathcal{H}} = \mathcal{H}$ if and only if the stability region of FRASA is* **p***-convex.*

Proof. Notice that $\mathcal{H}$ is the convex hull of $\overline{\mathcal{H}}$. The corner points either lie on the boundary of $\mathcal{H}$ or in the interior of $\mathcal{H}$. If the stability region of FRASA is **p**-convex, we only need to show

that all corner points lie on the boundary of $\mathcal{H}$. It is because if all corner points are on the boundary of $\mathcal{H}$, then the union $\bigcup_{\hat{n}\in\mathcal{M}} \mathcal{H}_{\hat{n}}$ is convex and hence $\overline{\mathcal{H}} = \mathcal{H}$. Consider $M = 2$. When forming the convex hull $\mathcal{H}$, either

1. $\Pi^{\mathbf{p}^{\mathcal{M}}(\mathcal{M})}$ lies on $\Omega^{\mathcal{M}}$, meaning that $\Omega^{\mathcal{M}}$ is part of the boundary of $\mathcal{H}$; or
2. $\Pi^{\mathbf{p}^{\mathcal{M}}(\mathcal{M})}$ and $\mathbf{0}$ lie on opposite sides of $\Omega^{\mathcal{M}}$, which means $\Omega^{\mathcal{M}}$ will not be the boundary of $\mathcal{H}$ because there is a corner point $\Pi^{\mathbf{p}^{\mathcal{M}}(\mathcal{M})}$ lying beyond $\Omega^{\mathcal{M}}$.

In both cases, $\Pi^{\mathbf{p}^{\mathcal{M}}(\mathcal{M})}$ lies on the boundary of $\mathcal{H}$. For general values of M greater than two, we consider all $\mathcal{M}' \subseteq \mathcal{M}$ where $2 \leq |\mathcal{M}'| < M$ in ascending order of $|\mathcal{M}'|$. Because the stability region of FRASA with link set $\mathcal{M}'$ is also $\mathbf{p}$-convex, by repeating the arguments as above, we see that now all corner points except $\Pi^{\mathbf{p}^{\mathcal{M}}(\mathcal{M})}$ are on the boundary of $\mathcal{H}$ and $\Omega^{\mathcal{M}}$ is the boundary of the stability region farthest away from $\mathbf{0}$. Now we consider the corner point $\Pi^{\mathbf{p}^{\mathcal{M}}(\mathcal{M})}$. We can apply similar arguments as above to show that $\Pi^{\mathbf{p}^{\mathcal{M}}(\mathcal{M})}$ lies on the boundary of $\mathcal{H}$. Hence, $\overline{\mathcal{H}} = \mathcal{H}$. On the other hand, if the stability region of FRASA is not $\mathbf{p}$-convex, then $\Pi^{\mathbf{p}^{\mathcal{M}}(\mathcal{M})}$ lies in between $\mathbf{0}$ and $\Omega^{\mathcal{M}}$. Therefore, at least one corner point does not lie on the boundary of $\mathcal{H}$ and $\overline{\mathcal{H}} \subsetneq \mathcal{H}$. □

From Theorems 6.4 and 6.5, we know that (6.11) guarantees the stability region of FRASA to be $\mathbf{p}$-convex. Then, can (6.11) assure the convexity of the stability region of FRASA? Recall Theorem 6.1 that the boundary of the stability region of FRASA consists of M hypersurfaces, *i.e.*, $\mathsf{F}_{\hat{n}}$ for all $\hat{n} \in \mathcal{M}$. Also, Lemma 6.2 says that for each $\hat{n} \in \mathcal{M}$, the hypersurface $\mathsf{F}_{\hat{n}}$ is contained inside the convex hull $\mathsf{H}_{\hat{n}}$. If (6.11) holds, we need an additional condition to guarantee the convexity of the stability region of FRASA: for all $\hat{n} \in \mathcal{M}$, $\mathsf{F}_{\hat{n}}$ is a hyperplane, meaning that $\mathsf{F}_{\hat{n}} = \mathsf{H}_{\hat{n}}$. This additional condition is satisfied

when $M = 2$ as illustrated in Section 6.2. Therefore, for $M = 2$, **p**-convexity is equivalent to convexity and (6.11) guarantees the convexity of the stability region of FRASA. However, this is not the case for $M > 2$ since if such a hyperplane exists for some $\hat{n}$, the boundary of the stability region of FRASA is linear in $\lambda_{\hat{n}}$, contradicting to the non-parametric form (6.3) that the boundary is of degree at least two in $\lambda_{\hat{n}}$ when $M > 2$. Hence, the nonconvexity of the stability region of FRASA when $M > 2$ follows.

Consider again the examples in Figs. 6.9 and 6.10. In Fig. 6.9, $\sum_{n\in\mathcal{M}} p_n = 0.9 \leq 1$, therefore the stability region is **p**-convex and $\overline{\mathcal{H}} = \mathcal{H}$. On the other hand, in Fig. 6.10, $\sum_{n\in\mathcal{M}} p_n = 1.8 > 1$, and $\overline{\mathcal{H}} \subsetneq \mathcal{H}$. In other words, the convex hull bound is tighter if and only if the stability region is **p**-convex. We remark that even if the stability region may not be **p**-convex, the convex hull bound is still a valid convex and piecewise linear outer bound on the stability region of FRASA.

To illustrate the importance of **p**-convexity, we also compute the "CHB" value, *i.e.*, the upper bound from Theorem 6.3 in Tables 6.2-6.11. We observe that when the stability region of FRASA is **p**-convex, the convex hull bound is tighter than the bound given by [3]; otherwise, the convex hull bound is looser. By Theorems 6.3 and 6.5, the convex hull bound is loose when the stability region is not **p**-convex. This demonstrates that there is a tradeoff between the convexity and the tightness of the bounds.

6.6 Supporting Hyperplane Bound

In this Section, we give a convex and piecewise linear inner bound on the stability region of FRASA by using *supporting*

hyperplanes. Recall that a supporting hyperplane of a convex set is a hyperplane such that it intersects with the convex set and the convex set entirely belongs to only one of the closed half spaces generated by the hyperplane. This inner bound is obtained based on the result of Lemma 6.2.

Theorem 6.6 (Supporting Hyperplane Bound)**.** *For each $\hat{n} \in \mathcal{M}$, we construct a supporting hyperplane $\mathsf{P}_{\hat{n}}$ which supports the convex hull $\mathsf{H}_{\hat{n}}$ in Lemma 6.2 at $\Pi^{\mathsf{p}^{\mathcal{M}}(\mathcal{M})}$ such that*

1. *it lies below $\mathsf{H}_{\hat{n}}$; and*
2. *it has positive intercepts on all coordinate axes.*

We let $\mathcal{S}_{\hat{n}}$ be the closed half space below $\mathsf{P}_{\hat{n}}$. Then the intersection of all these half spaces in the positive orthant, i.e., $\mathcal{S} = \bigcap_{\hat{n}\in\mathcal{M}} \mathcal{S}_{\hat{n}} \cap \{\boldsymbol{\lambda} \colon \lambda_n \geq 0, \forall n \in \mathcal{M}\}$, is a convex and piecewise linear inner bound on the stability region of FRASA.

Proof. Consider the bound of convex hull union $\overline{\mathcal{H}}$ in Theorem 6.2. Choose an arbitrary $\hat{n} \in \mathcal{M}$. When $\overline{\mathcal{H}}$ is intersected with the closed half space $\mathcal{S}_{\hat{n}}$, the resultant polytope does not contain the convex hull $\mathsf{H}_{\hat{n}}$ by construction. Therefore, this resultant polytope excludes the hypersurface $\mathsf{F}_{\hat{n}}$. We repeat this argument for all $\hat{n} \in \mathcal{M}$, then for all $\hat{n} \in \mathcal{M}$, the convex hull $\mathsf{H}_{\hat{n}}$ together with the hypersurface $\mathsf{F}_{\hat{n}}$ are removed. The boundary of the resultant polytope is consisted of $\mathsf{P}_{\hat{n}}$ for all $\hat{n} \in \mathcal{M}$ and the boundary of the positive orthant only, and hence the polytope is $\mathcal{S}$. Therefore, $\mathcal{S}$ is a subset of $\overline{\mathcal{R}}$ and constitutes an inner bound on the stability region of FRASA. This bound is convex and piecewise linear since half spaces are convex and piecewise linear, and these two properties are preserved under intersection. □

Consider the case that $M = 2$ as in Fig. 6.11. First we choose the hyperplanes as stated in Theorem 6.6. Specifically, the line segment between $(p_1, 0)$ and $(p_1\overline{p}_2, p_2\overline{p}_1)$ is the convex hull H_1. Then we choose any point $(p_1', 0)$ on λ_1-axis such that

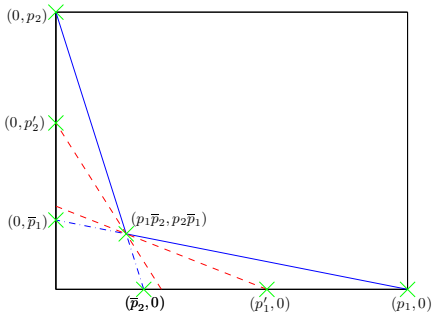

Figure 6.11: Supporting hyperplane bound.

$p_1\overline{p}_2 \leq p_1' \leq p_1$ and form the hyperplane P_1, *i.e.*, the line passing through $(p_1', 0)$ and $(p_1\overline{p}_2, p_2\overline{p}_1)$. Similarly, we choose a point $(0, p_2')$ on λ_2-axis such that $p_2\overline{p}_1 \leq p_2' \leq p_2$ and form the hyperplane P_2. These hyperplanes are shown as the red dashed lines in Fig. 6.11. The intersection of the closed half spaces below the red lines in the positive quadrant is the inner bound from Theorem 6.6.

This supporting hyperplane bound is arbitrary, in the sense that for each $\hat{n} \in \mathcal{M}$, as long as the hyperplane constructed satisfies the requirements listed, $\mathcal{S}$ will be an inner bound. If we require the inner bound to occupy the maximum hypervolume, then this problem is equivalent to finding a maximum-hypervolume convex subset of the stability region of FRASA. To the best of our knowledge, this is studied only for $M = 2$ [27]. In this case, the problem is to find the maximum-area convex subset of a polygon. We recall some related definitions. A *reflex vertex* is a vertex of a polygon such that the angle at the vertex inside the polygon is reflex. A *chord* is a maximal line segment contained in the polygon.

First we consider the case that $p_1 + p_2 > 1$, *i.e.*, the stability region of FRASA is not **p**-convex. In this case, as depicted in Fig. 6.11, the reflex vertex is $(p_1\overline{p}_2, p_2\overline{p}_1)$. By calculus, the maximum-hypervolume convex subset is either the region below

the chord between $(p_1, 0)$ and $(0, \overline{p}_1)$, or the region below the chord between $(0, p_2)$ and $(\overline{p}_2, 0)$, depending on the values of p_1 and p_2. This is a special case of the result in [27]. Suppose the region below the chord between $(p_1, 0)$ and $(0, \overline{p}_1)$ is the maximum-hypervolume convex subset of the stability region of FRASA. If we partition this chord about $(p_1\overline{p}_2, p_2\overline{p}_1)$, we obtain two line segments: one of these lies on a supporting hyperplane of the boundary between $(p_1, 0)$ and $(p_1\overline{p}_2, p_2\overline{p}_1)$, while the other lies on a supporting hyperplane of the boundary between $(0, p_2)$ and $(p_1\overline{p}_2, p_2\overline{p}_1)$. Similar observations can also be found when the region below the chord between $(0, p_2)$ and $(\overline{p}_2, 0)$ is the maximum-hypervolume convex subset of the stability region of FRASA. This means when the stability region is not **p**-convex, if we require the inner bound to have the maximum hypervolume, the supporting hyperplanes we need in Theorem 6.6 coincide.

On the other hand, if the stability region of FRASA is **p**-convex, as stated in previous Section, **p**-convexity is equivalent to convexity. When $p_1 + p_2 \leq 1$, the stability region is **p**-convex and also convex, and the stability region itself is the maximum-hypervolume convex subset. In this case, the line segments of the boundary are already the supporting hyperplanes we need.

6.7 Extension to Partial Interference

In this Section, we extend the results in previous Sections to partial interference. Towards this, we introduce $\mathsf{q}_{n,\mathcal{A}}^{\mathcal{M}}$ for $n \in \mathcal{A} \subseteq \mathcal{M}$ as in Chapter 5. We remark that our results here automatically applies to binary interference, if we allow $\mathsf{q}_{n,\mathcal{A}}^{\mathcal{M}}$ to be either zero or one only by comparing the corresponding SNR, *i.e.*, $\gamma_{n,\mathcal{A}}^{\mathcal{M}}$, against a predefined threshold γ_0. We illustrate the results of the following Theorems by the ring topology in Fig. 6.12.

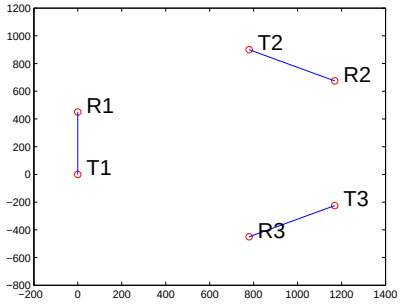

Figure 6.12: A sample topology.

6.7.1 FRASA under Partial Interference

Assume identical settings as in Section 6.2. Let $p'_n = \chi_n p_n$ and $\overline{p}'_n = 1 - \chi_n p_n$. Introduce the following notations:

$$\overline{\mathcal{Q}}^{\mathcal{M}}_{(x,y)} = \sum_{\mathcal{A}\subseteq\mathcal{M}\setminus\{x,y\}} \prod_{n'\in\mathcal{A}} p'_{n'} \prod_{n''\in\mathcal{M}\setminus(\mathcal{A}\cup\{x,y\})} \overline{p}'_{n''} \mathsf{q}^{\mathcal{M}}_{x,\mathcal{A}\cup\{x\}}, \quad (6.14)$$

$$\overline{\mathcal{Q}}^{\mathcal{M}}_{(x,y)'} = \sum_{\mathcal{A}\subseteq\mathcal{M}\setminus\{x,y\}} \prod_{n'\in\mathcal{A}} p'_{n'} \prod_{n''\in\mathcal{M}\setminus(\mathcal{A}\cup\{x,y\})} \overline{p}'_{n''} \mathsf{q}^{\mathcal{M}}_{x,\mathcal{A}\cup\{x,y\}}, \quad (6.15)$$

$$\overline{\mathcal{Q}}^{\mathcal{M}}_{(x)} = \sum_{\mathcal{A}\subseteq\mathcal{M}\setminus\{x\}} \prod_{n'\in\mathcal{A}} p'_{n'} \prod_{n''\in\mathcal{M}\setminus(\mathcal{A}\cup\{x\})} \overline{p}'_{n''} \mathsf{q}^{\mathcal{M}}_{x,\mathcal{A}\cup\{x\}}. \quad (6.16)$$

(6.14) is the probability of successful transmission of link x given that link x is active but link y is not. (6.15) is the probability of successful transmission of link x given that both links x and y are active. (6.16) is the probability of successful transmission of link x given that link x is active. Then the parametric form of the stability region of $\overline{\mathsf{S}}_{\hat{n}}$ will be $\lambda_n = \overline{\lambda}_n, \forall n \in \mathcal{M}$ where

$$\overline{\lambda}_n = \begin{cases} \chi_n p_n \left[p_{\hat{n}} \overline{\mathcal{Q}}^{\mathcal{M}}_{(n,\hat{n})'} + \overline{p}_{\hat{n}} \overline{\mathcal{Q}}^{\mathcal{M}}_{(n,\hat{n})} \right], & n \neq \hat{n} \\ p_{\hat{n}} \overline{\mathcal{Q}}^{\mathcal{M}}_{(\hat{n})}, & n = \hat{n} \end{cases}$$

with $\overline{\lambda}_{\hat{n}} > 0$ and χ_n is between zero and one for all $n \in \mathcal{M} \setminus \{\hat{n}\}$.

With this parametric form, we obtain the stability region of FRASA under partial interference as in the following Theorem.

Theorem 6.7. *For each $\hat{n} \in \mathcal{M}$, we construct a hypersurface $\mathsf{F}_{\hat{n}}$, which is represented by $\lambda_n = \overline{\lambda}_n, \forall n \in \mathcal{M}$, where*

$$\overline{\lambda}_n = \begin{cases} \chi_n p_n \Big[p_{\hat{n}} \overline{\mathcal{Q}}^{\mathcal{M}}_{(n,\hat{n})'} + \overline{p}_{\hat{n}} \overline{\mathcal{Q}}^{\mathcal{M}}_{(n,\hat{n})} \Big], & n \neq \hat{n} \\ p_{\hat{n}} \overline{\mathcal{Q}}^{\mathcal{M}}_{(\hat{n})}, & n = \hat{n} \end{cases} \tag{6.17}$$

with $\overline{\lambda}_{\hat{n}} > 0$ and χ_n is between zero and one for all $n \in \mathcal{M} \setminus \{\hat{n}\}$. Then $\overline{\mathcal{R}}$, the stability region of FRASA under partial interference, is enclosed by $\mathsf{F}_{\hat{n}}, \forall \hat{n} \in \mathcal{M}$ in the positive orthant.

Proof. Every point $\boldsymbol{\lambda} = (\lambda_n)_{n \in \mathcal{M}}$ with

$$\lambda_n = \sum_{\mathcal{A}:\, n \in \mathcal{A} \subseteq \mathcal{M}} \prod_{n' \in \mathcal{A}} \chi_{n'} p_{n'} \prod_{n'' \in \mathcal{M} \setminus \mathcal{A}} (1 - \chi_{n''} p_{n''}) \mathsf{q}^{\mathcal{M}}_{n,\mathcal{A}}, \forall n \in \mathcal{M},$$

where χ_n is between zero and one for all $n \in \mathcal{M}$, lies in the stability region of FRASA under partial interference. Observe that when $\chi_n < 1, \forall n \in \mathcal{M}$, the corresponding $\boldsymbol{\lambda}$ lies in the interior of the stability region. Therefore we only need to consider those $\boldsymbol{\lambda}$ with $\chi_n = 1$ for some $n \in \mathcal{M}$. When $\chi_n = 1$, it means link n has infinite backlog or operate in persistent conditions, while in non-persistent conditions, we allow χ_n to vary arbitrarily between zero and one. Notice that we can never reduce the successful transmission probabilities of all links by changing the links from operating in persistent conditions to non-persistent conditions, because this reduces the amount of interference experienced by all links. Mathematically, we partition $\mathcal{M}$ into three disjoint sets $\mathcal{P}, \{\bar{n}\}, \overline{\mathcal{P}}$. We first let $\mathcal{P} \cup \{\bar{n}\}$ be the set of persistent links. Then the successful transmission probability of

link n is

$$\sum_{(\mathcal{A}',\mathcal{A}''):\ \mathcal{A}'\subseteq\mathcal{P},\mathcal{A}''\subseteq\overline{\mathcal{P}}} \Bigg\{ \Bigg[\prod_{n'\in\mathcal{A}''} \chi_{n'} p_{n'} \prod_{n''\in\overline{\mathcal{P}}\setminus\mathcal{A}''} (1-\chi_{n''}p_{n''}) \Bigg] \times \Bigg[p_{\bar{n}} \prod_{n'\in\mathcal{A}'} p_{n'} \prod_{n''\in\mathcal{P}\setminus\mathcal{A}'} (1-p_{n''}) \Bigg] \mathsf{q}^{\mathcal{M}}_{n,\mathcal{A}'\cup\mathcal{A}''\cup\{\bar{n}\}} + \Bigg[\prod_{n'\in\mathcal{A}''} \chi_{n'} p_{n'} \prod_{n''\in\overline{\mathcal{P}}\setminus\mathcal{A}''} (1-\chi_{n''}p_{n''}) \Bigg] \times \Bigg[(1-p_{\bar{n}}) \prod_{n'\in\mathcal{A}'} p_{n'} \prod_{n''\in\mathcal{P}\setminus\mathcal{A}'} (1-p_{n''}) \Bigg] \mathsf{q}^{\mathcal{M}}_{n,\mathcal{A}'\cup\mathcal{A}''} \Bigg\}. \tag{6.18}$$

If we let $\mathcal{P}$ be the set of persistent links, the successful transmission probability of link n is

$$\sum_{(\mathcal{A}',\mathcal{A}''):\ \mathcal{A}'\subseteq\mathcal{P},\mathcal{A}''\subseteq\overline{\mathcal{P}}} \Bigg\{ \Bigg[\chi_{\bar{n}} p_{\bar{n}} \prod_{n'\in\mathcal{A}''} \chi_{n'} p_{n'} \prod_{n''\in\overline{\mathcal{P}}\setminus\mathcal{A}''} (1-\chi_{n''}p_{n''}) \Bigg] \times \Bigg[\prod_{n'\in\mathcal{A}'} p_{n'} \prod_{n''\in\mathcal{P}\setminus\mathcal{A}'} (1-p_{n''}) \Bigg] \mathsf{q}^{\mathcal{M}}_{n,\mathcal{A}'\cup\mathcal{A}''\cup\{\bar{n}\}} + \Bigg[(1-\chi_{\bar{n}}p_{\bar{n}}) \prod_{n'\in\mathcal{A}''} \chi_{n'} p_{n'} \prod_{n''\in\overline{\mathcal{P}}\setminus\mathcal{A}''} (1-\chi_{n''}p_{n''}) \Bigg] \times \Bigg[\prod_{n'\in\mathcal{A}'} p_{n'} \prod_{n''\in\mathcal{P}\setminus\mathcal{A}'} (1-p_{n''}) \Bigg] \mathsf{q}^{\mathcal{M}}_{n,\mathcal{A}'\cup\mathcal{A}''} \Bigg\}. \tag{6.19}$$

It is easy to see that the successful transmission probability in (6.19) is larger than that in (6.18), because

$$\begin{aligned} &\Big[\chi_{\bar{n}} p_{\bar{n}} \mathsf{q}^{\mathcal{M}}_{n,\mathcal{A}'\cup\mathcal{A}''\cup\{\bar{n}\}} + (1-\chi_{\bar{n}}p_{\bar{n}}) \mathsf{q}^{\mathcal{M}}_{n,\mathcal{A}'\cup\mathcal{A}''}\Big] \\ &\quad - \Big[p_{\bar{n}} \mathsf{q}^{\mathcal{M}}_{n,\mathcal{A}'\cup\mathcal{A}''\cup\{\bar{n}\}} + (1-p_{\bar{n}}) \mathsf{q}^{\mathcal{M}}_{n,\mathcal{A}'\cup\mathcal{A}''}\Big] \\ &= (1-\chi_{\bar{n}}) p_{\bar{n}} \Big(\mathsf{q}^{\mathcal{M}}_{n,\mathcal{A}'\cup\mathcal{A}''} - \mathsf{q}^{\mathcal{M}}_{n,\mathcal{A}'\cup\mathcal{A}''\cup\{\bar{n}\}} \Big) \geq 0, \end{aligned}$$

where we assume $\mathsf{q}^{\mathcal{M}}_{n,\mathcal{A}'\cup\mathcal{A}''} - \mathsf{q}^{\mathcal{M}}_{n,\mathcal{A}'\cup\mathcal{A}''\cup\{\bar{n}\}} \geq 0$, which is in general true because the probability of successful transmission is larger when there are less interferers. This implies that the stability region of FRASA obtained by assuming all links in $\mathcal{P} \subseteq \mathcal{M}$ in persistent conditions is contained inside the stability region of FRASA obtained by assuming all links in $\mathcal{P}' \subseteq \mathcal{P}$ in persistent conditions. Hence, to obtain the boundary of stability region of FRASA under partial interference, we only have to consider the case that only one link is persistent. Then we can use the parametric form (6.17) to obtain the boundary when $\chi_{\hat{n}} = 1$. By repeating over all possible values of $\hat{n}$, we get the desired result. □

An illustration of the results of Theorem 6.7 with the topology in Fig. 6.12 is given in Fig. 6.13. Figs. 6.13(a), 6.13(b) and 6.13(c) depict F_1, F_2 and F_3 respectively. The union of these hypersurfaces, which is the boundary of the stability region of FRASA under partial interference, is shown in Fig. 6.13(d).

6.7.2 Convex Hull Bound

We can obtain similar results as Lemma 6.2, Theorems 6.2 and 6.3 under partial interference by using the corner points. The definition of corner points under partial interference is identical to those in Theorem 5.1 in Chapter 5.

Lemma 6.5. *The boundary of the stability region of $\overline{\mathsf{S}}_{\hat{n}}$ under partial interference, i.e., the hypersurface $\mathsf{F}_{\hat{n}}$ in Theorem 6.7, is contained in the convex hull $\mathsf{H}_{\hat{n}}$ generated by the corner points $\Pi^{\mathsf{p}^{\mathcal{M}}(\mathcal{M}'\cup\{\hat{n}\})}$ for all $\mathcal{M}' \subseteq \mathcal{M} \setminus \{\hat{n}\}$, i.e., every point satisfying (6.17) is a convex combination of the corner points $\Pi^{\mathsf{p}^{\mathcal{M}}(\mathcal{M}'\cup\{\hat{n}\})}$ for all $\mathcal{M}' \subseteq \mathcal{M} \setminus \{\hat{n}\}$.*

Proof. Let $\Pi = (\Pi_n)_{n\in\mathcal{M}}$ be a point satisfying (6.17). When

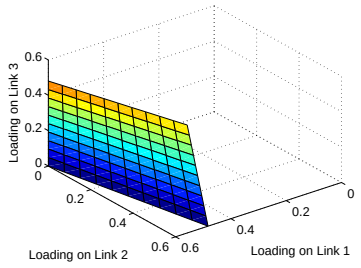

(a) F_1, boundary of stability region with link 1 infinitely backlogged.

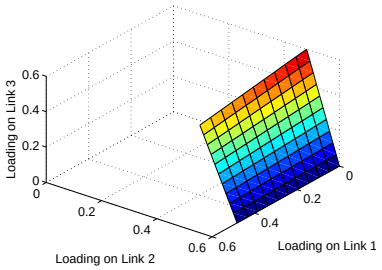

(b) F_2, boundary of stability region with link 2 infinitely backlogged.

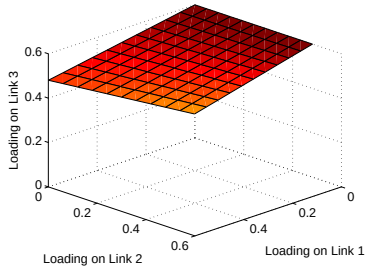

(c) F_3, boundary of stability region with link 3 infinitely backlogged.

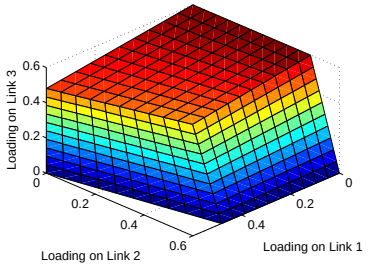

(d) $\overline{\mathcal{R}}$, the whole stability region.

Figure 6.13: Stability region of FRASA under partial interference with $M = 3$, transmission probabilities 0.6 and topology in Fig. 6.12 by Theorem 6.7.

$n \neq \hat{n}$,

$$\Pi_n = \chi_n p_n \Bigg[p_{\hat{n}} \sum_{\mathcal{A} \subseteq \mathcal{M} \setminus \{n,\hat{n}\}} \prod_{n' \in \mathcal{A}} p'_{n'} \prod_{n'' \in \mathcal{M} \setminus (\mathcal{A} \cup \{n,\hat{n}\})} \overline{p}'_{n''} \mathsf{q}^{\mathcal{M}}_{n,\mathcal{A} \cup \{n,\hat{n}\}} + \overline{p}_{\hat{n}} \sum_{\mathcal{A} \subseteq \mathcal{M} \setminus \{n,\hat{n}\}} \prod_{n' \in \mathcal{A}} p'_{n'} \prod_{n'' \in \mathcal{M} \setminus (\mathcal{A} \cup \{n,\hat{n}\})} \overline{p}'_{n''} \mathsf{q}^{\mathcal{M}}_{n,\mathcal{A} \cup \{n\}} \Bigg], \quad (6.20)$$

and

$$\Pi_{\hat{n}} = p_{\hat{n}} \sum_{\mathcal{A} \subseteq \mathcal{M} \setminus \{\hat{n}\}} \prod_{n' \in \mathcal{A}} p'_{n'} \prod_{n'' \in \mathcal{M} \setminus (\mathcal{A} \cup \{\hat{n}\})} \overline{p}'_{n''} \mathsf{q}^{\mathcal{M}}_{\hat{n},\mathcal{A} \cup \{\hat{n}\}} \quad (6.21)$$

where $p'_n = \chi_n p_n$ and $\overline{p}'_n = 1 - \chi_n p_n$. If Π is a convex combination

of $\Pi^{\mathsf{p}^{\mathcal{M}}(\mathcal{M}'\cup\{\hat{n}\})}$ for all $\mathcal{M}' \subseteq \mathcal{M} \setminus \{\hat{n}\}$, then when $n \neq \hat{n}$,

$$\Pi_n = p_n \sum_{\mathcal{M}':\, n\in\mathcal{M}'\subseteq\mathcal{M}\setminus\{\hat{n}\}} \phi_{\mathcal{M}'} \left[p_{\hat{n}} \sum_{\mathcal{A}\subseteq\mathcal{M}'\setminus\{n\}} \prod_{n'\in\mathcal{A}} p_{n'} \prod_{n''\in\mathcal{M}'\setminus(\mathcal{A}\cup\{n\})} \overline{p}_{n''} \mathsf{q}^{\mathcal{M}}_{n,\mathcal{A}\cup\{n,\hat{n}\}} + \overline{p}_{\hat{n}} \sum_{\mathcal{A}\subseteq\mathcal{M}'\setminus\{n\}} \prod_{n'\in\mathcal{A}} p_{n'} \prod_{n''\in\mathcal{M}'\setminus(\mathcal{A}\cup\{n\})} \overline{p}_{n''} \mathsf{q}^{\mathcal{M}}_{n,\mathcal{A}\cup\{n\}} \right], \quad (6.22)$$

and

$$\Pi_{\hat{n}} = p_{\hat{n}} \sum_{\mathcal{M}'\subseteq\mathcal{M}\setminus\{\hat{n}\}} \phi_{\mathcal{M}'} \sum_{\mathcal{A}\subseteq\mathcal{M}'} \prod_{n'\in\mathcal{A}} p_{n'} \prod_{n''\in\mathcal{M}'\setminus\mathcal{A}} \overline{p}_{n''} \mathsf{q}^{\mathcal{M}}_{\hat{n},\mathcal{A}\cup\{\hat{n}\}} \quad (6.23)$$

where

$$\sum_{\mathcal{M}'\subseteq\mathcal{M}\setminus\{\hat{n}\}} \phi_{\mathcal{M}'} = 1 \text{ and } \phi_{\mathcal{M}'} \geq 0, \forall \mathcal{M}' \subseteq \mathcal{M} \setminus \{\hat{n}\}.$$

We will show that $\{\phi_{\mathcal{M}'}\}_{\mathcal{M}'\subseteq\mathcal{M}\setminus\{\hat{n}\}}$ always exists. When $n = \hat{n}$, we get

$$\sum_{\mathcal{M}'\subseteq\mathcal{M}\setminus\{\hat{n}\}} \phi_{\mathcal{M}'} \sum_{\mathcal{A}\subseteq\mathcal{M}'} \prod_{n'\in\mathcal{A}} p_{n'} \prod_{n''\in\mathcal{M}'\setminus\mathcal{A}} \overline{p}_{n''} \mathsf{q}^{\mathcal{M}}_{\hat{n},\mathcal{A}\cup\{\hat{n}\}} = \sum_{\mathcal{A}\subseteq\mathcal{M}\setminus\{\hat{n}\}} \prod_{n'\in\mathcal{A}} p'_{n'} \prod_{n''\in\mathcal{M}\setminus(\mathcal{A}\cup\{\hat{n}\})} \overline{p}'_{n''} \mathsf{q}^{\mathcal{M}}_{\hat{n},\mathcal{A}\cup\{\hat{n}\}}. \quad (6.24)$$

Consider this as a multinomial in $\left\{\mathsf{q}^{\mathcal{M}}_{\hat{n},\mathcal{M}''\cup\{\hat{n}\}}\right\}_{\mathcal{M}''\subseteq\mathcal{M}\setminus\{\hat{n}\}}$. By equating the coefficient of $\mathsf{q}^{\mathcal{M}}_{\hat{n},\mathcal{M}''\cup\{\hat{n}\}}$ for all $\mathcal{M}'' \subseteq \mathcal{M} \setminus \{\hat{n}\}$, we get

$$\sum_{\mathcal{M}':\, \mathcal{M}''\subseteq\mathcal{M}'\subseteq\mathcal{M}\setminus\{\hat{n}\}} \phi_{\mathcal{M}'} \prod_{n''\in\mathcal{M}'\setminus\mathcal{M}''} \overline{p}_{n''} = \prod_{n'\in\mathcal{M}''} \chi_{n'} \prod_{n''\in\mathcal{M}\setminus(\mathcal{M}''\cup\{\hat{n}\})} (1 - \chi_{n''} p_{n''}). \quad (6.25)$$

Also by equating the coefficient of $\mathsf{q}^{\mathcal{M}}_{n,\mathcal{M}''\cup\{n\}}$ and $\mathsf{q}^{\mathcal{M}}_{n,\mathcal{M}''\cup\{n,\hat{n}\}}$ for all $\mathcal{M}'' \subseteq \mathcal{M}\setminus\{n,\hat{n}\}$ with $n \neq \hat{n}$ respectively, we get

$$\begin{aligned}&\sum_{\mathcal{M}':\, \mathcal{M}''\subseteq\mathcal{M}'\setminus\{n\}\subseteq\mathcal{M}\setminus\{n,\hat{n}\}} \phi_{\mathcal{M}'} \prod_{n''\in\mathcal{M}'\setminus(\mathcal{M}''\cup\{n\})} \overline{p}_{n''}\\ =&\prod_{n'\in\mathcal{M}''\cup\{n\}} \chi_{n'} \prod_{n''\in\mathcal{M}\setminus(\mathcal{M}''\cup\{n,\hat{n}\})} (1-\chi_{n''}p_{n''}).\end{aligned}$$

Observe that this is only a special case of (6.25), it suffices to consider (6.25) only. Notice that (6.25) is a system of linear equations. By Gaussian elimination, we see that for all $\mathcal{M}'' \subseteq \mathcal{M}\setminus\{\hat{n}\}$,

$$\phi_{\mathcal{M}''} = \prod_{n'\in\mathcal{M}''} \chi_{n'} \prod_{n''\in\mathcal{M}\setminus(\mathcal{M}''\cup\{\hat{n}\})} (1-\chi_{n''}) \geq 0.$$

Also, by considering $\mathcal{M}'' = \emptyset$ in (6.25), let $\chi_n = 1$ and $p_n = 0$ for all $n \in \mathcal{M}\setminus\{\hat{n}\}$, then we obtain

$$\sum_{\mathcal{M}'\subseteq\mathcal{M}\setminus\{\hat{n}\}} \phi_{\mathcal{M}'} = 1.$$

Therefore, every point satisfying (6.17) is a convex combination of $\Pi^{\mathsf{p}^{\mathcal{M}}(\mathcal{M}'\cup\{\hat{n}\})}$ for all $\mathcal{M}' \subseteq \mathcal{M}\setminus\{\hat{n}\}$. □

Theorem 6.8 (Bound of Upper Convex-Hull Union under Partial Interference)**.** *For each $\hat{n} \in \mathcal{M}$, denote by $\overline{\mathsf{H}}_{\hat{n}}$ the upper convex hull of the hypersurface $\mathsf{F}_{\hat{n}}$ in Theorem 6.7, i.e., the set of hyperplanes forming the convex hull $\mathsf{H}_{\hat{n}}$ in Lemma 6.5 while lying above $\mathsf{F}_{\hat{n}}$. Consider the union $\overline{\mathsf{H}} = \bigcup_{\hat{n}\in\mathcal{M}} \overline{\mathsf{H}}_{\hat{n}}$. The region $\overline{\mathcal{H}}$ below $\overline{\mathsf{H}}$ in the positive orthant is a piecewise linear outer bound on the stability region of FRASA under partial interference.*

Proof. The stability region of FRASA under partial interference, *i.e.*, $\overline{\mathcal{R}}$ in Theorem 6.7, is enclosed by the hyperplanes $\lambda_n = 0, \forall n \in \mathcal{M}$ and the hypersurfaces $\mathsf{F}_{\hat{n}}, \forall \hat{n} \in \mathcal{M}$. To obtain

a piecewise linear outer bound on $\overline{\mathcal{R}}$, we only have to find a piecewise linear outer bound on $\mathsf{F}_{\hat{n}}$ for each $\hat{n} \in \mathcal{M}$. The upper convex hull $\overline{\mathsf{H}}_{\hat{n}}$ suffices for this purpose because it lies above $\mathsf{F}_{\hat{n}}$ and it is piecewise linear. Therefore the union $\overline{\mathsf{H}} = \bigcup_{\hat{n}\in\mathcal{M}} \overline{\mathsf{H}}_{\hat{n}}$ lies above $\mathsf{F}_{\hat{n}}, \forall \hat{n} \in \mathcal{M}$ and the region $\overline{\mathcal{H}}$ below $\overline{\mathsf{H}}$ in the positive orthant constitutes a piecewise linear outer bound on $\overline{\mathcal{R}}$. □

Theorem 6.9 (Convex Hull Bound under Partial Interference)**.** *$\mathcal{H}$, the convex hull generated by $\Pi^{\mathsf{p}^{\mathcal{M}}(\mathcal{M}')}$ for all $\mathcal{M}' \subseteq \mathcal{M}$, is a convex and piecewise linear outer bound on the stability region of FRASA.*

Proof. The proof is identical to that of Theorem 6.3. □

We demonstrate in Fig. 6.14 the results of Theorems 6.8 and 6.9 with the topology in Fig. 6.12. The upper convex hulls of F_1, F_2 and F_3, *i.e.*, $\overline{\mathsf{H}}_1$, $\overline{\mathsf{H}}_2$ and $\overline{\mathsf{H}}_3$, are shown in Figs. 6.14(a), 6.14(b) and 6.14(c) respectively. Fig. 6.14(d) is $\overline{\mathcal{H}}$, the bound of upper convex hull union under partial interference, while Fig. 6.14(e) is $\mathcal{H}$, the convex hull bound under partial interference. As shown in Fig. 6.14(d) and Fig. 6.14(e), these two bounds are identical.

6.7.3 p-Convexity

Introduce the following notations:

$$\mathcal{Q}^{\mathcal{M}}_{(x,y)} = \sum_{\mathcal{A}\subseteq\mathcal{M}\setminus\{x,y\}} \prod_{n'\in\mathcal{A}} p_{n'} \prod_{n''\in\mathcal{M}\setminus(\mathcal{A}\cup\{x,y\})} \overline{p}_{n''}\mathsf{q}^{\mathcal{M}}_{x,\mathcal{A}\cup\{x\}}, \quad (6.26)$$

$$\mathcal{Q}^{\mathcal{M}}_{(x)} = \sum_{\mathcal{A}\subseteq\mathcal{M}\setminus\{x\}} \prod_{n'\in\mathcal{A}} p_{n'} \prod_{n''\in\mathcal{M}\setminus(\mathcal{A}\cup\{x\})} \overline{p}_{n''}\mathsf{q}^{\mathcal{M}}_{x,\mathcal{A}\cup\{x\}}. \quad (6.27)$$

(6.26) and (6.27) have the same meaning as (6.14) and (6.16) in Section 6.7.1 respectively, except that (6.26) and (6.27) assume

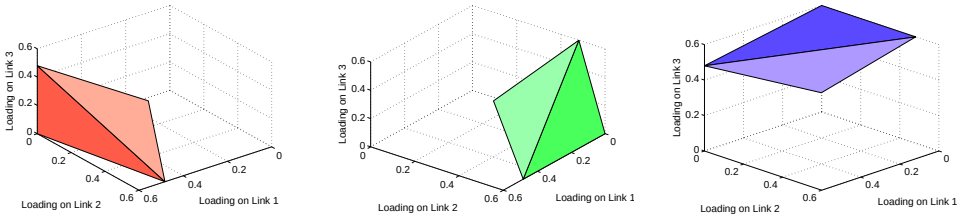

(a) $\overline{\mathsf{H}}_1$, upper convex hull of F_1.

(b) $\overline{\mathsf{H}}_2$, upper convex hull of F_2.

(c) $\overline{\mathsf{H}}_3$, upper convex hull of F_3.

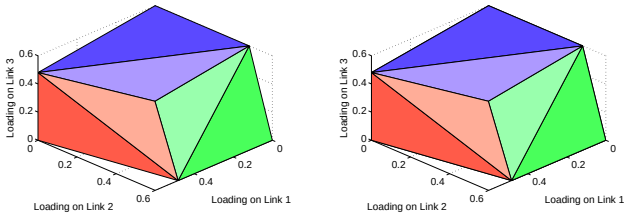

(d) $\overline{\mathcal{H}}$, bound of upper convex-hull union under partial interference.

(e) $\mathcal{H}$, convex hull bound under partial interference.

Figure 6.14: Convex hull bound on stability region of FRASA under partial interference with $M = 3$, transmission probabilities 0.6 and topology in Fig. 6.12 by Theorems 6.8 and 6.9.

every link is either persistent or empty. With some modifications, we obtain the following Theorems as the counterpart of Theorems 6.4 and 6.5 under partial interference.

Theorem 6.10. *The stability region of FRASA under partial interference is* **p***-convex if and only if*

$$\left|\mathcal{X}'_{\mathcal{M}}\right| \left|\mathcal{Y}'_{\mathcal{M}}\right| \leq 0, \tag{6.28}$$

where $\mathcal{X}'_{\mathcal{M}}$ *and* $\mathcal{Y}'_{\mathcal{M}}$ *are* $M \times M$ *matrices, the* $(\bar{n}, n)$*-th element in* $\mathcal{X}'_{\mathcal{M}}$ *is*

$$\begin{cases} \mathcal{Q}^{\mathcal{M}}_{(n,\bar{n})}, & n \neq \bar{n} \\ 0, & n = \bar{n} \end{cases}.$$

and the $(\bar{n}, n)$*-th element in* $\mathcal{Y}'_{\mathcal{M}}$ *is*

$$\begin{cases} \mathcal{Q}^{\mathcal{M}}_{(n,\bar{n})} - \mathcal{Q}^{\mathcal{M}}_{(n)}, & n \neq \bar{n} \\ -\mathcal{Q}^{\mathcal{M}}_{(n)}, & n = \bar{n} \end{cases}.$$

Proof. Using the notations in (6.26) and (6.27), we let $\Pi^{\mathsf{p}^{\mathcal{M}}(\mathcal{M}\setminus\{\bar{n}\})} = \left(\Pi_n^{\mathsf{p}^{\mathcal{M}}(\mathcal{M}\setminus\{\bar{n}\})}\right)_{n\in\mathcal{M}}$ with

$$\Pi_n^{\mathsf{p}^{\mathcal{M}}(\mathcal{M}\setminus\{\bar{n}\})} = \begin{cases} p_n \mathcal{Q}^{\mathcal{M}}_{(n,\bar{n})}, & n \neq \bar{n} \\ 0, & n = \bar{n} \end{cases},$$

$\Pi^{\mathsf{p}^{\mathcal{M}}(\mathcal{M})} = \left(\Pi_n^{\mathsf{p}^{\mathcal{M}}(\mathcal{M})}\right)_{n\in\mathcal{M}}$ with

$$\Pi_n^{\mathsf{p}^{\mathcal{M}}(\mathcal{M})} = p_n \mathcal{Q}^{\mathcal{M}}_{(n)}, \forall n \in \mathcal{M},$$

and modify Lemmas 6.3 and 6.4 as follows.

Lemma 6.6. *Let $\mathcal{X}_{\mathcal{M}}$ be a $M \times M$ matrix, with the first row equals $\mathbf{0} - \Pi^{\mathsf{p}^{\mathcal{M}}(\mathcal{M}\setminus\{1\})}$, and for $n \in \mathcal{M}\setminus\{1\}$, the n-th row is $\Pi^{\mathsf{p}^{\mathcal{M}}(\mathcal{M}\setminus\{n\})} - \Pi^{\mathsf{p}^{\mathcal{M}}(\mathcal{M}\setminus\{1\})}$. Then*

$$\left|\mathcal{X}_{\mathcal{M}}\right| = -\left|\mathcal{X}'_{\mathcal{M}}\right| \prod_{n'\in\mathcal{M}} p_{n'}, \tag{6.29}$$

where the $(\bar{n}, n)$-th element in $\mathcal{X}'_{\mathcal{M}}$ is

$$\begin{cases} \mathcal{Q}^{\mathcal{M}}_{(n,\bar{n})}, & n \neq \bar{n} \\ 0, & n = \bar{n} \end{cases}.$$

Lemma 6.7. *Let $\mathcal{Y}_{\mathcal{M}}$ be a $M \times M$ matrix, with the first row equals $\Pi^{\mathsf{p}^{\mathcal{M}}(\mathcal{M})} - \Pi^{\mathsf{p}^{\mathcal{M}}(\mathcal{M}\setminus\{1\})}$, and for $n \in \mathcal{M}\setminus\{1\}$, the n-th row is $\Pi^{\mathsf{p}^{\mathcal{M}}(\mathcal{M}\setminus\{n\})} - \Pi^{\mathsf{p}^{\mathcal{M}}(\mathcal{M}\setminus\{1\})}$. Then*

$$\left|\mathcal{Y}_{\mathcal{M}}\right| = -\left|\mathcal{Y}'_{\mathcal{M}}\right| \prod_{n'\in\mathcal{M}} p_{n'}, \tag{6.30}$$

where the $(\bar{n}, n)$-th element in $\mathcal{Y}'_{\mathcal{M}}$ is

$$\begin{cases} \mathcal{Q}^{\mathcal{M}}_{(n,\bar{n})} - \mathcal{Q}^{\mathcal{M}}_{(n)}, & n \neq \bar{n} \\ -\mathcal{Q}^{\mathcal{M}}_{(n)}, & n = \bar{n} \end{cases}.$$

By similar arguments in proving Theorem 6.4, **p**-convexity is achieved if and only if $\left|\mathcal{X}_{\mathcal{M}}\right|\left|\mathcal{Y}_{\mathcal{M}}\right| \leq 0$. From Lemmas 6.6 and 6.7, the condition is equivalent to

$$(-1)^2\left|\mathcal{X}'_{\mathcal{M}}\right|\left|\mathcal{Y}'_{\mathcal{M}}\right|\prod_{n'\in\mathcal{M}} p_{n'}^2 \leq 0.$$

After simplification, it reduces to (6.28). □

Theorem 6.11. *$\overline{\mathcal{H}} = \mathcal{H}$ if and only if the stability region of FRASA under partial interference is* **p***-convex.*

Proof. The proof is identical to that of Theorem 6.5. □

With the topology in Fig. 6.12, we can calculate the followings: $\left|\mathcal{X}'_{\mathcal{M}}\right| = -1.5225$, $\left|\mathcal{Y}'_{\mathcal{M}}\right| = 0.2308$, therefore

$$\left|\mathcal{X}'_{\mathcal{M}}\right|\left|\mathcal{Y}'_{\mathcal{M}}\right| = -0.3514 \leq 0$$

and the stability region is **p**-convex.

As another illustration, consider $M = 2$. In this case, **p**-convexity is equivalent to convexity as in collision channel. We first evaluate $\left|\mathcal{X}'_{\mathcal{M}}\right|$ and $\left|\mathcal{Y}'_{\mathcal{M}}\right|$ as follows. According to Lemma 6.6,

$$\left|\mathcal{X}'_{\mathcal{M}}\right| = -\mathsf{q}^{\mathcal{M}}_{1,\{1\}}\mathsf{q}^{\mathcal{M}}_{2,\{2\}},$$

and from Lemma 6.7,

$$\begin{aligned}\left|\mathcal{Y}'_{\mathcal{M}}\right| = &-\mathsf{q}^{\mathcal{M}}_{1,\{1\}}\mathsf{q}^{\mathcal{M}}_{2,\{2\}} + \mathsf{q}^{\mathcal{M}}_{1,\{1\}}\left(\overline{p}_1\mathsf{q}^{\mathcal{M}}_{2,\{2\}} + p_1\mathsf{q}^{\mathcal{M}}_{2,\{1,2\}}\right)\\ &+\mathsf{q}^{\mathcal{M}}_{2,\{2\}}\left(\overline{p}_2\mathsf{q}^{\mathcal{M}}_{1,\{1\}} + p_2\mathsf{q}^{\mathcal{M}}_{1,\{1,2\}}\right).\end{aligned}$$

The **p**-convexity condition in Theorem 6.10, *i.e.*, (6.28), becomes

$$\begin{aligned}-\mathsf{q}^{\mathcal{M}}_{1,\{1\}}\mathsf{q}^{\mathcal{M}}_{2,\{2\}}\Big[&-\mathsf{q}^{\mathcal{M}}_{1,\{1\}}\mathsf{q}^{\mathcal{M}}_{2,\{2\}} + \mathsf{q}^{\mathcal{M}}_{1,\{1\}}\left(\overline{p}_1\mathsf{q}^{\mathcal{M}}_{2,\{2\}} + p_1\mathsf{q}^{\mathcal{M}}_{2,\{1,2\}}\right)\\ &+\mathsf{q}^{\mathcal{M}}_{2,\{2\}}\left(\overline{p}_2\mathsf{q}^{\mathcal{M}}_{1,\{1\}} + p_2\mathsf{q}^{\mathcal{M}}_{1,\{1,2\}}\right)\Big] \leq 0\end{aligned}$$

$$\frac{\overline{p}_2\mathsf{q}^{\mathcal{M}}_{1,\{1\}} + p_2\mathsf{q}^{\mathcal{M}}_{1,\{1,2\}}}{\mathsf{q}^{\mathcal{M}}_{1,\{1\}}} + \frac{\overline{p}_1\mathsf{q}^{\mathcal{M}}_{2,\{2\}} + p_1\mathsf{q}^{\mathcal{M}}_{2,\{1,2\}}}{\mathsf{q}^{\mathcal{M}}_{2,\{2\}}} \geq 1,$$

which is equivalent to the condition for convexity proved in Theorem 3 in [10] when $p_1 = p_2 = 1$.

6.7.4 Supporting Hyperplane Bound

The following Theorem is the counterpart of Theorem 6.6, for the convex and piecewise linear inner bound on the stability region of FRASA under partial interference.

Theorem 6.12 (Supporting Hyperplane Bound under Partial Interference)**.** *For each $\hat{n} \in \mathcal{M}$, we construct a supporting hyperplane $\mathsf{P}_{\hat{n}}$ which supports the convex hull $\mathsf{H}_{\hat{n}}$ in Lemma 6.5 at $\Pi^{\mathsf{p}^{\mathcal{M}}(\mathcal{M})}$ such that*

1. *it lies below $\mathsf{H}_{\hat{n}}$; and*
2. *it has positive intercepts on all coordinate axes.*

We let $\mathcal{S}_{\hat{n}}$ be the closed half space below $\mathsf{P}_{\hat{n}}$. Then the intersection of all these half spaces in the positive orthant, i.e., $\mathcal{S} = \bigcap_{\hat{n} \in \mathcal{M}} \mathcal{S}_{\hat{n}} \cap \{\boldsymbol{\lambda} \colon \lambda_n \geq 0, \forall n \in \mathcal{M}\}$, is a convex and piecewise linear inner bound on the stability region of FRASA under partial interference.

Proof. The proof is identical to that of Theorem 6.6. □

6.8 Chapter Summary

In this Chapter, we proposed FRASA, Feedback Retransmission Approximation for Slotted ALOHA, to serve as a surrogate to approximate finite-link slotted ALOHA. From FRASA, we obtained in closed form the boundary of the stability region for any number of links in the system under collision channel. We illustrated that the result from FRASA is identical to the analytical result of finite-link slotted ALOHA when there are two links in the system. Simulations showed that the stability region obtained from FRASA is a good approximation to the stability region of finite-link slotted ALOHA. We demonstrated that our results from FRASA has a wider range of applicability than the existing bounds. We also established a convex hull bound, which is convex and piecewise linear, to outer-bound the stability region of FRASA. This convex hull bound can be generated by using the transmission probability vector only. Moreover, we introduced **p**-convexity, which is essential to ensure the convex hull bound to be close to the boundary of the stability region of FRASA. From this, we deduced that the stability region of FRASA is nonconvex when there are more than two links. A separate convex and piecewise linear inner bound, supporting hyperplane bound, was also introduced. Furthermore, we extended the results to cover other interference models like binary and partial interference. Since the convex hull bound and the supporting hyperplane bound are convex and piecewise linear, they can be used to formulate the traffic engineering problem in wireless mesh networks with random access protocols as linear programming, which can be solved by standard techniques. These bounds may also be useful in the design of traffic engineering algorithms in such networks.

□ **End of chapter.**

Table 6.2: Comparison for λ_M for $M = 3$ and $p_1 = p_2 = p_3 = 0.5$.

	λ_1	λ_2	CHB	Upper	FRASA (Exact Sim.)	Lower
G1	0	0	0.5	0.5	0.5 (0.499596)	0.5
	0	0.12	0.38	0.38	0.38 (0.383064)	0.38
G2	0.06	0.06	0.38	0.38	0.370278 (0.365150)	0.340526
G3	0.12	0.123	0.257	0.257	0.17036 (0.158455)	0.140231
G4	0.12	0.13*	0.25	0.25	0.13 (0.131462)	0.13

Table 6.3: Comparison for λ_M for $M = 3$ and $p_1 = 0.6, p_2 = 0.7, p_3 = 0.8$.

	λ_1	λ_2	CHB	Upper	FRASA (Exact Sim.)	Lower
G1	0	0	0.8	0.8	0.8 (0.801918)	0.8
	0	0.05	0.742857	0.6	0.6 (0.601158)	0.6
	0.03	0	0.76	0.68	0.68 (0.682747)	0.68
G2	0.018	0.028	0.744	0.616	0.602618 (0.593758)	0.508
G3	0.03	0.05	0.702857	0.48	0.423303 (0.375008)	0.24
G4	0.035	0.0561*	0.689219	0.4356	0.344373 (0.203636)	0.115187
	0.025	0.0563*	0.702324	0.4748	0.421353 (0.359871)	0.277705

Table 6.4: Comparison for λ_M for $M = 3$ and $p_1 = 0.63, p_2 = 0.52, p_3 = 0.51$.

	λ_1	λ_2	CHB	Upper	FRASA (Exact Sim.)	Lower
G1	0	0	0.51	0.51	0.51 (0.509758)	0.51
	0	0.045	0.465865	0.463163	0.463163 (0.464256)	0.463163
	0.07	0	0.453333	0.437143	0.437143 (0.440437)	0.437143
G2	0.07	0.045	0.409199	0.390306	0.381358 (0.374840)	0.340919
G3	0.14	0.09	0.308397	0.270612	0.203557 (0.164070)	0.122806
G4	0.12	0.095*	0.319684	0.286224	0.233287 (0.203133)	0.167073
	0.15*	0.093	0.297360	0.257082	0.166100 (0.117348)	0.092458

Table 6.5: Comparison for λ_M for $M = 3$ and $p_1 = 0.1, p_2 = 0.1, p_3 = 0.1$. (Note: [3]'s bound is not applicable for the example in G4)

	λ_1	λ_2	CHB	Upper	FRASA (Exact Sim.)	Lower
G1	0	0	0.1	0.1	0.1 (0.099937)	0.1
	0	0.03	0.096667	0.096667	0.096667 (0.097374)	0.096667
G2	0.04	0.04	0.091111	0.091111	0.090894 (0.091423)	0.090749
G3	0.078	0.078	0.08175	0.082667	0.081748 (0.081703)	0.081723
G4	0.078	0.082*	0.076	0.082222	0.075971 (0.076836)	0.081260

Table 6.6: Comparison for λ_M for $M = 3$ and $p_1 = 0.3, p_2 = 0.2, p_3 = 0.1$.

	λ_1	λ_2	CHB	Upper	FRASA (Exact Sim.)	Lower
G1	0	0	0.1	0.1	0.1 (0.101570)	0.1
	0	0.06	0.093333	0.093333	0.093333 (0.094032)	0.093333
G2	0.11	0.06	0.081111	0.081111	0.080094 (0.079323)	0.079039
G3	0.21	0.12	0.058	0.063333	0.057966 (0.057121)	0.057731
G4	0.11	0.13*	0.071778	0.073333	0.070841 (0.071236)	0.070503

Table 6.7: Comparison for λ_M for $M = 5$ and $p_1 = p_2 = p_3 = p_4 = p_5 = 0.5$.

	λ_1	λ_2	λ_3	λ_4	CHB	Upper	FRASA (Exact Sim.)	Lower
G1	0	0	0	0	0.5	0.5	0.5 (0.499870)	0.5
	0	0	0	0.015	0.485	0.485	0.485 (0.487190)	0.485
	0	0	0.015	0.015	0.47	0.47	0.469521 (0.468605)	0.462021
	0	0.015	0.015	0.015	0.455	0.455	0.453495 (0.455147)	0.421588
G2	0.015	0.015	0.015	0.015	0.44	0.44	0.436838 (0.433372)	0.337257
G3	0.03	0.03	0.03	0.03	0.38	0.38	0.364349 (0.347664)	0.048165
G4	0.03	0.03	0.03	0.033*	0.377	0.377	0.360352 (0.343758)	0.045835
	0.033*	0.032*	0.031	0.03	0.374	0.374	0.356292 (0.330086)	0.039261
	0.0325*	0.032*	0.0315*	0.03	0.374	0.374	0.356289 (0.329231)	0.037718

Table 6.8: Comparison for λ_M for $M = 5$ and $p_1 = 0.4, p_2 = 0.5, p_3 = 0.6, p_4 = 0.7, p_5 = 0.8$.

	λ_1	λ_2	λ_3	λ_4	CHB	Upper	FRASA (Exact Sim.)	Lower
G1	0	0	0	0	0.8	0.8	0.8 (0.801848)	0.8
	0	0	0	0.005	0.794286	0.78	0.78 (0.781746)	0.78
	0	0	0.005	0.005	0.787619	0.76	0.759473 (0.761162)	0.744333
	0	0.005	0.005	0.005	0.779619	0.74	0.738360 (0.737206)	0.685500
G2	0.002	0.003	0.005	0.005	0.779619	0.74	0.738223 (0.730949)	0.629233
G3	0.004	0.006	0.01	0.01	0.759238	0.68	0.672075 (0.664101)	0.409069
G4	0.004	0.006	0.01	0.017*	0.751238	0.652	0.640030 (0.626106)	0.172513
	0.004	0.006	0.011*	0.017*	0.749905	0.648	0.635225 (0.617195)	0.152455
	0.002	0.0073*	0.011*	0.017*	0.751025	0.6508	0.638890 (0.621284)	0.312233

Table 6.9: Comparison for λ_M for $M = 5$ and $p_1 = 0.77, p_2 = 0.74, p_3 = 0.63, p_4 = 0.52, p_5 = 0.51$.

	λ_1	λ_2	λ_3	λ_4	CHB	Upper	FRASA (Exact Sim.)	Lower
G1	0	0	0	0	0.51	0.51	0.51 (0.513695)	0.51
	0	0	0	0.0025	0.507548	0.507398	0.507398 (0.507195)	0.507398
	0	0	0.003	0.0025	0.505120	0.504276	0.504259 (0.507851)	0.502567
	0	0.007	0.003	0.0025	0.500295	0.496990	0.496889 (0.496086)	0.481862
G2	0.0005	0.007	0.003	0.0025	0.499964	0.496469	0.496355 (0.495522)	0.475539
G3	0.001	0.014	0.006	0.005	0.489928	0.482939	0.482467 (0.485847)	0.439008
G4	0.001	0.014	0.006	0.0057*	0.489241	0.482210	0.481704 (0.482933)	0.437699
	0.001	0.014	0.0089*	0.0057*	0.486894	0.479192	0.478545 (0.476540)	0.424837
	0.001	0.015*	0.0089*	0.0057*	0.486205	0.478151	0.477467 (0.479027)	0.420479

Table 6.10: Comparison for λ_M for $M = 5$ and $p_1 = p_2 = p_3 = p_4 = p_5 = 0.1$.

	λ_1	λ_2	λ_3	λ_4	CHB	Upper	FRASA (Exact Sim.)	Lower
G1	0	0	0	0	0.1	0.1	0.1 (0.099510)	0.1
	0	0	0	0.03	0.096667	0.096667	0.096667 (0.096855)	0.096667
	0	0	0.03	0.03	0.093333	0.093333	0.093214 (0.092705)	0.093084
	0	0.03	0.03	0.03	0.09	0.09	0.089623 (0.090675)	0.089205
G2	0.03	0.03	0.03	0.03	0.8625	0.086667	0.085870 (0.085167)	0.084971
G3	0.064	0.064	0.064	0.064	0.066685	0.071556	0.066673 (0.066963)	0.066451
G4	0.064	0.064	0.064	0.066*	0.066352	0.071333	0.066345 (0.067406)	0.066231
	0.061	0.062	0.066*	0.066*	0.066852	0.071667	0.066838 (0.067879)	0.066713

Table 6.11: Comparison for λ_M for $M = 5$ and $p_1 = 0.05, p_2 = 0.15, p_3 = 0.2, p_4 = 0.25, p_5 = 0.3$.

	λ_1	λ_2	λ_3	λ_4	CHB	Upper	FRASA (Exact Sim.)	Lower
G1	0	0	0	0	0.3	0.3	0.3 (0.302818)	0.3
	0.008	0	0	0	0.296571	0.296571	0.296571 (0.294838)	0.296571
	0.008	0.03	0	0	0.283714	0.283714	0.283559 (0.283699)	0.283324
	0.008	0.03	0.04	0	0.266571	0.266571	0.265342 (0.263649)	0.263498
G2	0.008	0.03	0.04	0.06	0.241294	0.240857	0.235673 (0.236382)	0.228304
G3	0.015	0.05	0.08	0.1	0.175240	0.195	0.171271 (0.169823)	0.164827
G4	0.008	0.03	0.04	0.115*	0.212478	0.217286	0.207391 (0.207954)	0.202430
	0.006	0.02	0.09*	0.115*	0.188218	0.201	0.184594 (0.183449)	0.181481

Table 6.12: Comparison for λ_M for $M = 10$ and $p_1 = p_2 = p_3 = p_4 = p_5 = p_6 = p_7 = p_8 = p_9 = p_{10} = 0.5$.

	λ_1	λ_2,λ_3	λ_4,λ_5	λ_6,λ_7,λ_8	λ_9	Upper	FRASA (Exact Sim.)	Lower
G1	0	0	0	0	0	0.5	0.5 (0.500313)	0.5
	0	0.00045	0.00045	0.00045	0.00045	0.4964	0.496389 (0.495384)	0.436516
G2	0.00045	0.00045	0.00045	0.00045	0.00045	0.49595	0.495935 (0.491676)	0.361677
G3	0.0009	0.0009	0.0009	0.0009	0.0009	0.4919	0.491840 (0.487785)	0.005261
G4	0.00097	0.00097	0.000977*	0.000977*	0.00098*	0.491225	0.491155 (0.491508)	0.002443
	0.00097	0.00097	0.00097	0.000977*	0.00098*	0.491239	0.491169 (0.492485)	0.002524

Table 6.13: Comparison for λ_M for $M = 10$ and $p_1 = p_2 = p_3 = 0.1, p_4 = 0.2, p_5 = 0.3, p_6 = 0.4, p_7 = 0.5, p_8 = 0.6, p_9 = 0.7, p_{10} = 0.8$.

	λ_1 $\times 10^{-3}$	λ_2, λ_3 $\times 10^{-3}$	λ_4 $\times 10^{-3}$	λ_5 $\times 10^{-3}$	λ_6 $\times 10^{-3}$	λ_7 $\times 10^{-3}$	λ_8 $\times 10^{-3}$	λ_9 $\times 10^{-3}$	Upper	FRASA (Exact Sim.)	Lower
G1	0	0	0	0	0	0	0	0	0.8	0.8 (0.801064)	0.8
	0	0.15	0.35	0.5	0.5	1	2	3	0.7694	0.768940 (0.765617)	0.654316
G2	0.15	0.15	0.35	0.5	0.5	1	2	3	0.7688	0.768316 (0.768196)	0.637086
G3	0.3	0.3	0.7	1	1	2	4	6	0.7376	0.735560 (0.734688)	0.412179
G4	0.3	0.3	0.7	1	1	2	4	6.86*	0.73416	0.731926 (0.730537)	0.402376
	0.01	0.327*	0.735*	1.26*	1.96*	2.94*	4.41*	6.86*	0.724684	0.721594 (0.719353)	0.041246

Table 6.14: Comparison for λ_M for $M = 10$ and $p_1 = p_2 = p_3 = p_4 = p_5 = p_6 = p_7 = p_8 = p_9 = p_{10} = 0.1$.

	λ_1	λ_2,λ_3,λ_4	λ_5,λ_6,λ_7,λ_8,λ_9	Upper	FRASA (Exact Sim.)	Lower
G1	0	0	0	0.1	0.1 (0.099754)	0.1
	0	0.019	0.019	0.083111	0.081498 (0.081612)	0.077453
G2	0.019	0.019	0.019	0.081	0.078832 (0.079277)	0.073177
G3	0.036	0.036	0.036	0.064	0.050075 (0.049960)	0.04286
G4	0.039*	0.036	0.036	0.063667	0.049130 (0.049294)	0.042554
	0.039*	0.039*	0.036	0.062667	0.045913 (0.046425)	0.041415

Table 6.15: Comparison for λ_M for $M = 10$ and $p_1 = p_2 = p_3 = p_4 = p_5 = 0.1, p_6 = p_7 = p_8 = p_9 = p_{10} = 0.05$.

	λ_1,λ_2,λ_3,λ_4,λ_5	λ_6	λ_7,λ_8	λ_9	Upper	FRASA (Exact Sim.)	Lower
G1	0	0	0	0	0.05	0.05 (0.049782)	0.05
	0	0.01	0.01	0.01	0.047895	0.047860 (0.048058)	0.047789
G2	0.025	0.01	0.01	0.01	0.041316	0.040460 (0.040962)	0.038908
G3	0.05	0.02	0.02	0.02	0.032632	0.026879 (0.026375)	0.025804
G4	0.025	0.018	0.018	0.025*	0.039263	0.037808 (0.037468)	0.036269
	0.015	0.015	0.025*	0.025*	0.041316	0.040447 (0.040123)	0.039497

Chapter 7

Conclusion and Future Works

7.1 Conclusion

The capacity of a wireless mesh network is significantly affected by the interference among the links in the network. Therefore, to maximize the performance of a wireless mesh network in terms of capacity, it is crucial for wireless mesh traffic engineering algorithms to accurately model the interference among the links. However, existing traffic engineering algorithms assumed an overly simplified binary interference model, which is verified as an imprecise model for interference. Also, these works presumed the existence of an ideal scheduler which can control when each link can be active in transmission. Hence, we believe there is a need to design new traffic engineering algorithms without assuming binary interference and perfect scheduling.

The contribution of this thesis includes the followings:

- an introduction of a new interference model: partial interference, and the illustration of the potential gain in capacity by exploiting partial interference;
- a numerical characterization of the stability region of 802.11 networks under partial interference with two links;
- an analytical characterization of the stability region of slotted ALOHA networks under partial interference with two links, and analytical results on part of the boundary of

the stability region for the case of more than two links in slotted ALOHA networks;

- an introduction of the FRASA model as a surrogate of slotted ALOHA to approximate the stability region of slotted ALOHA networks, the analytical results on the stability region of FRASA with any number of links under collision channel, binary and partial interference, and the convex and piecewise linear outer and inner bounds on the stability region of FRASA that can be used to find upper and lower bounds on network capacity.

7.2 Future Works

In view of this work, one of the possible future works is to consider partial interference when computing the capacity of any wireless mesh network with arbitrary topology. We may modify the interference constraints in the capacity-finding problem to take into account partial interference, and evaluate how much will be gained by considering partial interference in scheduling in wireless networks.

Another possibility is to consider the capacity-finding problem with random access MAC protocols like 802.11 or slotted ALOHA, and design traffic engineering algorithms for these networks. This can be used to provide QoS guarantees without assuming the existence of perfect global schedulers, therefore it does not require modifying existing MAC protocols.

The model in this work only covers the case of single-hop networks. Therefore, towards designing traffic engineering algorithms with random access MAC protocols, we have to generalize the results of this work to multi-hop wireless networks. The stability region, the convex hull bound and the supporting hyperplane bound obtained in this work may be used in designing traffic engineering algorithms in wireless random ac-

cess networks. Extending the results on finding the maximum-hypervolume convex subset to cover the case of more than two links helps providing a better inner bound on the stability region of FRASA.

In this thesis, we have only considered networks with one channel. In reality, links on different channels may also interfere with each other. Therefore, we may also extend our framework to consider partial interference in wireless networks with multiple channels.

□ **End of chapter.**

Appendix A

Proof of (4.13) in Chapter 4

In Chapter 4, we use $\Pr(j_1, k_1|j_0, k_0)$ to denote the transition probability from (j_0, k_0) to (j_1, k_1). For convenience, we drop the subscripts for τ_n, c_n, q_n, i_n and repeat the transition probabilities in (4.1)-(4.12) as follows:

$$\Pr(j, k|j, k+1) = 1, \quad j \in [0, m], k \in [0, W_j - 2], \tag{A.1}$$

$$\Pr(0, k|-1, k+1) = q, k \in [0, W_0 - 2], \tag{A.2}$$

$$\Pr(-1, k|-1, k+1) = 1 - q, k \in [0, W_0 - 2], \tag{A.3}$$

$$\Pr(0, k|j, 0) = \frac{(1-c)q}{W_0}, \quad j \in [0, m-1], k \in [0, W_0 - 1], \tag{A.4}$$

$$\Pr(-1, k|j, 0) = \frac{(1-c)(1-q)}{W_0}, \quad j \in [0, m-1], k \in [0, W_0 - 1], \tag{A.5}$$

$$\Pr(0, k|m, 0) = \frac{q}{W_0}, k \in [0, W_0 - 1], \tag{A.6}$$

$$\Pr(-1, k|m, 0) = \frac{1-q}{W_0}, k \in [0, W_0 - 1], \tag{A.7}$$

$$\Pr(j, k|j-1, 0) = \frac{c}{W_j}, \quad j \in [1, m], k \in [0, W_j - 1], \tag{A.8}$$

$$\Pr(0,k|-1,0) = \frac{q(1-i)+q^2i(1-c)}{W_0}, \quad k \in [0, W_0-1], \tag{A.9}$$

$$\Pr(1,k|-1,0) = \frac{qic}{W_1}, k \in [0, W_1-1], \tag{A.10}$$

$$\Pr(-1,k|-1,0) = \frac{qi(1-c)(1-q)}{W_0}, \quad k \in [1, W_0-1], \tag{A.11}$$

$$\Pr(-1,0|-1,0) = \frac{qi(1-c)(1-q)}{W_0} + (1-q). \tag{A.12}$$

As in Chapter 4, we use $\pi_{j,k}$ to denote the stationary probability of the state (j,k) in the Markov chain. We follow the steps listed below to solve the Markov chain and obtain the transmission probability, *i.e.*, (4.13).

Step 1: Express $\pi_{j,k}$ in terms of $\pi_{j-1,0}$ for $j \in [2,m], k \in [0, W_j-1]$. From (A.8), we get for $j \in [2,m]$,

$$\pi_{j,W_j-1} = \pi_{j-1,0}\frac{c}{W_j}.$$

Also for $j \in [2,m]$, $k \in [0, W_j-2]$, from (A.1) and (A.8),

$$\begin{aligned}\pi_{j,k} &= \pi_{j-1,0}\frac{c}{W_j} + \pi_{j,k+1} \\ &= \pi_{j,W_j-1} + \pi_{j,k+1}.\end{aligned}$$

Therefore, for $j \in [2,m]$, $k \in [0, W_j-1]$,

$$\pi_{j,k} = \pi_{j-1,0}\frac{c(W_j-k)}{W_j}. \tag{A.13}$$

Step 2: Express $\pi_{j,0}$ in terms of $\pi_{1,0}$ for $j \in [1,m]$. From (A.13), we obtain for $j \in [2,m]$,

$$\pi_{j,0} = \pi_{j-1,0}c.$$

Therefore, for $j \in [1,m]$,

$$\pi_{j,0} = \pi_{1,0}c^{j-1}. \tag{A.14}$$

Step 3: Express $\pi_{1,k}$ in terms of $\pi_{-1,0}$ and $\pi_{0,0}$ for $k \in [0, W_1 - 1]$. From (A.8) and (A.10),

$$\pi_{1,W_1-1} = \pi_{0,0}\frac{c}{W_1} + \pi_{-1,0}\frac{qic}{W_1}.$$

Also, from (A.1), (A.8) and (A.10), for $k \in [0, W_1 - 2]$,

$$\begin{aligned}\pi_{1,k} &= \pi_{0,0}\frac{c}{W_1} + \pi_{-1,0}\frac{qic}{W_1} + \pi_{1,k+1} \\ &= \pi_{1,W_1-1} + \pi_{1,k+1}.\end{aligned}$$

We obtain for $k \in [0, W_1 - 1]$,

$$\pi_{1,k} = \pi_{0,0}\frac{c(W_1 - k)}{W_1} + \pi_{-1,0}\frac{qic(W_1 - k)}{W_1}. \tag{A.15}$$

In particular,

$$\pi_{1,0} = \pi_{0,0}c + \pi_{-1,0}qic. \tag{A.16}$$

Step 4: Compute $\sum_{j=0}^{m-1} \pi_{j,0}$ in terms of $\pi_{0,0}$ and $\pi_{-1,0}$. From (A.14) and (A.16),

$$\begin{aligned}\sum_{j=0}^{m-1} \pi_{j,0} &= \pi_{0,0} + \sum_{j=1}^{m-1} \pi_{1,0}c^{j-1} \\ &= \pi_{0,0} + (\pi_{0,0}c + \pi_{-1,0}qic)\sum_{j=1}^{m-1} c^{j-1} \\ &= \pi_{0,0}\sum_{j=0}^{m-1} c^j + \pi_{-1,0}qi\sum_{j=1}^{m-1} c^j. \end{aligned} \tag{A.17}$$

Step 5: Express $\pi_{0,k}$ in terms of π_{0,W_0-1} for $k \in [1, W_0 - 2]$. From (A.4), (A.6) and (A.9),

$$\pi_{0,W_0-1} = \sum_{j=0}^{m-1} \pi_{j,0}\frac{(1-c)q}{W_0} + \pi_{m,0}\frac{q}{W_0} + \pi_{-1,0}\frac{q(1-i) + q^2 i(1-c)}{W_0}.$$

And from (A.14), (A.16) and (A.17),

$$\begin{aligned}\pi_{0,W_0-1} &= \pi_{0,0}\frac{(1-c^m)q}{W_0} + \pi_{-1,0}\frac{q^2ic(1-c^{m-1})}{W_0} \\ &\quad +(\pi_{0,0}c + \pi_{-1,0}qic)\frac{c^{m-1}q}{W_0} + \pi_{-1,0}\frac{q(1-i)+q^2i(1-c)}{W_0} \\ &= \pi_{0,0}\frac{q}{W_0} + \pi_{-1,0}\frac{q^2i+q(1-i)}{W_0}. \end{aligned} \tag{A.18}$$

From (A.1), (A.2), (A.4), (A.6) and (A.9), we obtain for $k \in [1, W_0-2]$,

$$\begin{aligned}\pi_{0,k} &= \sum_{j=0}^{m-1}\pi_{j,0}\frac{(1-c)q}{W_0} + \pi_{m,0}\frac{q}{W_0} + \pi_{-1,0}\frac{q(1-i)+q^2i(1-c)}{W_0} \\ &\quad +\pi_{0,k+1} + \pi_{-1,k+1}q \\ &= \pi_{0,W_0-1} + \pi_{0,k+1} + \pi_{-1,k+1}q\end{aligned}$$

Therefore, for $k \in [1, W_0-2]$,

$$\sum_{k'=k}^{W_0-2}(\pi_{0,k'} - \pi_{0,k'+1}) = \sum_{k'=k}^{W_0-2}(\pi_{0,W_0-1} + \pi_{-1,k'+1}q),$$

or

$$\pi_{0,k} = \pi_{0,W_0-1}(W_0-k) + q\sum_{k'=k}^{W_0-2}\pi_{-1,k'+1}. \tag{A.19}$$

Step 6: Express $\pi_{-1,k}$ in terms of π_{-1,W_0-1} for $k \in [1, W_0-1]$. From (A.5), (A.7) and (A.11),

$$\begin{aligned}\pi_{-1,W_0-1} &= \sum_{j=0}^{m-1}\pi_{j,0}\frac{(1-c)(1-q)}{W_0} \\ &\quad +\pi_{m,0}\frac{1-q}{W_0} + \pi_{-1,0}\frac{qi(1-c)(1-q)}{W_0},\end{aligned}$$

then from (A.14), (A.16) and (A.17),

$$\begin{aligned}\pi_{-1,W_0-1} &= \pi_{0,0}\frac{(1-c^m)(1-q)}{W_0} + \pi_{-1,0}\frac{qic(1-c^{m-1})(1-q)}{W_0} \\ &\quad +(\pi_{0,0}c + \pi_{-1,0}qic)\frac{c^{m-1}(1-q)}{W_0} \\ &\quad +\pi_{-1,0}\frac{qi(1-c)(1-q)}{W_0} \\ &= \pi_{0,0}\frac{1-q}{W_0} + \pi_{-1,0}\frac{qi(1-q)}{W_0}. \end{aligned} \tag{A.20}$$

Also, from (A.3), (A.5), (A.7) and (A.11), for $k \in [1, W_0 - 2]$

$$\begin{aligned}\pi_{-1,k} &= \sum_{j=0}^{m-1}\pi_{j,0}\frac{(1-c)(1-q)}{W_0} \\ &\quad +\pi_{m,0}\frac{1-q}{W_0} + \pi_{-1,0}\frac{qi(1-c)(1-q)}{W_0} + \pi_{-1,k+1}(1-q) \\ &= \pi_{-1,W_0-1} + \pi_{-1,k+1}(1-q).\end{aligned}$$

Therefore, for $k \in [1, W_0 - 1]$,

$$\begin{aligned}\pi_{-1,k} &= \sum_{k'=0}^{W_0-k-1}\pi_{-1,W_0-1}(1-q)^{k'} \\ &= \pi_{-1,W_0-1}\frac{1-(1-q)^{W_0-k}}{q}. \end{aligned} \tag{A.21}$$

Step 7: Express $\pi_{0,0}$ in terms of $\pi_{-1,0}$. From (A.3), (A.5), (A.7), (A.11) and (A.12),

$$\begin{aligned}\pi_{-1,0} &= \sum_{j=0}^{m-1}\pi_{j,0}\frac{(1-c)(1-q)}{W_0} \\ &\quad +\pi_{m,0}\frac{1-q}{W_0} + \pi_{-1,0}\frac{qi(1-c)(1-q)}{W_0} \\ &\quad +\pi_{-1,1}(1-q) + \pi_{-1,0}(1-q) \\ &= \pi_{-1,W_0-1} + \pi_{-1,1}(1-q) + \pi_{-1,0}(1-q)\end{aligned}$$

Therefore, from (A.20) and (A.21),

$$\begin{aligned}\pi_{-1,0}q &= \pi_{-1,W_0-1} + \pi_{-1,1}(1-q)\\ &= \pi_{-1,W_0-1}\left\{1 + \frac{1-q}{q}\left[1-(1-q)^{W_0-1}\right]\right\}\\ &= \left\{\pi_{0,0}\frac{1-q}{W_0} + \pi_{-1,0}\frac{qi(1-q)}{W_0}\right\}\\ &\quad\times\left\{1 + \frac{1-q}{q}\left[1-(1-q)^{W_0-1}\right]\right\}.\end{aligned}$$

On solving, we obtain

$$\pi_{0,0} = \pi_{-1,0}\frac{q}{1-q}\frac{qW_0 - i(1-q)\left[1-(1-q)^{W_0}\right]}{1-(1-q)^{W_0}}. \tag{A.22}$$

Step 8: Compute the aggregate probability for stage $j=-1$ in terms of $\pi_{-1,0}$. From (A.20) and (A.22),

$$\begin{aligned}\pi_{-1,W_0-1} &= \pi_{0,0}\frac{1-q}{W_0} + \pi_{-1,0}\frac{qi(1-q)}{W_0}\\ &= \pi_{-1,0}\left\{\frac{qi(1-q)}{W_0}\right.\\ &\quad\left.+\frac{1-q}{W_0}\frac{q}{1-q}\frac{qW_0 - i(1-q)\left[1-(1-q)^{W_0}\right]}{1-(1-q)^{W_0}}\right\}\\ &= \pi_{-1,0}\frac{q^2}{1-(1-q)^{W_0}}.\end{aligned} \tag{A.23}$$

From (A.21) and (A.23),

$$\begin{aligned}\sum_{k=0}^{W_0-1}\pi_{-1,k} &= \pi_{-1,0} + \sum_{k=1}^{W_0-1}\pi_{-1,W_0-1}\frac{1-(1-q)^{W_0-k}}{q}\\ &= \pi_{-1,0}\left\{1 + \frac{q}{1-(1-q)^{W_0}}\right.\\ &\quad\left.\times\left(W_0 - 1 - \frac{1-q}{q}\left[1-(1-q)^{W_0-1}\right]\right)\right\}\\ &= \pi_{-1,0}\frac{qW_0}{1-(1-q)^{W_0}}.\end{aligned} \tag{A.24}$$

Step 9: Compute the aggregate probability for stage $j = 0$ in terms of $\pi_{-1,0}$. Using (A.18), (A.19), (A.21) and (A.23), we obtain for $k \in [1, W_0 - 2]$,

$$\begin{aligned}
\pi_{0,k} &= \pi_{0,0}\frac{q(W_0-k)}{W_0} + \pi_{-1,0}\frac{[q^2 i + q(1-i)](W_0-k)}{W_0} \\
&\quad + \pi_{-1,0}\frac{q^2}{1-(1-q)^{W_0}} \sum_{k'=k}^{W_0-2} \left[1-(1-q)^{W_0-k'-1}\right] \\
&= \pi_{0,0}\frac{q(W_0-k)}{W_0} + \pi_{-1,0}\frac{[q^2 i + q(1-i)](W_0-k)}{W_0} \\
&\quad + \pi_{-1,0}\frac{q^2}{1-(1-q)^{W_0}} \\
&\quad \times \left\{ (W_0-k-1) - \frac{1-q}{q}\left[1-(1-q)^{W_0-k-1}\right] \right\} \\
&= \pi_{0,0}\frac{q(W_0-k)}{W_0} + \pi_{-1,0}\frac{[q^2 i + q(1-i)](W_0-k)}{W_0} \\
&\quad + \pi_{-1,0}\frac{q^2(W_0-k)-q}{1-(1-q)^{W_0}} + \pi_{-1,0}\frac{q(1-q)^{W_0-k}}{1-(1-q)^{W_0}}. \quad \text{(A.25)}
\end{aligned}$$

In (A.25), if we let $k = W_0 - 1$, we get (A.18). If we substitute $k = 0$ into (A.25), we obtain (A.22), hence (A.25) holds for $k \in [0, W_0 - 1]$, and,

$$\begin{aligned}
\sum_{k=0}^{W_0-1} \pi_{0,k} &= \pi_{0,0}\frac{q(W_0+1)}{2} + \pi_{-1,0}\frac{[q^2 i + q(1-i)](W_0+1)}{2} \\
&\quad + \pi_{-1,0}\frac{q^2 W_0(W_0+1) - 2qW_0}{2[1-(1-q)^{W_0}]} + \pi_{-1,0}(1-q) \\
&= \pi_{-1,0}\Bigg\{ \frac{q}{1-q}\frac{qW_0 - i(1-q)[1-(1-q)^{W_0}]}{1-(1-q)^{W_0}}\frac{q(W_0+1)}{2} \\
&\quad + \frac{[q^2 i + q(1-i)](W_0+1)}{2} \\
&\quad + \frac{q^2 W_0(W_0+1) - 2qW_0}{2[1-(1-q)^{W_0}]} + (1-q) \Bigg\},
\end{aligned}$$

or

$$\sum_{k=0}^{W_0-1}\pi_{0,k}=\pi_{-1,0}\Bigg\{\frac{q}{1-q}\frac{W_0+1}{2}\times\frac{q^2W_0+(1-q)(1-i)[1-(1-q)^{W_0}]}{1-(1-q)^{W_0}}+\frac{qW_0(qW_0+q-2)}{2[1-(1-q)^{W_0}]}+(1-q)\Bigg\}. \tag{A.26}$$

Step 10: Compute the aggregate probability for stage $j=1$ in terms of $\pi_{-1,0}$. From (A.15) and (A.22),

$$\begin{aligned}\sum_{k=0}^{W_1-1}\pi_{1,k}&=\pi_{0,0}\frac{c(W_1+1)}{2}+\pi_{-1,0}\frac{qic(W_1+1)}{2}\\&=\pi_{-1,0}\frac{c(W_1+1)}{2}\\&\quad\times\Bigg\{\frac{q}{1-q}\frac{qW_0-i(1-q)[1-(1-q)^{W_0}]}{1-(1-q)^{W_0}}+qi\Bigg\}\\&=\pi_{-1,0}\frac{q^2cW_0}{(1-q)[1-(1-q)^{W_0}]}\frac{W_1+1}{2}.\end{aligned}$$

Step 11: Compute the aggregate probability for stage $j\in[2,m]$ in terms of $\pi_{-1,0}$. From (A.16) and (A.22),

$$\begin{aligned}\pi_{1,0}&=\pi_{0,0}c+\pi_{-1,0}qic\\&=\pi_{-1,0}\Bigg\{\frac{qc}{1-q}\frac{qW_0-i(1-q)[1-(1-q)^{W_0}]}{1-(1-q)^{W_0}}+qic\Bigg\}\\&=\pi_{-1,0}\frac{q^2cW_0}{(1-q)[1-(1-q)]^{W_0}}.\end{aligned} \tag{A.27}$$

From (A.13), (A.14) and (A.27), for $j\in[2,m]$, $k\in[0,W_j-1]$,

$$\begin{aligned}\pi_{j,k}&=\pi_{1,0}\frac{c^{j-1}(W_j-k)}{W_j}\\&=\pi_{-1,0}\frac{q^2c^jW_0(W_j-k)}{W_j(1-q)[1-(1-q)^{W_0}]}.\end{aligned}$$

Therefore, for $j \in [2, m]$,

$$\sum_{k=0}^{W_j-1} \pi_{j,k} = \pi_{-1,0} \frac{q^2 c^j W_0}{(1-q)[1-(1-q)^{W_0}]} \frac{W_j+1}{2}. \tag{A.28}$$

So (A.28) also applies to the case when $j = 1$.

Step 12: Normalization. From (A.24), (A.26) and (A.28),

$$\begin{aligned}
1 &= \sum_{k=0}^{W_0-1} \pi_{-1,k} + \sum_{j=0}^{m} \sum_{k=0}^{W_j-1} \pi_{j,k} \\
&= \pi_{-1,0} \Bigg\{ \frac{qW_0}{1-(1-q)^{W_0}} \\
&\quad + \frac{q}{1-q} \frac{W_0+1}{2} \frac{q^2 W_0 + (1-q)(1-i)[1-(1-q)^{W_0}]}{1-(1-q)^{W_0}} \\
&\quad + \frac{qW_0(qW_0+q-2)}{2[1-(1-q)^{W_0}]} + (1-q) \\
&\quad + \frac{q^2 W_0}{2(1-q)[1-(1-q)^{W_0}]} \sum_{j=1}^{m} c^j (W_j+1) \Bigg\}.
\end{aligned}$$

Therefore,

$$\begin{aligned}
\pi_{-1,0} &= \Bigg\{ \frac{qW_0}{1-(1-q)^{W_0}} \\
&\quad + \frac{q}{1-q} \frac{W_0+1}{2} \frac{q^2 W_0 + (1-q)(1-i)[1-(1-q)^{W_0}]}{1-(1-q)^{W_0}} \\
&\quad + \frac{qW_0(qW_0+q-2)}{2[1-(1-q)^{W_0}]} + (1-q) \\
&\quad + \frac{q^2 W_0}{2(1-q)[1-(1-q)^{W_0}]} \sum_{j=1}^{m} c^j (W_j+1) \Bigg\}^{-1} \\
&= \Bigg\{ \frac{q^2 W_0}{2(1-q)[1-(1-q)^{W_0}]} \sum_{j=0}^{m} c^j (W_j+1) \\
&\quad + \frac{1}{2} q(1-i)(W_0+1) + (1-q) \Bigg\}^{-1}.
\end{aligned} \tag{A.29}$$

Step 13: Compute the transmission probability. Therefore, from (A.14), (A.22), (A.27) and (A.29), the transmission probability is

$$\begin{aligned}
\tau &= \sum_{j=0}^{m} \pi_{j,0} + \pi_{-1,0} q i \\
&= \pi_{-1,0} \Bigg\{ qi + \frac{q}{1-q} \frac{qW_0 - i(1-q)[1-(1-q)^{W_0}]}{1-(1-q)^{W_0}} \\
&\quad + \frac{q^2 c W_0}{(1-q)[1-(1-q)^{W_0}]} \sum_{j=1}^{m} c^{j-1} \Bigg\} \\
&= \pi_{-1,0} \frac{q^2 W_0}{(1-q)[1-(1-q)^{W_0}]} \sum_{j=0}^{m} c^j \\
&= \left(2q^2 W_0 \sum_{j=0}^{m} c^j \right) \Bigg\{ q^2 W_0 \sum_{j=0}^{m} c^j (W_j + 1) \\
&\quad + (1-q)\big[1-(1-q)^{W_0}\big]\big[q(1-i)(W_0+1) + 2(1-q)\big] \Bigg\}^{-1},
\end{aligned}$$

which is (4.13).

□ **End of chapter.**

Bibliography

[1] R. Gupta, J. Musacchio, and J. Walrand, "Sufficient Rate Constraints for QoS Flows in Ad-Hoc Networks," *Ad Hoc Networks*, 2006.

[2] R. R. Rao and A. Ephremides, "On the Stability of Interacting Queues in a Multiple-Access System," *IEEE Trans. Inf. Theory*, vol. 34, no. 5, pp. 918–930, Sep. 1988.

[3] W. Luo and A. Ephremides, "Stability of N Interacting Queues in Random-Access Systems," *IEEE Trans. Inf. Theory*, vol. 45, no. 5, pp. 1579–1587, Jul. 1999.

[4] P. Gupta and P. R. Kumar, "The Capacity of Wireless Networks," *IEEE Trans. Inf. Theory*, vol. 46, no. 2, pp. 388–404, Mar. 2000.

[5] K. Jain, J. Padhye, V. Padmanabhan, and L. Qiu, "Impact of Interference on Multi-hop Wireless Network Performance," in *MobiCom 2003*, San Diego, California, USA, Sep. 2003.

[6] M. Kodialam and T. Nandagopal, "Characterizing the Capacity Region in Multi-Radio Multi-Channel Wireless Mesh Networks," in *MobiCom 2005*, Cologne, Germany, Aug./Sep. 2005.

[7] J. Padhye, S. Agarwal, V. N. Padmanabhan, L. Qiu, A. Rao, and B. Zill, "Estimation of Link Interference in

Static Multi-hop Wireless Networks," in *Internet Measurement Conference*, Berkeley, CA, Oct. 2005.

[8] A. Mishra, E. Rozner, S. Banerjee, and W. Arbaugh, "Exploiting Partially Overlapping Channels in Wireless Networks: Turning a Peril into an Advantage," in *Internet Measurement Conference*, Berkeley, CA, Oct. 2005.

[9] G. Bianchi, "Performance Analysis of the IEEE 802.11 Distributed Coordination Function," *IEEE J. Sel. Areas Commun.*, vol. 18, no. 3, pp. 535–547, Mar. 2000.

[10] V. Naware, G. Mergen, and L. Tong, "Stability and Delay of Finite-User Slotted ALOHA With Multipacket Reception," *IEEE Trans. Inf. Theory*, vol. 51, no. 7, pp. 2636–2656, Jul. 2005.

[11] B. S. Tsybakov and V. A. Mikhailov, "Ergodicity of a Slotted ALOHA System," *Probl. Inform. Transm.*, vol. 15, no. 4, pp. 73–87, 1979.

[12] W. Szpankowski, "Stability Conditions for Multidimensional Queueing Systems with Computer Applications," *Oper. Res.*, vol. 36, no. 6, pp. 944–957, Nov./Dec. 1988.

[13] V. Anantharam, "The Stability Region of the Finite-User Slotted ALOHA Protocol," *IEEE Trans. Inf. Theory*, vol. 37, no. 3, pp. 535–540, May 1991.

[14] W. Szpankowski, "Stability Conditions for Some Multiqueue Distributed Systems: Buffered Random Access Systems," *Adv. Appl. Probab.*, vol. 26, pp. 498–515, Jun. 1994.

[15] S. Ghez, S. Verdú, and S. C. Schwartz, "Stability Properties of Slotted Aloha With Multipacket Reception Capability," *IEEE Trans. Autom. Control*, vol. 33, no. 7, pp. 640–649, Jul. 1988.

[16] S. J. Shellhammer, "Estimation of Packet Error Rate Caused by Interference using Analytic Techniques - A Coexistence Assurance Methodology," IEEE 802.19 Technical Advisory Group Document Archive, Qualcomm, Inc., Oct. 2005.

[17] T. S. Rappaport, *Wireless Communications: Principles and Practice*, 2nd ed. Prentice Hall, 2002.

[18] G. Mergen and L. Tong, "Stability and Capacity of Regular Wireless Networks," *IEEE Trans. Inf. Theory*, vol. 51, no. 6, pp. 1938–1953, Jun. 2005.

[19] H. Wu, Y. Peng, K. Long, S. Cheng, and J. Ma, "Performance of Reliable Transport Protocol over IEEE 802.11 Wireless LAN: Analysis and Enhancement," in *INFOCOM 2002*, Jun. 2002.

[20] *Wireless LAN Medium Access Control (MAC) and Physical Layer (PHY) Specifications*, IEEE Std. 802.11, 1999.

[21] D. Malone, K. Duffy, and D. J. Leith, "Modeling the 802.11 Distributed Coordination Function in Non-saturated Heterogeneous Conditions," *IEEE/ACM Trans. Netw.*, vol. 15, no. 1, 2007.

[22] D. Kincaid and W. Cheney, *Numerical Analysis: Mathematics of Scientific Computing*, 3rd ed. Brooks/Cole, 2002.

[23] The Network Simulator - ns-2. [Online]. Available: http://www.isi.edu/nsnam/ns/

[24] R. M. Loynes, "The Stability of a Queue with Non-Independent Interarrival and Service Times," *Proc. Cambridge Phil. Soc.*, vol. 58, pp. 494–520, 1962.

[25] S. S. Lam, "Store-and-Forward Buffer Requirements in a Packet Switching Network," *IEEE Trans. Commun.*, vol. 24, no. 4, Apr. 1976.

[26] J. R. Wieland, R. Pasupathy, and B. W. Schmeiser, "Queueing-Network Stability: Simulation-Based Checking," in *Proceedings of the 2003 Winter Simulation Conference*, vol. 1, Dec. 2003, pp. 520–527.

[27] J.-S. Chang and C.-K. Yap, "A Polynomial Solution for Potato-Peeling and Other Polygon Inclusion and Enclosure Problems," in *25th Annual Symposium on Foundations of Computer Science*, Oct. 1984, pp. 408–416.